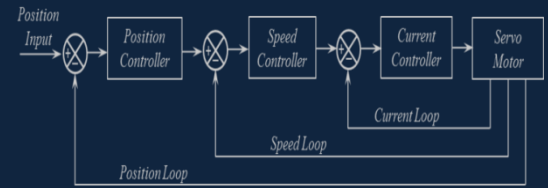




e-ISSN: 2618-575X



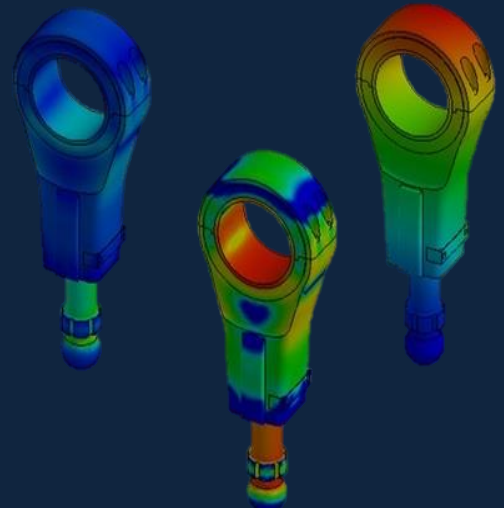
International Advanced Researches and Engineering Journal

Aerospace Engineering,
Aquaculture and Fisheries Engineering,
Architecture,
Bioengineering,
Chemical Engineering,
Civil Engineering,
Computer Engineering,
Electrical and Electronics,
Energy,
Environmental Engineering,
Food Engineering,
Geomatics Engineering,
Industrial Engineering,
Industrial Applications,
Machine Theory and Dynamics,
Manufacturing,
Mechanical Engineering,
Mechanics,
Mechatronics,
Medical,
Modeling and Simulation,
Physics Engineering,
Robotics,
Textile Engineering
Health in Engineering

$$F=ma$$

$$E=mc^2$$

$$\int \frac{dy}{dx} dt$$



Volume: 03 / Issue: 01 / April 2019




e-ISSN: 2618-575X

Available online at www.dergipark.gov.tr

INTERNATIONAL ADVANCED RESEARCHES
and
ENGINEERING JOURNAL

Journal homepage: www.dergipark.gov.tr/iarej

International
Open Access 

Volume 03
Issue 01

April, 2019

International Advanced Researches and Engineering Journal (IAREJ) is a double-blind peer-reviewed and publicly available online journal that has Editorial Board (<http://dergipark.gov.tr/iarej/board>). The editor in chief of IAREJ welcomes the submissions that cover theoretical and/or applied researches on **Engineering** and related science with Engineering. The publication language of the Journal is **English**. **Writing Rules** are given in Author Guidelines (<http://dergipark.gov.tr/iarej/writing-rules>). IAREJ publishes **original papers** that are research papers and technical review papers.

IAREJ publication, which is **open access**, is **free of charge**. There is no article submission and processing charges (APCs).

IAREJ is indexed & abstracted in:

Directory of Open Access Scholarly Researches (ROAD)
Directory of Research Journals Indexing (DRJI)
Google Scholar
Journal Factor
J-Gate
Index Copernicus
Rootindexing
Scientific Indexing Services (SIS)

Authors are responsible from the copyrights of the figures and the contents of the manuscripts, accuracy of the references, quotations and proposed ideas and the Publication Ethics (<http://dergipark.gov.tr/iarej/page/4240>).

All rights of the issue are reserved by International Advanced Researches and Engineering Journal (IAREJ). IAREJ also allows the author(s) to hold the copyright of own articles.

©

IAREJ

15 April 2019



This is an open access issue under the CC BY-NC license (<http://creativecommons.org/licenses/by-nc/4.0/>).



e-ISSN: 2618-575X

Available online at www.dergipark.gov.tr

INTERNATIONAL ADVANCED RESEARCHES
and
ENGINEERING JOURNAL

Journal homepage: www.dergipark.gov.tr/iarej

International
Open Access



Volume 03
Issue 01

April, 2019

Table of Contents

Review Articles	Pages
The effect of dairy cow feeding regime on functional milk production <i>Habip Muruz and Nurcan Çetinkaya</i>	001-006
Research Articles	
Convective hot airdrying characteristics of selected vegetables <i>Eda Elgin Kılıç and, İnci Çınar</i>	007-013
Evaluation of some agronomical characteristics and essential oil ratio of coriander (<i>Coriandrum sativum</i> L.) cultivars cultivated by applying different humic acid doses <i>Hanifi Cinarlidere and Belgin Cosge Senkal</i>	014-019
Production of red fluorescent protein (mCherry) in an inducible E. coli expression system in a bioreactor, purification and characterization <i>Hülya Kuduğ, Bahadır Ataman, Rizvan İmamoğlu, Duygu Düzgün and İsa Gökçe</i>	020-025
Use of various plant extracts to provide hygiene in mattresses and antibacterial film production <i>Gülsemin SavaşTuna, Efe Şafak, Beyza Kara, Gülce Mülayim, Ceren Sert, Nazlıcan Ulu, Kemal Göktuğ Eken and Sercen Cansu Sertel</i>	026-031
Determination of highly effective attributes in fold level classification of proteins <i>Özlem Polat</i>	032-039
Resource based view in the Turkish construction sector and resource selection with ANP technique <i>Ozlem Geylani and H. Attila Dikbas</i>	040-047
The evaluation on the effect of effective and repetitive vibration to compressive strength with the fuzzy method <i>Ferhat Pakdamar and Mahmut Kahraman</i>	048-054
Investigation of mechanical and microstructural performance of alkali activated electrical arc furnace slag mortars <i>Murat Ozturk, Umur Korkut Sevim, Muzeyyen Balcikanli Bankir and Omer Saltuk Bolukbasi</i>	055-059
Comparison of contamination on yarns produced from local and us blend cotton types <i>Gülbin Fidan and Yasemin Korkmaz</i>	060-064
Biosynthesis and characterization of iron oxide nanoparticles from <i>Enteromorpha</i> spp. extract: determination of adsorbent properties for copper (II) ions <i>Gizem Ercan, Deniz Uzunoğlu, Memduha Ergüt and Ayla Özer</i>	065-074
Removal of Acid Orange 74 from wastewater with TiO₂ nanoparticle <i>Gamze Topal, Neşe Keklikçioğlu Çakmak, Atakan Eroğlu and Ünsal Açıkel</i>	075-080



Review Article

The effect of dairy cow feeding regime on functional milk production**Habip Muruz^{a,*}** **and Nurcan Çetinkaya^a** ^a Faculty of Veterinary Medicine, Ondokuz Mayıs University, 55139, Samsun, Turkey

ARTICLE INFO

Article history:

Received 21 March 2018

Revised 21 October 2018

Accepted 13 January 2019

Keywords:

Functional milk

Conjugated linoleic acid

Nutrition

Dairy cow

ABSTRACT

The purpose of this paper is to evaluate nutritional strategies that will increase the concentration of the conjugated linoleic acid in milk to produce functional milk with regard to health benefits in dairy cow. Conjugated linoleic acid isomers are natural fatty acids in foods obtained from ruminants. The main substrates for biohydrogenation are linoleic acid and linolenic acid, an essential fatty acid. It has been identified 54 different conjugated linoleic acid isomers that have beneficial biological activity. *cis-9, trans-11 18:2* and *trans-10, cis-12 18:2* are most bioactive isomers of CLA. In milk fat, the *cis-9, trans-11* conjugated linoleic acid is found in major amounts more than *trans-10, cis-12* conjugated linoleic acid. Conjugated linoleic acid is first produced as an intermediate product during the biohydrogenation in the rumen of dietary linoleic acid and linolenic acid. Another major pathway of conjugated linoleic acid synthesis in dairy cows is endogenous synthesis in the mammary gland. Dietary *cis-9, trans-11* conjugated linoleic acid is of great interest due to its health benefits known to a cancer chemopreventive and antiatherogenic. Therefore, many researchers have looked for ways of increasing the amount of conjugated linoleic acid in cow milk. For this purpose, researchers have adopted two approaches. The first approach is to make dietary changes to increase the natural conjugated linoleic acid production of cow. The second approach is to feed with mixtures of conjugated linoleic acid isomers protected against microbial biological hydrogenation in the rumen. As a result, as consumers continue to be aware of the relationship between diet and health, increased conjugated linoleic acid level of milk may provide new market opportunities for milk and milk products as functional food.

© 2019, Advanced Researches and Engineering Journal (IAREJ) and the Author(s).

1. Introduction

Dairy products from ruminants are the most important sources of nutrient quality protein, energy, minerals and vitamins. Recent studies have shown that dairy products have many bioactive compounds with associated health effects for the consumer beyond simple nutrition [1]. The Conjugated linoleic acid (CLA), which cannot be synthesized by the human body, is mostly found in the raw milk derived from cows. The discovery of a “functional food” role for CLA occurred over the past decade. CLA is considered an essential nutrient for human. Therefore, this fatty acid, human can only obtain from ruminant products [2]. Data from several studies in both animal and human models suggest that CLA has several the physiological properties such as anticarcinogenic, antilipogenic, antidiabetic, modulate

immune function and inflammatory response, antihypertensive, antiatherosclerotic [3].

The term CLA refers to a group mixture of positional and geometric isomers (*cis, trans*) of linoleic acid or linolenic acid that have conjugated double bonds. It has been determined that great numbers of isomers of CLA found in milk and meat products [4], but *cis-9, trans-11 18:2* (*c9, t11* CLA), also called rumenic acid, and *trans-10, cis-12 18:2* (*t10, c12* CLA) are most bioactive isomers of CLA [5]. It reported that physiological effect of *c9, t11* CLA is principal anticarcinogenic, while *t10, c12* CLA isomer is antidiabetic, antiobese and anticarcinogenic [6].

A portion of CLA is produced uncompleted ruminal biohydrogenation of linoleic acid and another portion derives from Δ -9 desaturase on vaccenic acid (C18:1 *trans-11*) (occurs during biohydrogenation linoleic acid, linolenic acid and oleic acid) within mammary gland and

* Corresponding author. Tel.: +90 362 312 1919; Fax: +90 362 457 69 22
E-mail addresses: habip.muruz@omu.edu.tr (H. Muruz), nurcanc@omu.edu.tr (N. Çetinkaya)
ORCID: 0000-0002-1975-4545 (H. Muruz), 0000-0002-9977-2937 (N. Çetinkaya)

in the other body tissues [7,8]. McCrorie et al. [9] demonstrated that the CLA content in milk fat ranged from 2 to 37 mg/g fat due to breed, species, lactation period, age, feeding strategy and the fatty acid composition of diet [10]. However, among these factors, diet plays a central role on CLA composition in milk fat [11].

In this review, dietary change to increase the natural CLA production in dairy cows will be discussed here.

2. The Fatty Acids in Cow Milk Fat

Whole cow's milk contains 3.2-4.7% fat depending on particularly feeding strategies (generally increased with increasing fiber content) and lactation stage. Approximately 98% of the total milk fat consists of triglycerides. Other milk lipids include: diacylglycerides (0.25-0.48%); monoacylglycerides (0.02-0.04%); phospholipids (0.6-1.0%); cholesterol (0.2-0.4%); glycolipids (0.006%); and FAs in milk (0.1-0.4%). Milk fat contains saturated FA (SFA), monounsaturated FA (MUFA), and polyunsaturated FA (PUFA), approximately 70%, 25 and 5, respectively, but this can be modified by changing the animal diet [12]. PUFA includes linolenic acid (C18:3 n-3) and rumenic acid (C18:2 *cis*-9, *trans*-11). Milk MUFA consists mainly of oleic acid (C18:1 *cis*-9) and also *trans* vaccenic acid (C18:1 *trans*-11). Both rumenic and vaccenic acid are *trans*-11 FA produced by rumen microorganisms. There are approximately 400 different types of FA [13]. The milk FAs, which range from 4 to 20C chain length, are derived from the feed and the microbial biohydrogenation in the rumen. The FAs in ruminant milk are synthesized either in the mammary gland (carbon chains: <C15 and a portion of C16) from acetate and to a lesser extent from β -hydroxybutyrate or approximately one half of the FAs (a portion of C16 and >C17) from dietary lipids and adipose tissue reserves [14].

CLA, which is unsaturated FAs and constitute up to 5% of all FAs [15]. Up to now, total of 54 different isomers of CLA were identified [16]. Within this group, *c*9, *t*11 CLA and *t*10, *c*12 CLA are believed to be the most common natural two isoforms of the group of CLAs [17]. It has been shown that CLAs are formed both during the biohydrogenation of PUFA originated from the diet in the rumen and mammary synthesis from vaccenic acid [18]. The *c*9, *t*11 CLA isomer is found in more abundance (72 to 94% of total CLA) than the *t*10, *c*12 CLA in milk and meat products [19, 20].

3. The Fatty Acid Composition of Plants

Unlike short and medium-chain FA, long chain C18 FA can not be endogenously synthesized by ruminants desired in meat and milk. For this reason, these FA have to be ingested by feed ruminant.

The main substrates for ruminal biohydrogenation are C18 linoleic acid and linolenic acid. The lipids in the ruminant feeds are mainly triglycerides as well as in lower proportion phospholipids and galactolipids. The lipid composition of forage is amply composed of glycolipids and phospholipids, and the main FA is linolenic acid which is unsaturated fatty acids, while seed oils are largely triglycerides containing linoleic and [21]. It has been

shown that the lipid fraction ranged from 30–100 g kg⁻¹ DM in the leaves of grasses and grasses. [22]. However, the lipids present in plants are not static structures, but are constantly exposed to turnover due to the lipid degradation in living plants by normally present lipases [22].

As shown in Table 1 [23], the FA profile of lipids in feeds is highly variable. Linolenic acid levels generally depend on plant and environmental factors such as wilting prior to ensiling, hay and haylage making, stage of maturity and light intensity. The pre-wilting process of ensiling causes about 40% reduction in total fatty acid level, 40% loss even for linolenic acid. An ensiling process and silage additives (formic acid) led to smaller losses. In contrast, the use of hay and haylage reduced total FA by 50% and 70%, respectively. [22]. It is reported that nitrogen fertilization was significantly increased for palmitic acid (18%), linoleic acid (12%) and linolenic acid (40%) in the herbage [24].

Many of the oil seeds are rich in linoleic, accounting for 53 to 69% of total FA, and but its composition is considerably variable. For example, in ground nuts, rapeseed and sesame seed: high in oleic acid; cotton seed, soybeans and sunflower seeds: high in linoleic acid and linseed: high in linolenic acid. Fish oil, the richest source of FA of 20 or 22 C, contains relatively low amounts of linoleic and linolenic [25].

Table 1. Fatty acid content of common dairy cow feeds [25]

Feed	Oleic	Linoleic	Linolenic	Other
	-fatty acid, % of total reported FAs-			
Pasture				
Grass	2.2	20.4	55.9	0.0
Clover	3.6	21.1	48.2	0.0
Grass+legume	4.2	18.9	51.6	0.0
Silage				
Grass	6.3	14.5	46.2	0.0
Corn	18.9	40.9	6.1	13.8
Hay alfalfa	4.9	18.1	23.5	25.0
Concentrates				
Barley	20.5	43.3	4.3	1.9
Corn	30.9	47.8	2.3	0.0
Oats	38.1	34.9	2.1	0.5
Wheat	17.5	55.8	4.5	0.2
Byproduct				
Gluten meal	26.7	53.0	1.4	0.0
Distillers grains	24.2	54.5	1.8	1.2
Plantseed/oils				
Soybean	23.3	54.5	5.9	1.5
Extruded soybean	19.5	53.2	9.1	0.0
Extruded cottonseed	16.5	57.4	0.0	0.0
Sunflower	21.2	69.4	0.0	0.0
Peanut	51.5	30.2	0.0	2.8
Linseed	22.7	15.4	51.4	0.0
Fish oil	21.0	2.0	1.0	32.0
Animal tallow	45.9	5.9	0.3	0.0

4. Synthesis of CLA in the Dairy Cows

In the ruminal biohydrogenation of lipid, ruminal bacteria play a key role and the formation of lipid in the rumen occurs in two important steps: The initial step is lipolysis, releasing free FAs with bacterial lipases of dietary lipids entering the rumen [26]. Another step is

biohydrogenation of FAs by rumen bacteria to produce saturated [1]. The main substrates for biohydrogenation are linoleic acid and linolenic acid. The first linoleic is rapidly converted to *c*9, *t*11 CLA in the rumen, except for linolenic acid, afterwards *c*9, *t*11 is converted to C18:1, *t*11 vaccenic acid during biohydrogenation process. C18:1, *t*11 vaccenic acid is then reduced to stearic acid as the end product. As for linolenic acid, this is transformed to C18:2 *t*11, *c*15 after that C18:2 *t*11, *c*15 is converted to C18:1, *t*11 vaccenic acid. Similarly, vaccenic acid is reduced to stearic acid (Figure 1). Both linoleic acid and linolenic acid are converted to vaccenic acid which is the common intermediate product in the rumen during biohydrogenation. Generated vaccenic acid is leaving the rumen and is absorbed across the small intestine, and incorporated into milk fat. In the mammary gland, vaccenic acid is converted to *cis*-9, *trans*-11CLA by action of the Δ -9 desaturase enzyme [27]. According to Corl et al. [28], endogenously synthesized CLA in mammary gland is about 78% of the CLA in milk fat. Therefore, the key to increasing CLA concentration in milk is to increase vaccenic acid production in the rumen [1].

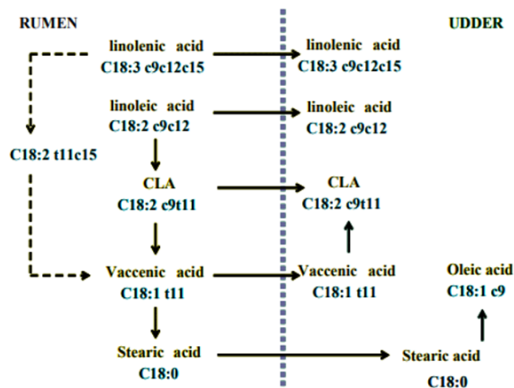


Figure 1. Simplified scheme of biohydrogenation and desaturation pathways of C18 fatty acids in rumen and udder of dairy cow [27]

5. The Feeding Regime to Increase the Content of CLA in Milk

A number of factors are known to affect the level of milk fat CLA; these are presented in Table 2. However, the dietary factors affecting the content of CLA in milk could be grouped into two categories [29]. (a) The first approach is to make dietary changes: the use of lipid sources as pasture (rich in linoleic) and vegetable fats (rich in linoleic and linolenic acid). (b) The second approach is to feed with mixtures of CLA isomers in the rumen protected. In Table 2 are shown the nutritional factors that affect CLA amount in milk fat. Dietary supplementation of plant oils (sunflower, soybean, corn, canola, linseed, and peanut) have been shown to increase CLA in milk fat due to give the greatest response plant oils high in linoleic acid [31], and this response is a dose-dependent.

In generally, ruminant diets no include the plant oils because they has potentially toxic effects on rumen microbial growth. To minimize this effect, Ca salts of the FAs is added to diet so as to bypass from rumen and only a small part are exposed to biohydrogenation. Plant oils, which is unsaturated, have been found to increase CLA in

milk fat more than saturated animal fat due to the available lipid substrate for biohydrogenation [30].

Table 2. Dietary factors that affect content of CLAs in milk fat [18, 23, 30]

Dietary factor	Content of CLA
I. Lipid substrate	
Unsaturated Plant oils	Increased type, level and dose-dependent increase
High-oil plant seeds	
Raw seeds	No effect
Processed seeds	Increased over raw seeds
Calcium salts of plant oils	Increased with increasing amounts
High-oil corn grain and silage	Minimal effect
Animal fat by-products	Minimal effect
Fish oil	Increased in relation to level fed in the diet
II. Forage:concentrate ratio	Increased with high forage diet
III. High forage diet	Increased
VI. Nonstructural carbohydrate level	Minor effect
V. Low energ diets	Probably positive
VI. Pasture related	
Pasture versus TMR	Increased with consumption of pasture
Fresh cut pasture	Higher than conserved forages
Fresh/Green	Highly positive
Pasture+ full fat extruded soybean	No effect
Pasture+Soy oil	No effect
Pasture+Fish oil	Increased
Diversity in plant species	Increased
Maturity of forage	Increased with less mature forage
Elevation of pasture	Highland>mountain>lowland
VII. CLA supplement	Dose-dependent increase

As another method, fat seeds are added to diet [21]. However, the result of researches have showed that feeding full-fed seeds have not effect on the concentration of CLA in milk fat due to unavailability by rumen bacteria responsible for biohydrogenation of the PUFA in these seeds [32].

Fish oils, containing mainly FA of 20 or 22 C as the main FA, produced to a higher CLA than an evenly of plant oils [22, 33]. A meta-analysis of comparison of averages of dry matter intake (DMI), milk yield and composition, and CLA in milk of different fat sources and processing method suggested that the best strategy to enrich milk with CLA were the combination of fish oil and vegetable fats (395 mg of *cis*-9, *trans*-11CLA/l vs. 188 mg of *cis*-9, *trans*-11 CLA/l; increase of 2.1 times) (Table 3) [34].

Data from several studies suggest that milk CLA content significantly increased in dairy cows feeding with processed seeds than feeding unprocessed seeds [33], but for extruded seeds [37]. Recent evidence suggests that

Table 3. The effect on milk yield and composition of dietary ingredient [34]

	Treatments									SEM	P-Value
	Control	Fresh Pasture	Rapeseed	Corn	Soybean	Sunflower	Linseed	Fish Oil	Fish Oil+Vegetable Fats		
Total fatty acids, g/kg DM	30.0d	25.9d	54.1ab	44.1bc	49.0ab	59.3a	55.2ab	37.1cd	45.5abc	1.78	<0.01
DMI, Kg/d	21.3ab	19.0	21.1	21.8	20.4	19.6	20.8	21.0	20.9	0.51	<0.01
Milk yield, Kg/kg	31.1a	27.0c	29.6ab	32.4a	30.6ab	28.8bc	29.2b	31.0ab	31.4ab	0.87	<0.01
Fat, g/Kg	36.1a	38.0a	34.2ab	34.4ab	33.2b	33.6b	36.5a	32.2b	31.2b	00.63	<0.01
Fat yield, Kg/d	1.11c	0.94ab	1.04ab	1.13a	1.02ab	0.94b	1.07a	1.03ab	1.01ab	0.039	<0.01
<i>cis-9,trans-11</i> CLA, g/d	0.61c	1.13ab	0.83bc	0.84bc	1.00ab	1.04ab	0.90b	0.67bc	1.34a	0.044	<0.01
<i>cis-9,trans-11</i> CLA, g/d	5.67c	8.56abc	7.78bc	8.75ab	9.24ab	10.1ab	8.50bc	5.91c	12.4a	0.399	<0.01

Menas within a row differ with treatment (p<0.05)

extrusion of oil seeds (0.57 vs. 1.11 g of CLA/100 g of FA) and oils (0.57 vs. 1.10 g of CLA/100 g of FA) are the best processing method to increase milk CLA, and but extruded seeds and oils decreased milk yield (30.4 vs. 28.9 kg/d) and milk fat (36.1 vs. 33.1 g/kg), respectively [34].

In general, high consumption of pasture shows a higher effect on CLA amount in milk fat compared with diets rich in silage, hay, concentrate feeds [14] and total mixed rations (TMR) based on conserved forage and grain [38].

Table 4. Feeding pasture versus total mixed ration (TMR) on the level of CLA in milk fat [30]

Research Location	TMR mg CLA/g fat	Pasture mg CLA/g fat
Penn State	5.4	10.9
Wisconsin	5.6	22.7

A study at Penn State and Wisconsin demonstrated that a two-fold and four-fold, respectively increase in CLA with pasture (Table 4) [30]. Previous studies have reported that grazing has contributed to the increase in CLA due to probably enables selection of leafy plant parts with higher lipid concentration.

This view is supported by Dhiman et al. [25] who writes that milk CLA content of grazing animals presented 500% greater than animals with fed with 50:50 concentrate and conserved forage diet. Previous research comparing total mixed ration (TMR), pasture + TMR and pasture plus concentrate has found that feeding pasture plus TMR and pasture plus concentrate were enhanced the CLA [30]. Similarly, a recent study by Marin et al. [39] observed that cows with more intensive grazing and

low levels of concentrate presented higher levels of CLA and omega-3 fatty acids than cows with low grazing and higher concentrate. Forage maturity is also a significant impact on CLA content. Previous research has establish that diets containing forage at less mature forage was increased milk fat CLA compared to late-growth [40].

Dietary supplements of CLA can also increase the CLA content. Chouinard et al [36] suggested that supplements of CLA isomers to dairy cow diet, mainly consisting of *cis/trans* 9, 11; *cis/trans* 10,12, and *cis/trans* 11,13, were transferred to milk fat. However, these supplements also caused a reduction in the milk fat content [14]. Therefore, it recommended that CLA isomers are protected from ruminal biohydrogenation. In other hand, as plant oils increased in diets, milk fat tended to decrease, generally so called as milk fat depression [21]. In a study on the effect of different fatty acids on the CLA content of milk, *cis-9, trans-11* CLA was higher in diets rich in linoleic acid compared with control and diets rich in linolenic acid, and lower in control compared with other diets (Table5) [34].

6. Conclusion

Cows' milk fat is the richest natural source of CLA, which is produced in the rumen and mammary gland. Milk fat is naturally included many isomers of CLA, but *c9, t11* is predominant. Diet is a key factor that could be enhanced CLA content in milk fat. Allowing dairy cows to graze pasture, vegetable fats, dietary fish oil supplementation, feeding the fat as a calcium salt and encapsulation of the CLA isomers is the best strategy to increase the CLA content in milk

Table 5. The Effect on milk yield and composition of different fatty acids. [34]

	Treatments				SEM	P-Value
	Control	Oleic acid	Linoleic acid	Linolenic acid		
Total fatty acids, g/kg DM	28.8	52.6	50.1	50.3	2.03	<0.01
DMI, Kg/d	21.1	21.0	20.2	20.7	0.55	<0.01
Milk yield, Kg/kg	30.0	30.1	30.1	28.8	0.92	<0.01
Fat, g/Kg	36.3	34.4	33.9	36.8	00.64	<0.01
Fat yield, Kg/d	1.11	1.06	1.02	1.05	0.040	<0.01
<i>cis-9,trans-11</i> CLA, g/100g fatty acids	0.62	0.82	1.00	0.83	0.044	<0.01
<i>cis-9,trans-11</i> CLA, g/d	5.79	7.82	9.66	7.54	0.390	<0.01

References

1. Badinga, L. and Miles R.D. *Adding value to milk by increasing its conjugated linoleic acid content*. AN265, one of a series of the Animal Sciences Department, UF/IFAS Extension. Original publication date July 2011. Reviewed October.
2. Benjamin, S., Prakasan, P., Sreedharan, S., Wright, A.D. and Spener, F. *Pros and cons of CLA consumption: an insight from clinical evidences*. Nutr Metab. 2015. **12**: p.4–23.
3. Du, R., Zhong, T., Zhang, W.Q., Song, P., Song, W.D., Zhao, Y., C. Wang, Tang, Y.Q., Zhang, X. and Zhang, Q. *Antitumor effect of iRGD-modified liposomes containing conjugated linoleic acid-paclitaxel (CLA-PTX) on B16-F10 melanoma*. Int J Nanomedicine. 2014. **9**: p. 3091–3105.
4. Delmonte, P., Roach, J., Mossoba, M., Losi, G. and Yurawecz, M. *Synthesis, isolation, and GC analysis of all the 6, 8-to 13, 15-cis/trans conjugated linoleic acid isomers*. Lipids. 2004. **39**: p. 185–191.
5. Pariza, M. W., Park, Y. and Cook, M. E. *The biologically active isomers of conjugated linoleic acid*. Prog. Lipid Res. 2001. **40**: p. 283–298.
6. Koba, K., Yanagita, T. *Health benefits of conjugated linoleic acid (CLA)*. Obes Res Clin Pract. 2014. **8**(6). (Abstr).
7. Mosley, E.E., Powell, G.L., Riley, M.B., Jenkins, T.C. *Microbial biohydrogenation of oleic acid to trans isomers in vitro*. Journal of Lipid Research. 2002. **43**: p. 290–296.
8. Rodriguez-Alcala, L. M., Braga, T., Xavier Malcata, F., Gomes, A., Fontecha, J. *Quantitative and qualitative determination of CLA produced by Bifidobacterium and lactic acid bacteria by combining spectrophotometric and AgC -HPLC techniques*. Food Chem. 2011. **125**: p. 1373–1378.
9. McCrorie, T.A., Keaveney, E.M., Wallace, J.M.W., Binns, N., Livingstone, M.B.E. *Human health effects of conjugated linoleic acid from milk and supplements*. NutrResRev. 2011. **24**: p. 206–227.
10. Nagpal, R., Yadav, H., Puniya A.K., Singh, K., Jain, S. and Marotta, F. *Conjugated linoleic acid: sources, synthesis and potential health benefits- an overview*. Curr Top Nutraceutical Res. 2007. **5**: p. 55-66.
11. Khanal, R.C and Olsen, K.C. *Factors affecting conjugated linoleic acid (CLA) content in milk, meat and egg: A review*. Pakistan Journal of Nutrition. 2004. **3**(2): p. 82-98.
12. Grummer, R.R. *Effect of feed on the composition of milk fat*. J Dairy Sci. 1991. **74**: p.3244–3257.
13. Gottardo, P., Penasab, M., Righic, F., Lopez-Villalobos, N., Cassandro, M., De Marchi, M. *Fatty acid composition of milk from Holstein-Friesian, Brown Swiss, Simmental and Alpine Grey cows predicted by mid-infrared spectroscopy*. Italy J AnimSci. 2017. **16**(3): p. 380–389.
14. Harvatine, K.J., Boisclair, Y.R., Bauman, D.E. *Recent advances in the regulation of milk fat synthesis*. Animal. 2009. **3**: p. 40-54.
15. Glasser, F., Schmidely, R., Sauviant, D., Doreau, M. *Digestion of fatty acids in ruminants: a metaanalysis of flows and variation factors: 2. C18 fatty acids*. Animal. 2008. **2**: p. 691-704.
16. Delmonte, P., Roach, J., Mossoba, M., Losi, G. and Yurawecz, M. *Synthesis, isolation, and GC analysis of all the 6, 8-to 13, 15-cis/trans conjugated linoleic acid isomers*. Lipids. 2004. **39**: p. 185–191.
17. Samková, E., Spicka, J., Pesek, M., Pelikánová, T., Hanus, O. *Animal factors affecting fatty acid composition of cow milk fat: a review*. S Afr J Anim Sci. 2012. **42**: p. 83-100.
18. Bauman, D.E., Perfield, J.W.I., Harvatine, K.J. and Baumgard, L.H. *Regulation of fat synthesis by conjugated linoleic acid: lactation and the ruminant model*. J Nutr. 2008. **138**: p. 403–409.
19. Bhattacharya, A., Banu, J., Rahman, M. *Biological effects of conjugated linoleic acid in health and disease*. J Nutr Biochem. 2006. **17**: p. 789-810.
20. Park, Y. and Pariza, M.W. *Mechanisms of body fat modulation by conjugated linoleic acid (CLA)*. Food Res Int. 2007. **40**: p. 311-323.
21. Bauman, D.E., Baumgard, L.H., Corl, B.A., Griinari, J.M. *Biosynthesis of conjugated linoleic acid in ruminants*. J Anim Sci. 1999. p. 1-15.
22. Elgersma, A., Wever, A.C., Naęcz-Tarwacka, T. *Grazing versus indoor feeding: effects on milk quality*. Grassland Science in Europe. 2006. **11**: p.419-427.
23. Kalac, P. and Samková E. *The effects of feeding various forages on fatty acid composition of bovine milk fat: A review*. Czech J Anim Sci. 2010. **12**: p. 521–537.
24. Boufaied, H., Chouinard P.Y., Tremblay, G.F., Petit, H.V., Michaud, R., Belanger G. *Fatty acids in forages. I. Factors affecting concentrations*. Can J AnimSci. 2003. **83**: p. 501-511.
25. Dhiman, T., Nam, S. and Ure, A. 2005. *Factors affecting conjugated linoleic acid content in milk and meat*. Crit Rev Food Sci Nutr. 2005. **45**(6): p. 463–482.
26. Dawson, R.M., Hemington, N. and Hazlewood, G.P. *On the role of higher plant and microbial lipases in the ruminal hydrolysis of grass lipids*. Br J Nutr. 1977. **38**: p. 225-232.
27. Bauman, D. and Griinari, J. *Nutritional regulation of milk fat synthesis*. Annu Rev Nutr. 2003. **23**: p. 203–227.
28. Corl, B.A., Baumgard, L.H., Dwyer, D.A., Griinari, J.M., Phillips, B.S., and Bauman, D.E. *The role of delta(9)-desaturase in the production of cis-9, trans-11 CLA*. J Nutr Biochem. 2011. **12**: p. 622–630.
29. Whitlock, L.A., Schingoethe, D.J., AbuGhazaleh, A.A., Hippen, A.R. and Kalscheur, K.F. *Milk production and composition from cows fed small amounts of fish oil with extruded soybeans*. J Dairy Sci. 2006. **89**: p. 3972–3980.
30. Muller, L., Delahoy. *Conjugated linoleic acid (CLA) in animal production and human health*. Penn State Extension. [cited 2018 05 March]; Available from: <https://extension.psu.edu/conjugated-linoleic-acid-cla-in-animal-production-and-human-health>.

31. Kelly, M.L., Berry J.R., Dwyer, D.A., Griinari, J.M., Chouinard, P.Y., Van Amburgh, M. E. and Bauman D. E. *Dietary fatty acid sources affect conjugated linoleic acid concentrations in milk from lactating dairy cows.* J Nutr. 1998. **128**: p. 881-885.
32. Khanal, R.C and Olsen, K.C. *Factors affecting conjugated linoleic acid (CLA) content in milk, meat and egg: A review.* Pak J Nutr. 2004. **3(2)**: p. 82-98.
33. Chouinard, P.Y., Corneau, L., Bauman, D.E., Butler, W.R., Chilliard, Y. and Drackley, J.K. *Conjugated linoleic acid content of milk from cows fed different sources of dietary fat.* J Dairy Sci. 1998. **81**(Suppl. 1): p. 233 (Abstr.).
34. Siurana, A., Calsamiglia, S. *A meta analysis of feeding strategies to increase the content of conjugated linoleic acid (CLA) in dairy cattle milk and the impact on daily human consumption.* Anim Feed Sci Technol. 2016. **217**:p 13–26.
35. Ward, A.T., Witlenberg, K.M., Froebe, H.M., Pryzbyiski, R and Malcolmson, L. *Fresh forage and solin supplement on conjugated linoleic acid levels in plasma and milk.* J Dairy Sci. 2003. **86**: p. 1742-1750.
36. Siurana, A. and Calsamigli, A. *Metaanalysis of feeding strategies to increase the content of conjugated linoleic acid (CLA) in dairy cow milk and the impact on daily human consumption.* Anim Feed Sci Technol. 2016. **217**: p. 13-26.
37. Chouinard, P.Y., Corneau, L., Barbano, D.M., Metzger, L.E. and Bauman, D. E. *Conjugated linoleic acids alter milk fatty acid composition and inhibit milk fat secretion in dairy cows.* J Nutr. 1999. **129**:p. 1579-1584.
38. Dhiman, T.R., Anand, G.R., Satter, L.D. and Pariza, M.W. *Conjugated linoleic acid content of milk from cows fed different diets.* J Dairy Sci. 1999. **82**: p. 2146-2156.
39. Marina, M. P., Meléndez, P. G., Aranda, P. and Ríos, C. *Conjugated linoleic acid content and fatty acids profile of milk from grazing dairy cows in southern Chile fed varying amounts of concentrate.* J Appl Anim Res. 2018. **46**(1): p. 150–154.
40. Chouinard, P.Y., Corneau, L., Kelly, M.L., Griinari, J.M. and Bauman D.E. *Effect of dietary manipulation on milk conjugated linoleic acid concentrations.* J Dairy Sci. 1998. **81**(Suppl. 1): p. 233 (Abstr.).



Research Article

Convective hot air drying characteristics of selected vegetables

Eda Elgin Kılıç^a  and İnci Çınar^{b,*} ^a Gaziantep University, Naci Topçuoğlu Vocational School, Department of Food Processing, Gaziantep/Turkey^b Kahramanmaraş Sütçü İmam University, Faculty of Engineering and Architecture, Department of Food Engineering, Kahramanmaraş/Turkey

ARTICLE INFO

ABSTRACT

Article history:

Received 31 July 2018

Revised 31 October 2018

Accepted 27 November 2018

Keywords:

Drying models

Hot air drying

Natural convection

Rate constant

Thin layer drying

Vegetable

The objectives of the present work were to investigate and to model the convective hot air-drying characteristics of carrot, zucchini and eggplant at different drying air temperatures (60, 70 and 80 °C). Drying characteristics were determined by the plot of moisture loss of samples versus drying time in 10 min intervals for each drying air temperatures. The experimental moisture data were then fitted to selected thin layer drying models available in the literature, namely Henderson and Pabis, Newton and the two-term models and good agreements between experimental and predicted values of moisture contents were observed ($R^2 > 0.98$). Results showed that all drying took place in falling rate period for all samples at all drying air temperatures studied. Increase in drying air temperature from 60 °C to 80 °C resulted in a decrease of total drying time 35%, 45% and 50% for carrot, zucchini and eggplant respectively. Drying rate constants (a , b , k , k_0 and k_1) increased with the increasing drying air temperature. Comparison between experimental and predicted values of moisture content versus drying air temperature indicated that the most suitable models for carrot, zucchini and eggplant drying were two-term, Henderson and Pabis and Newton respectively at 60 °C, two-term, Henderson and Pabis and Newton model at 70 °C and two-term, Henderson and Pabis and Newton model at 80 °C drying air temperature respectively.

© 2019, Advanced Researches and Engineering Journal (IAREJ) and the Author(s).

1. Introduction

Turkey has a significant potential for fruit and vegetable production and export. Proper climate conditions along with other factors enable vegetable production in almost all regions. Being non-homogenous and porous in nature, fresh vegetables are highly perishable due to high water content in their structure and therefore long-term storage is impossible without being processed for preservation [1]. In this case, preservation technique plays an important role in terms of nutritional and economical losses. Removing the excess water from structure of vegetables can be possible through drying process.

Drying, for this matter, is one of the oldest preservation methods that is used to preserve fruits and vegetables. Drying is an important method to prolong the storage period by lowering deteriorative quality changes of the fruits and vegetables. Drying of foods requires high energy input and energy share in industrial usage is nearly 15% [2]. Drying, in terms of thermal processing,

involves simultaneous mass and heat transfer and therefore accuracy of spatial and temporal distribution of temperature and moisture of food depends highly on effective diffusivity [3].

During drying, the food is in contact with the surrounding hot air and therefore its temperature increases towards to dry bulb temperature as drying proceeds. In the initial period of hot air drying, moisture (un-bounded water) is transferred from the center of the food to the surface by diffusion and surface evaporation is observed while heat is transferred from the surface of the food to the center mainly by conduction as temperature of the food increases. Rate of moisture transfer to surface compensates the rate of evaporation from the surface and surface of food remains wet and wet bulb temperature is observed until the critical moisture level is reached. From this critical moisture point on, surface starts to dry out, dry patches on the surface is observed and temperature raises to dry bulb temperature [4], [5].

* Corresponding author. Tel.: +90 344 300 2087

E-mail addresses: edakilic@gantep.edu.tr (E.E.Kılıç), icinar@ksu.edu.tr (İ. Çınar)

ORCID: 0000-0002-9887-8377 (E.E.Kılıç), 0000-0002-7715-7423 (İ. Çınar)

Water removal from food to be dried is based on convective, conductive and radiative transfer of heat. In convective drying, the required heat to remove water is carried by a heated air. The hot air passes through the food and exits from the drier continuously during the process. Depending on the nature of the dried food material, the use of this technique needs different machinery and equipment. Cabin dryers, tunnel dryers, fluid bed dryers and spray dryers constitute common types of dryers used in air drying technique [6]. Air temperature and air flow rate are an important parameters in convective hot air drying. Drying behavior of food materials, drying costs and effects of drying parameters on nutritional and sensorial properties of foods are better determined by the use of empirical, semi-empirical and theoretical mathematical models that originate from Fick's law of diffusion and Fourier law [2].

In the literature, large number of studies investigating the drying behavior of food products both experimentally and numerically concentrate on the factors affecting drying behavior of the food namely drying air temperature, humidity, speed and pretreatment application [7]. During the drying process of the foods, thin layer drying models are frequently preferred with the aim of determining the moisture content which varies with time as seen in Table 1. Thin layer drying models are models developed to explain the change in moisture content over time during the drying of foods. The thin layer drying models usually cover describing drying process in agricultural materials fall into three categories [8], namely theoretical, semi-theoretical and empirical [9], [10] whereas theoretical models take into account internal resistances to moisture transfer and external influences between food and its environment are taken into account in semi-theoretical and empirical models [11]. The semi-theoretical models gave closer approaches in describing drying curves than the theoretical models and therefore were used more frequently in the literature.

There are many studies in the literature describing the drying behavior of food both experimentally and mathematically. Younis et.al. [12] studied garlic slices, Rushan and Mengeş [13] potatoes, Rabha et.al. [14] bitter pepper, Silva et.al. [15] banana, Aregbesola et.al. [16] hazelnut, Hasan et.al. [17] mushrooms, Alibaş [18] artichoke, Lee and Kim [19] onion slices and Kaya and Aydın [20] experimentally investigated the behavior of the apples.

The aim of this study to investigate and to model the convective hot air drying characteristics of carrot, zucchini and eggplant determined by the plot of moisture loss of samples versus drying time at different drying air temperatures (60 °C, 70 °C and 80 °C) and goodness of the fit was compared with the regression coefficients (R^2) of mathematical models (Newton, Henderson and Pabis, Two terms).

2. Materials and Methods

2.1 Material

In this study, carrot, zucchini and eggplant purchased from local markets in Gaziantep were used as research

Table 1. Thin layer drying models used in food drying.

Model name	Model	Reference
Newton	$MR = \exp(-kt)$	(21)
Page	$MR = \exp(-ktn)$	(22)
Henderson and Pabis	$MR = a \exp(-kt)$	(23)
Logarithmic	$MR = a \exp(-kt) + b$	(24)
Midilli	$MR = a \exp(-ktn) + bt$	(9,25)
Wang and Singh	$MR = 1 + at + bt^2$	(11)
Two Term	$MR = a \exp(-kt) + b \exp(-k_1t)$	(26)

material. The selected vegetables for drying experiments were free of impurities and stored at the refrigerator temperature (4 ± 0.5 °C) until they were analyzed.

2.2. Method

2.2.1. Preparation of samples

The selected vegetables were cut into 0.5 cm x 0.5 cm x 0.5 cm cubes before drying and prepared in three parallels for each drying experiment.

2.2.2. Drying experiments

In order to determine the effect of drying air temperature on drying kinetics, drying was carried out at natural convective conditions using drying air temperatures of 60 °C, 70 °C and 80 °C. To determine the variations of moisture content of carrot, eggplant and zucchini samples over time during drying experiments, moisture losses in certain time periods were measured. Drying process was carried out in laboratory type NÜVE brand FN 500 model drying oven at three different temperatures (60, 70 and 80) °C and with three parallels in natural convective conditions. During the drying process the water losses of the samples were determined with periods of 10 min. For this purpose, the samples taken from the drying cabinet were weighed with an accuracy of 0.0001 g on an AY-220 model analytical precision scale of Shimadzu brand.

2.2.3. Determination of moisture content

The moisture contents of the samples prepared for the determination of drying behavior during drying at different temperatures under natural convective drying conditions are calculated by Equation (1):

$$M_t = \frac{(m - KM)}{KM} \quad (1)$$

where:

M_t : the moisture content at anytime (g water / g dry matter)

m : the weight of sample at the time of t (g)

KM : the amount of dry matter of sample.

2.2.4. Determination of the equilibrium moisture content

In order to determine the equilibrium moisture content of materials at the drying temperatures, the difference between the two sample weighed was continued until the difference was less than 0.01g. The equilibrium moisture

content (M_e) was determined from the weight difference where the difference between the weights is negligible.

2.2.5. Calculation of dimensionless moisture content

The dimensionless humidity ratio frequently used in model equations and were given by Equation (2) [27] as follows:

$$MR = \frac{M_t - M_e}{M_0 - M_e} \quad (2)$$

where:

MR: moisture ratio(dimensionless),

M_t : the moisture content at anytime (g water / g dry matter),

M_e : the moisture content at the equilibrium (g water / g dry matter),

M_0 : the initial moisture content (g water / g dry matter).

2.3. Modeling of Drying

Thin layer drying methods were used to explain drying characteristics of fruits and vegetables and three semi theoretical models namely Newton, Two-term, Henderson and Pabis models were used for modelling of the drying kinetics at different drying temperatures.

2.3.1. Newton model

Newton model, which is one of the most used models to explain the drying kinetics of foods was given by Equation (3) [28] as:

$$MR = \exp(-kt) \quad (3)$$

where:

k: drying constant (min^{-1}),

t: drying time (min).

2.3.2. Henderson and Pabis model

Henderson and Pabis model was given in Equation (4) [23] as:

$$MR = a \exp(-kt) \quad (4)$$

where:

a: the coefficient of Henderson and Pabis model (unitless),

k: drying constant (min^{-1}),

t: drying time (min).

2.3.3. Two Term model

The two-term model equation was given in Equation (5) as suggested by Babalis et.al. [26] as follows:

$$MR = a \exp(-k_0 t) + b \exp(-k_1 t) \quad (5)$$

where:

k_0 and k_1 : Drying constant (min^{-1}),

a: the coefficient of the two-term model (unitless),

b: the coefficient of the two-term model (unitless),

t: drying time (min) .

2.4. Mathematical Modeling of Drying Curves

In this study, experimental non-dimensional humidity-drying time change data were used for modeling studies by regression analysis methods. The experimental dimensionless moisture content curves were applied to the thin layer drying models given in Table 2.1 below and the drying constants (k , k_0 , k_1), model constants (a , b) and regression coefficients (R^2) were determined by regression analysis. Sigma Plot 10.0 was used for regression analysis. The regression coefficient is the most important parameter that determines model suitability according to previous studies [29].

Table 2. Selected thin layer drying models for drying experiments.

Model Name	Model Equation	Reference
Newton	$MR = \exp(-kt)$	[30].
Hendersonand Pabis	$MR = a \exp(-kt)$	[23].
Two Term	$MR=a.\exp(k_0.t)+b.\exp(-k_1.t)$	[26].

3. Result and Discussion

Convective hot air drying is a process of simultaneous transfer of mass (moisture removal from the surface of the food material being dried) and heat (from the hot air to the surface of the food). Mass transfer is in the direction from center of the food to surface meanwhile heat is transferred from the surface of the food through the center by conduction. Drying experiments is carried on the determine optimum drying conditions for the specific food and operation.

Convective hot air drying characteristics of selected vegetables that are commonly used industrial food materials in hot air drying of foods namely eggplant, zucchini and carrot were studied for three different drying air temperatures (60 °C, 70 °C and 80 °C) as used in commercial driers. Convective hot air drying were conducted under natural convection conditions.

The results were expressed as the dimensionless moisture ratio that was builded from the resulting weight loss data. Plots from dimensionless moisture ratio to drying time were indicated that all drying experiments were proceeded in falling rate period and constant rate period was not observed for carrot, eggplant and zucchini samples. The total drying time for carrot, eggplant and zucchini decreased by 35%, 50% and 45% respectively when drying air temperature was increased from 60 °C to 80 °C. The drying times providing %50 reduction of the dimensionless moisture ratio at three different drying air temperatures studied were 150 min, 100 min, 90 min for carrot samples, 50 min, 40 min, 30 min for eggplant samples and 150, 80, min for zucchini samples, respectively. It has been determined that the increase in drying air temperature in all samples also resulted in an increase in the evaporation rate of the water from the surface of the vegetables as determined by moisture ratio, shortened the drying time and time to reach equilibrium moisture content was shorter as seen in Figure 1.

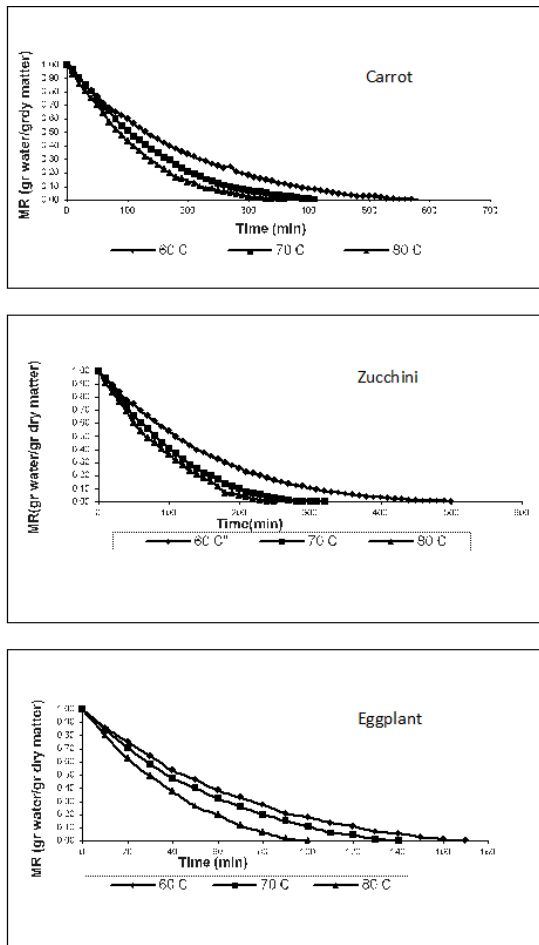


Figure 1. Change in dimensionless moisture ratios of carrot, eggplant and zucchini samples at different drying air temperatures.

Thin layer drying models are frequently used in the literature to design and optimize the hot air drying of food materials. Although they are empirical or semi-empirical in nature or consider some negligible changes in some model parameters, these models usually show considerably good agreements with the experimental data and fairly easy to use as compared to the models originate from the laws of thermodynamics. Therefore, experimental values of drying experiments were then fitted into the selected thin layer drying models from the literature and the goodness of the fit were determined by regression analyses of the selected models. Regression analyses were performed by the comparison between the experimental and predicted data obtained from drying models. Regression coefficients (R^2) and the drying rate constants namely a , b , k_1 and k_0 were calculated as seen in Table 3. Depending on the results, drying rate constants were increased with increasing drying air temperature.

Based on the data from regression analyses Newton, Henderson and Pabis, Two Terms dryer models were determined to be suitable in describing

experimental data of drying carrot, eggplant and zucchini at different drying air temperatures in the range of 60 to 80 °C. Comparisons of experimental and predicted model curves of dimensionless moisture ratio versus drying time at different drying temperatures were given in Figure 2. Each of the three thin layer drying models used was suitable for describing the experimental data obtained at different temperatures. R^2 regression coefficient value is found high ($R^2 > 0,98$) for each samples dried at different temperatures.

4. Conclusion

In this experimental study, drying kinetics of vegetables (eggplant, zucchini, carrot) were investigated as a function of drying conditions. In convective drying, which occurs at different temperatures in the laboratory type dryer, drying time is shortened as drying air temperature increases for all samples. Different drying behaviors were observed as respect to the drying air temperature. Henderson and Pabis, Newton and the two-term models were in good agreements between experimental and predicted values of moisture contents ($R^2 > 0,98$). Results showed that all drying took place in falling rate period for all samples at all drying air temperatures studied. Increase in drying air temperature from 60 to 80 °C resulted in a decrease of total drying time 35%, 45% and 50% for carrot, zucchini and eggplant respectively. Drying rate constants (a , b , k , k_0 and k_1) increased with the increasing drying air temperature. Comparison between experimental and predicted values of moisture content versus drying air temperature indicated that the most suitable models for carrot, zucchini and eggplant drying were Two-term, Henderson and Pabis and Newton respectively at 60 °C, Two-term, Henderson and Pabis and Newton model at 70 °C and Two-term, Henderson and Pabis and Newton model at 80 °C drying air temperature respectively.

Table 3. The results of regression analyses of carrot,eggplant, zucchini samples at different drying air temperatures.

	Drying Air Temperature (°C)	Newton		Two Terms		Henderson and Pabis	
		Model Coefficient	R ²	Model Coefficients	R ²	Model Coefficients	R ²
Carrot	60	8.7879E-005	0.9921	a=0.5255 k ₀ =9.0265E-005 b=0.5021 k ₁ =9.0266E-005	0.9930	a=1.0227 k=9.0266E-005	0.9930
	70	0.0001	0.9918	a= 0.5387 k ₀ =0.0001 b=0.5042 k ₁ =0.0001	0.9936	a=1,0430 k=0.0001	0.9936
	80	0.0001	0.9875	a=0.5234 k ₀ =0.0001 b=0.5366 k ₁ =0.0001	1.0000	a=1.0600 k=0.0001	0.9912
Eggplant	60	0.0003	0.9911	a=0.5062 k ₀ =0.0003 b=0.5526 k ₁ =0.0003	1.000	a=1.0289 k=0.0003	0.9921
	70	0.0003	0.9873	a= 0.5315 k ₀ =0.0003 b=0.5064 k ₁ =0.0003	0.9892	a=1,0379 k=0.0003	0.9892
	80	0.0004	0.9820	a=0.5359 k ₀ =0.0005 b=0.5057 k ₁ =0.0005	0.9844	a=1.0417 k=0.0005	0.9844
Zucchini	60	0.0001	0.9929	a=0.5158 k ₀ =0.0001 b=0.5275 k ₁ =0.0001	1.000	a=1.0433 k=0.0001	0.9948
	70	0.0002	0.9846	a= 0.5592 k ₀ =0.0002 b=0.5088 k ₁ =0.0002	0.9893	a=1.0622 k=0.0002	0.9833
	80	0.0002	0.9790	a=0.5222 k ₀ =0.0002 b=0.5400 k ₁ =0.0002	1.0000	a=1.0622 k=0.0002	0.9833

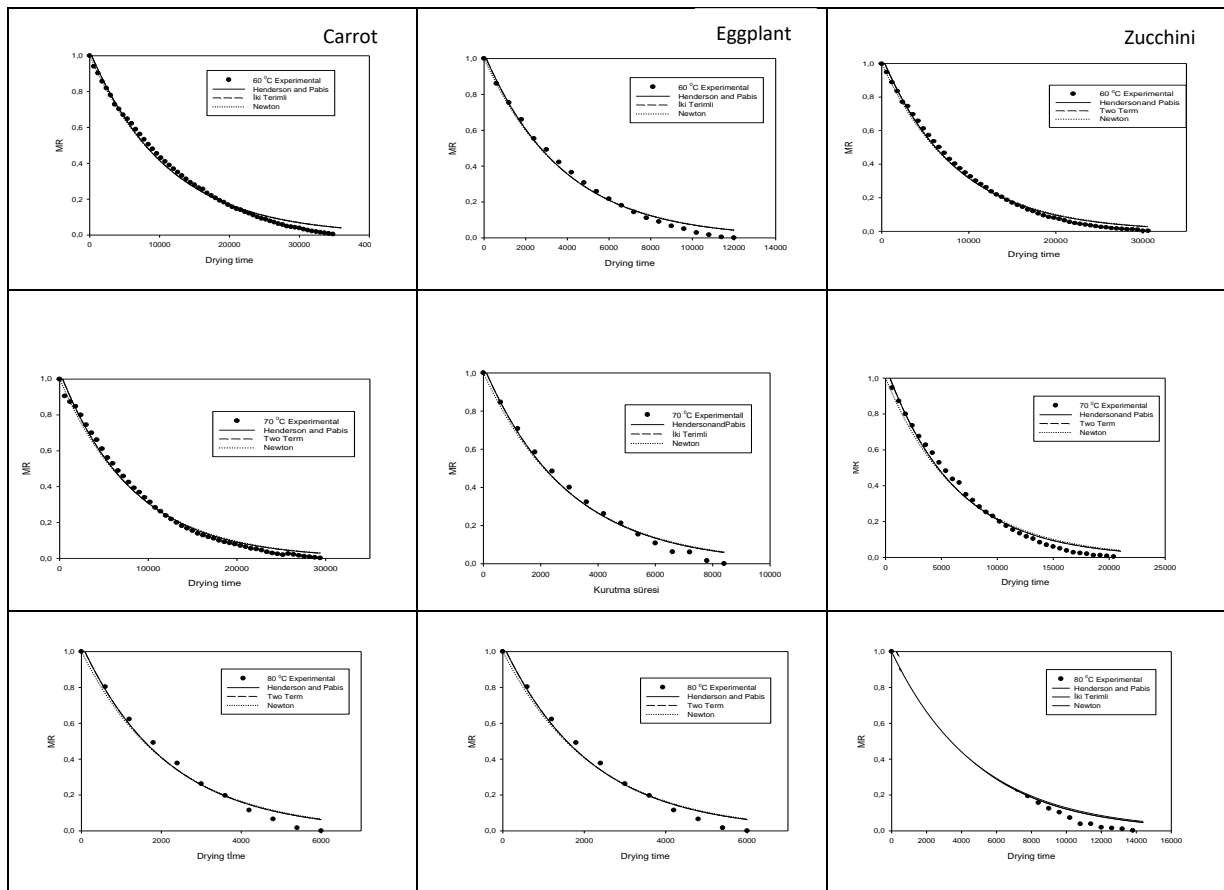


Figure 2. Comparisons of experimental and predicted thin layer model curves of carrot, eggplant and zucchini samples seen in columns respectively at different drying air temperatures.

References

- Aprajeeta, J., Gopirajah, R., Anandharamkrishnan, C. *Shrinkage and Porosity Effects on Heat and Mass Transfer During Potato Drying*, 2015. *Journal of Food Engineering*, 144:119-128.
- Perussello, C.A., Kumar, C., Castilhos, F., Karim, M.A. *Heat and Mass Transfer Modelling of the Osmoconvective Drying of Yacon Roots (Smallanthus sonchifolius)*, 2014. *Applied Thermal Engineering*, 63:23-32.
- Agrawal, S., Methekar, R.N. *Mathematical Model for Heat and Mass Transfer During Convective Drying of Zucchini*. *Food and Bioprocess Technology*, 2017. 101:68-73.
- Zang, M., Bhandari, B., Fang, Z. *Handbook of Drying of Vegetables and Vegetable Products*. CRC Press, 2017. (ISBN: 9781498753869-CAT#K27375), 538p.
- Krokida, M. K., Karathanos, V. T., Maroulis, Z.B. and Marinos-Kouris, D. *Drying Kinetics Of Some Vegetables*. *Journal Of Food Engineering*, 2003.59: 391-403.
- Cemeroğlu, B., Karadeniz, F., Özkan, M. *Meyve ve Sebze İşleme Teknolojisi, Bölüm: Kurutma Teknolojisi*. Gıda Teknolojisi Derneği Yayınları, 2003.28:541-675.
- Carlescu, P.M., Arsenoiaia, V., Roşca, R., Tenu, I. *CFD Simulation of Heat and Mass Transfer During Apricots Drying*. *LWT-Food Science and Technology*, 2017. 85:479-486.
- Akpinar, E.K., Bicer, Y. *Modelling of the drying of eggplants in thin-layers*. *International Journal of Food Science and Technology*, 2006 40 (3), 273–281.
- Midilli, A., Küçük, H., Yapar, Z. *Single Layer Drying*. *Drying Technology*, 2002 20(7):1503-1515.
- Panchariya, P.C., Popovic, D. and Sharma, A.L. *Thin-Layer Modeling of Black Tea Drying Process*. *Journal of Food Engineering*, 2002. 52:349-357.
- Özdemir, O., Devres, Y.O. *The Thin Layer Drying Characteristics of Hazelnuts During Roasting*. *Journal Of Food Engineering*, 1999 42:225-233.
- Younis, M., Abdelkarim, D., El-Abdein, A. *Kinetics and Mathematical Modeling of Infrared Thin-Layer Drying of Garlic Slices*. *Saudi Journal of Biological Sciences*, 2018.25: 332-338.
- Ruhanian, S., Movagharnejad, K. *Mathematical Modeling and Experimental of Potato Thin -Layer Drying in an Infrared -Convective Dryer*. *Engineering in Agriculture, Environment and Food*, 2016. 9, 84-91.
- Rabha, D.K., Muthukumar, P., Somayaji, C. *Experimental Investigation of Thin Layer Drying Kinetics Of Ghost Chilli Pepper (Capsicum Chinense Jacq.) Dried in A Forced Convection Solar Tunnel Dryer*. *Renewable Energy*. 2017. 105:583-589.
- Silva, W.P., Silva, C.M.D.P.S., Gama, F.J.A., Gomes, J.P. 2014. *Mathematical Models to Describe Thin-Layer Drying and to Determine Drying Rate of Whole Bananas*. *Journal of the Saudi Society Of Agricultural Sciences*, 2014. 13:67-74.

16. Aregbesola, O.A., Ogunsina, B.S., Sofolahan, A.E., Chime, N.N. *Mathematical Modeling Of Thin Layer Drying Characteristics Of dika (Irvingia gabonensis) nuts and kernels*. Nigerian Food Journal, 2015. 33, 83-89.
17. Hasan, A.A.M., Bala, B.K., Rowshon, M.K. *Thin Layer Drying of Hybrid Rice Seed*. Engineering in Agriculture, Environment and Food, 2014 7:169-175.
18. Alibaş, İ. *Sıcak Havayla Kurutulan Enginar (Cynara cardunculus L. Var. Scolymus) Dilimlerinin Kuruma Eğrilerinin Tanımlanmasında Yeni Bir Modelin Geliştirilmesi ve Mevcut Modellerle Kıyaslanması*. U. Ü. Ziraat Fakültesi Dergisi, Cilt, 2012. 26, sayı 1, 49.
19. Lee, H.J., Kim, J.H. *Drying Kinetics Of Onion Slices In A Hot –Air Dryer*. Journal Of Food Science And Nutrition, 2008. 13:225-230.
20. Kaya, A., Aydın, O. *Drying Kinetics of Red Delicious Apple*. Biosystems Engineering, 2007. 96(4):517 -524.
21. Erentürk, S., Gulaboglu, M.S., Gültekin, S. *The Thin Layer Drying Characteristics Of Rosehip*. Biosystems Engineering, 2004. 89(2), 159-166.
22. Aghbashlo, M., Kianmehr, M.H., Arabhosseini, A. *Modelling of Thin Layer Of Potato Slices In Length of Continous Band Dryer*. Energy Conversation An Management, 2009. 50, 1348-1355.
23. Singh, N. J., Pandey, R.K. *Convective Air Drying Characteristics Of Sweet Potato*, Food and Bioproducts Processing, 2012. 90:317-322.
24. Toğrul, İ., Pehlivan, D. *Modelling of Drying Kinetics Of Single Apricot*. Journal Of Food Engineering, 2003. 58:23 32.
25. Evin, D. *Thin Layer Drying Kinetics Of Gundelia tournefortii L*. Food And Bioproduct Processing, 2012. 90:323-332.
26. Babalis, S., Papanicolaou, E., Kyriakis, N., Belessiotis, V. *Evaluation Of Thin Layer Drying Models For Describing Drying Kinetics Of Figs*. Journal Of Food Engineering, 2006. 75, 205-214.
27. Karathanos, V.T. *Determination Of Water Content Of Dried Fruits By Drying Kinetics*. Journa Of Food Engineering, 1999. 39,337-344.
28. Tunde-Akintunde, Y. Ajala, A. *Air Drying Characteristics Of Chilli Pepper*. International Journal of Food Engineering, 2010. 58: 2, 13-32.
29. Sarsavadia, P. N., Sawhney, R. L., Pangavhane, D. R., & Singh, S. P. *Drying behaviour of brined onion slices*. Journal of Food Engineering, 1999 40, 219–226
30. Arıcı R. Ç., Mengeş, O. *Mantarın (Agaricus Bisporus) Kontrollü Sartlar Altında Kurutma Karakteristiklerinin Belirlenmesi Ve Kuruma Davranışının Modellenmesi*. Selçuk Üniversitesi, Selçuk Tarım Ve Gıda Bilimleri Dergisi, 2012. 26(1): 84-91.



Research Article

Evaluation of some agronomical characteristics and essential oil ratio of coriander (*Coriandrum sativum* L.) cultivars cultivated by applying different humic acid doses

Hanifi Cinarlidere ^a  and Belgin Cosge Senkal ^{a,*} 

^aBozok Universit, Faculty of Agriculture Engineering, Department of Field Crops, Yozgat, 66900,Turkey

ARTICLE INFO

Article history:

Received 02 March 2018
Revised 25 December 2018
Accepted 13 January 2019

Keywords:

Coriandrum sativum L.
Essential oil ratio
Humic acid
Seed yield

ABSTRACT

Coriander (*Coriandrum sativum* L.) is grown as a spice crop all over the World. Its essential oil is used as a flavor ingredient, but it also has a long history as a traditional medicine. Coriander essential oil and extracts possess promising antibacterial, antifungal and anti-oxidative activities as various chemical components in different parts of the plant, which thus play a great role in maintaining the shelf-life of foods by preventing their spoilage. This study was conducted to investigate the effects of different humic acid doses on some agronomical characteristics and essential oil ratio of coriander in Yozgat ecological condition at Research and Application Area of Gedikhasanlı, Faculty of Agriculture, Yozgat Bozok University during 2015-2016. Two coriander cultivars (Arslan and Gurbuz) and different humic acid doses (Dose-1: Control, Dose-2:100 L ha⁻¹, Dose-3:200 L ha⁻¹, and Dose-4: 300 L ha⁻¹) were used in the study. Spring and winter sowings were made on April 17, 2015 and on October 29, 2015, respectively. According the results of this study; the main values in plant height, number of branches per plant, number of umbel per plant, number of seed per umbel, first branch height, a thousand seed weight, biological yield, seed yield, stalk yield, harvest index, essential oil ratio, and yield were recorded as 39-77 cm, 3-5 number, 5-17 number, 21-52 number, 15-23 cm, 8-16 g, 1000-5900 kg ha⁻¹, 300-2300 kg ha⁻¹, 600-3700 kg ha⁻¹, 30-75%, 0.2-0.5%, and 60-800 L ha⁻¹, respectively. While values obtained from winter sowing are higher than spring sowing. The best results were obtained from cv. Arslan and 100-200 L ha⁻¹ humic acid doses.

© 2019 Advanced Researches and Engineering Journal (IAREJ) and the Author(s).

1. Introduction

Coriander (*Coriandrum sativum* L.) is an essential oil and spice plant cultivated throughout the world [1]. Coriander is belonging to the genus *Coriandrum* of the Apiaceae family. The native land of cultivated coriander plant is not fully known. However, it is cultivated in the Mediterranean countries, Southwest Asia and North Africa [2]. *Coriandrum* L. genus is represented by two species of flora in Turkey. These are *Coriandrum sativum* L. and *Coriandrum tordylium* (Fenzl) Bornm. When cultivating Coriander, 2 varieties of *Coriandrum sativum* L. are used: These are *Coriandrum sativum* L. *vulgare* Alef. (large seeded varieties) and *Coriandrum sativum* L. var. *microcarpum* D.C. (small seeded varieties) is known

as coriander [3].

Commercially used parts of the plant are fresh green leaves, ripe dried fruits (or seeds) and essential oil from these seeds. The use of coriander seeds relates to the chemical composition. The most important components of the seed are essential oil and fatty oil. The essential oil ratio of mature and dried seed varies between 0.03% and 2.6%, while the fatty oil varies between 9.9% and 27.7% [4]. Linalool (68%), α -pinene (11%), γ -terpinene (9%), geranylacetate (4%), camphor (3%), and geraniol (2%) are main components of the essential oil from coriander seeds [5]. Linalool is used as a raw material in the advanced technical processing stages while the commercial used oil is widely used by mixing sweet

* Corresponding author. Tel: +90 354 242 10 28 / 4462

E-mail addresses: h.cinarlidere@hotmail.com (H. Cinarlidere), belgin.senkal@bozok.edu.tr (B. Cosge Senkal)
ORCID: 0000-0003-3984-2937 (H. Cinarlidere), 0000-0001-7330-8098 (B. Cosge Senkal)

orange oil, cedar wood oil, terementi and anethol or anise oil [6].

Humic substances are natural organic materials which have colloidal properties in soils, lakes, rivers and waters and are the most common distribution in nature [7]. Soil humic substances play an important role directly and indirectly in the development of plants [8]. Studies have shown that humic acid has positive effects on plant growth [9], it was observed that plant growth was positive effect in low amount humic acid application (0.6-60 pmm) and negative effect in high amount one [10], also, humic acid increased plant dry weight, plant phosphorus concentration and useful phosphorus concentration in the soil [11].

The aim of this study was investigate the effects of spring and winter sowing times and the humic acid applied at different times and doses on some agricultural characteristics and essential oil content of coriander (*Coriandrum sativum* L.), a medicinal and aromatic plant.

2. Material and Method

2.1 Material

In this study, Arslan (large seeded) and Gurbuz (small seeded) coriander cultivars registered by the Ankara University, Faculty of Agriculture, Field Crops Department and humic acid with a commercial name of Phila-22 (Table 1) was used.

2.2 Method

The study was carried out in Application Area of Gedikhasanlı, Faculty of Agriculture, Yozgat Bozok University during 2015-2016. In the experimental area, total rainfall, mean relative humidity and temperature in 2015 and 2016 were recorded to be 554.2 mm and 421.5 mm, 64.45% and 63.16%, and 11.7 °C and 10.04 °C, respectively. According to the results of soil taken from 0-20 cm depth from the experiment area; the soil was loamy (46.31%), poor in organic matter (1.47%), lime content was low (4.04%), slightly alkaline (pH:7.67), phosphorus (P_2O_5) content (58.3 kg ha⁻¹) is low, but is rich in potassium (K_2O) (794.8 kg ha⁻¹).

The cultivars used in this study were sown in 40 cm row spacing and 3 m row length on April 17, 2015, in spring, and October 29, 2015, in winter. Experiment was established randomized complete design in split plot arrangements with three replications by using two cultivars as main plots and humic acid treatments (Dose-1: control, Dose-2: 100 L ha⁻¹, Dose-3: 200 L ha⁻¹, Dose-4: 300 L ha⁻¹) as split plots (Figure 1). After germination of the sown seeds, weed control and humic acid application were performed as needed during the growing season. Humic acid was diluted with water at a rate of 1/10 and the plants which are about 10-15 cm high were given in the designed doses and after each application, the soil was mixed by hoeing. Harvest was made by hand on August 15, 2015 in

spring sowing and on July 27, 2016 in winter sowing. In harvested plants, plant height (cm), first branch height (cm), number of branches per plant, number of umbrellas per plant, number of seeds per umbrella, a thousand seed weight (g), seed yield (kg ha⁻¹), stem yield (kg ha⁻¹), biological yield (kg ha⁻¹), harvest index (%), essential oil ratio (%) and essential oil yield (L ha⁻¹) were determined.

100 g of seed was ground from each parcel and 500 mL of water was added. The distillation was carried out using a Clevenger apparatus for 3h to determine the essential oil content (w/w).

The differences between the averages of the characters examined in the statistical evaluation of the results were grouped according to the Duncan test. SPSS 23 package program was used for statistical analysis.

Table 1. Commercial humic acid content used in the experiment

Content	W/W
Total Organic Matter (%)	36
Total Nitrogen (N) (%)	1.5
Organic Nitrogen (%)	1
Total Humic + Fulvic Acid (%)	22
Water Soluble Potassium Oxide (K_2O) (%)	4
pH	4-6

3. Results and Discussion

According to research findings (Table 2); plant height was found to be between 39.40 cm (cv. Arslan, Dose-3, spring sowing) and 77.00 cm (cv. Gurbuz, Dose-2, winter sowing) and the plants grown in winter sowing were longer than those grown in spring sowing. When previous studies were examined, plant height ranged from 37.75 cm to 120 cm [12-14]. In our study, the number of branches per plant was higher in winter sowing than spring sowing. The average number of branches per plant varied from 3 to 5. It has been stated that cultural factors such as sowing time, fertilization, irrigation and climatic factors and genetic characteristics have been effective on the number of branches per plant [13-15].

The number of umbrella per plant was between 5.13 (cv. Gurbuz, Dose-2, in spring sowing) - 16.33 (cv. Arslan, Dose-3, winter sowing) and the number of umbrella in winter sowing was higher than that of spring sowing. The number of seeds in the umbrella was 21.33 (cv. Arslan, Dose-3, spring sowing) and 51.33 (cv. Arslan, Dose-3, winter sowing). In the studies carried out, the number of umbrella per plant was found between 5 and 100, and it was changed according to ecological factors and cultural processes applied [13-18]. The number of seeds in the umbrella was determined between 15 and 22.85 seeds in previous studies. In our study, the value from the winter sowing was higher than ones from the other studies, but it has values close to the average in spring sowing [15, 17, 19].

Table 2. Performance of coriander cultivars (Arslan and Gurbuz)

Humic Acid Doses (L ha ⁻¹)	Plant height (cm)						Number of branches per plant (number)					
	Winter Sowing			Spring Sowing			Winter Sowing			Spring Sowing		
	Arslan	Gurbuz	Mean	Arslan	Gurbuz	Mean	Arslan	Gurbuz	Mean	Arslan	Gurbuz	Mean
Control	64.33	76.33	70.33	43.33	45.80	44.55	4.33	3.67	4.00	3.20	3.60	3.40
100	68.33	77.00	72.66	41.87	42.07	41.97	3.50	5.00	4.25	3.53	3.33	3.43
200	73.00	63.67	68.30	39.40	48.67	44.05	4.67	4.00	4.33	3.40	3.73	3.56
300	71.67	66.00	68.83	43.87	43.13	43.50	5.00	4.67	4.83	3.60	3.83	3.75
Mean	69.33	70.75	70.03	42.15	44.95	43.51	4.29	4.33	4.35	3.45	3.65	3.55
Humic Acid Doses (L ha ⁻¹)	Number of seeds per umbrella (number)						Biological yield (kg ha ⁻¹)					
	Winter Sowing			Spring Sowing			Winter Sowing			Spring Sowing		
	Arslan	Gurbuz	Mean	Arslan	Gurbuz	Mean	Arslan	Gurbuz	Mean	Arslan	Gurbuz	Mean
Control	51.33	41.33	46.33	22.00	26.33	24.15	3979.7	477.0.3	437.5.0	1126.7	1526.2	1326.5
100	45.66	46.00	45.83	23.33	24.67	24.00	4133.0	508.0.2	460.6.6	1069.3	1183.8	1126.5
200	51.33	45.66	50.00	21.33	23.67	22.50	4312.0	417.5.7	424.3.8	1002.9	1484.3	1246.8
300	44.33	41.33	42.83	23.67	23.33	23.50	5872.0	326.5.3	456.8.6	1263.6	1205.3	1234.4
Mean	48.16	43.58	46.24	22.55	24.50	23.55	4574.1	432.2.8	444.8.5	1115.5	1349.9	1233.5
Humic Acid Doses (L ha ⁻¹)	Stem yield (kg ha ⁻¹)						First branch height (cm)					
	Winter Sowing			Spring Sowing			Winter Sowing			Spring Sowing		
	Arslan	Gurbuz	Mean	Arslan	Gurbuz	Mean	Arslan	Gurbuz	Mean	Arslan	Gurbuz	Mean
Control	2340.3	3226.3	2783.3	696.7	1154.3	925.5	22.33	16.00	19.16 ^a	17.00	15.00	16.00
100	2408.9	3496.5	2952.7	678.7	843.6	761.5	15.67	20.00	17.83 ^a	14.13	19.00	16.55
200	2728.9	2896.3	2812.6	690.3	1107.7	899.0	12.33	13.67	13.00 ^b	13.00	18.07	15.55
300	3628.3	2172.3	2900.3	864.3	896.3	880.3	16.00	15.00	15.50 ^{ab}	16.73	17.67	17.20
Mean	2776.6	2947.8	2862.2	732.5	1000.5	866.5	16.58	16.16	16.37	15.25	17.45	16.35
Humic Acid Doses (L ha ⁻¹)	Number of umbrellas per plant (numbers)						Seed yield (kg ha ⁻¹)					
	Winter Sowing			Spring Sowing			Winter Sowing			Spring Sowing		
	Arslan	Gurbuz	Mean	Arslan	Gurbuz	Mean	Arslan	Gurbuz	Mean	Arslan	Gurbuz	Mean
Control	16.00	8.67	12.33	5.93	6.13	6.03	1639.7	1543.6	1591.6	430.5	381.9	406.2
100	15.00	13.67	14.33	5.93	5.13	5.53	1739.0	1595.3	1667.1	391.3	340.7	366.0
200	16.33	11.00	13.66	6.93	6.53	6.73	1583.0	1279.0	1431.0	312.7	378.3	345.5
300	15.67	13.66	14.66	6.60	6.13	6.35	2243.3	1093.0	1668.1	399.7	309.0	354.5
Mean	15.75	11.75	13.74	6.35	5.98	6.16	1801.2	1377.7	1589.4	383.5	352.5	368.5
Humic Acid Doses (L ha ⁻¹)	Harvest index (%)						A thousand seed weight (g)					
	Winter Sowing			Spring Sowing			Winter Sowing			Spring Sowing		
	Arslan	Gurbuz	Mean	Arslan	Gurbuz	Mean	Arslan	Gurbuz	Mean	Arslan	Gurbuz	Mean
Control	41.68	32.77	37.22	74.03	62.07	68.05	14.45	9.02	11.73	14.57	9.07	11.82
100	41.94	31.13	36.53	70.57	65.43	68.00	12.93	8.90	10.91	14.93	10.13	12.53
200	38.29	30.03	34.16	68.95	61.97	65.46	13.17	9.03	11.10	14.37	9.87	12.12
300	38.50	32.57	35.53	67.07	64.72	65.85	13.89	8.94	11.40	15.04	10.17	12.65
Mean	40.10 ^a	31.62 ^b	35.86	70.15	63.55	66.84	13.61 ^a	8.97 ^b	11.28	14.75 ^a	9.81 ^b	12.28
Humic Acid Doses (L ha ⁻¹)	Essential oil ratio (%)						Essential oil yield (L ha ⁻¹)					
	Winter Sowing			Spring Sowing			Winter Sowing			Spring Sowing		
	Arslan	Gurbuz	Mean	Arslan	Gurbuz	Mean	Arslan	Gurbuz	Mean	Arslan	Gurbuz	Mean
Control	0.40	0.33	0.36	0.24	0.18	0.21 ^b	647.3	511.3	579.3	98.7	69.7	84.2
100	0.43	0.38	0.41	0.26	0.20	0.23 ^{ab}	720.3	593.4	659.8	96.7	62.7	79.7
200	0.43	0.33	0.38	0.28	0.23	0.25 ^a	650.7	468.3	559.5	78.3	79.8	79.5
300	0.36	0.44	0.40	0.30	0.23	0.26 ^a	778.8	500.7	639.7	106.7	63.8	85.5
Mean	0.40	0.37	0.38	0.25	0.21	0.25	69.9.2	518.4	609.5	95.1	69.0	82.1

* The difference between the meanings indicated in different letters in the same column is statistically significant.

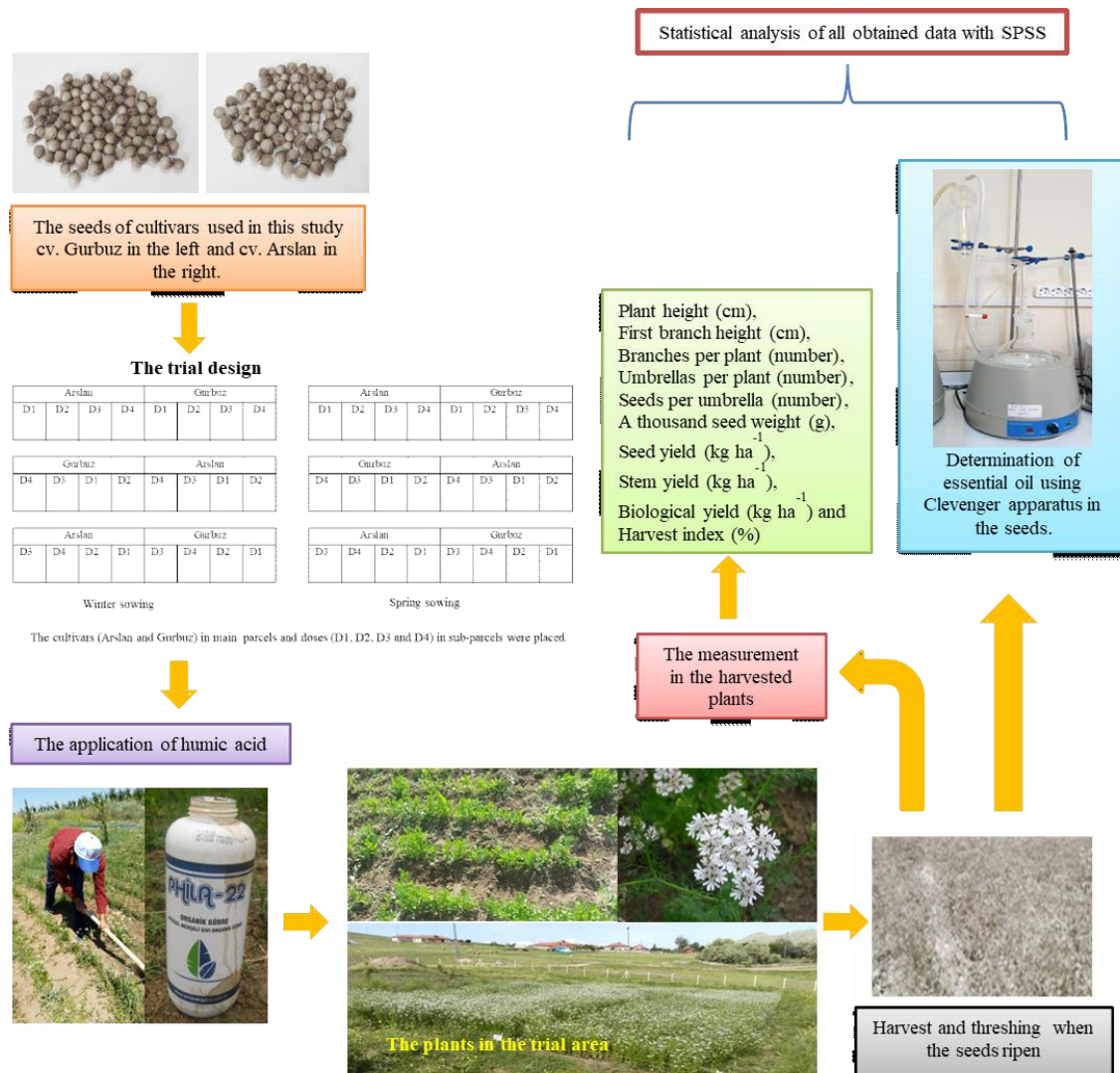


Figure 1. Schematic presentation of the all applications in this study.

The biological yield values obtained from two different cultivars were between $1002.9 \text{ kg ha}^{-1}$ (cv. Arslan, Dose-3, spring sowing) – $5872.0 \text{ kg ha}^{-1}$ (cv. Arslan, Dose-4, winter sowing) and the biological yield of winter sowing was higher than that of spring sowing. Our findings obtained from this study are similar to those reported by [5, 13, 15-17, 20]. Seed yield was recorded between 309.0 kg ha^{-1} (cv. Gurbuz, Dose-4, spring sowing) and $2243.3 \text{ kg ha}^{-1}$ (cv. Arslan, Dose-4, winter sowing). The values obtained from our study were in agreement with those obtained from other studies ($450.8\text{-}3591.3 \text{ kg ha}^{-1}$) [5, 12-14, 2, 22]. The stalk yield values obtained from coriander varieties were found at 678.7 kg ha^{-1} (cv. Arslan, Dose-2, spring sowing) – $3628.3 \text{ kg ha}^{-1}$ (cv. Arslan, Dose-4, winter sowing). The first branch height was between 13.00 cm (cv. Arslan, Dose-3, spring sowing) - 22.33 cm (cv. Arslan, Dose-1, winter sowing). In our study, the first branch height was found higher in winter and spring sowings than the other studies [23]. In our study, the harvest index was between 30.03% (cv. Gurbuz, Dose-3, winter sowing) and 74.03% (cv.

Gurbuz, Dose-1, spring sowing), many researchers found similar findings with the harvest index (8.6%-117.54%) of coriander [13, 15, 17, 23]. A thousand seed weight were obtained between 8.90 g (cv. Gurbuz, Dose-2, winter sowing) - 15.04 g (cv. Arslan, Dose-4, spring sowing). In the previous studies conducted, the lowest one thousand seed weight was determined as 5.03 g and the maximum value was determined as 19.88 g [12-20, 22, 24, 25]. In our study, essential oil ratio obtained from mature seed and essential oil yield were respectively; 0.18% (cv. Gurbuz, Dose-1, spring sowing) - 0.43% (cv. Arslan, Dose-2 and Dose-3, winter sowing); 62.7 L ha^{-1} (cv. Gurbuz, Dose-2, spring sowing) – 778.8 L ha^{-1} (cv. Arslan, Dose-4, winter sowing). In different studies, the essential oil ratio of coriander seeds were reported as 0.27-0.60% by Gök [19], 0.26-0.36% by Tunçtürk [25], 0.35% by Bahadırılı et al. [26], 0.32-0.71% by Yalçın [27], and 0.23-0.39% by Beyzi and Güneş [28]. Generally, findings related essential oil ratio were found within these limits with many studies (0.18%-0.77%) [5, 12-16, 18, 22, 24, 25, 29, 30]. According to other studies,

essential oil yield was recorded as 0.61 L ha⁻¹ and the highest was 16.5 L ha⁻¹. In our study, the essential oil yield of the mature seed was higher in winter and summer sowings than in other studies [12, 15, 18, 19, 21, 24, 31]. According to our study, four humic acid doses applied showed statistically significant effects on the first branch height and the essential oil ratio. Dose-2 and Dose-3 for the essential oil ratio and Dose-1 and Dose-2 for the first branch height showed the highest effect. Soil humic substances play an important direct and indirect role in the development of plants. Indirect effects are the uptake of water-soluble forms by water retention, drainage, aeration, and formation of chelating compounds or metallic-hydroxides with metallic ions. Direct effects in plants are promoting root development of the plant and the metabolism of nutrient elements absorbed by plants [32]. For the positive effects of humic acid to occur, it has to be applied to the same field for several years [33]. Due to the fact that the study was carried out for a single year, no significant effect of humic acid on the investigated properties was observed. According to our findings, the yield of winter sowing was higher than that of spring sowing. The reason for this is that the vegetation during in winter sowing is longer, the root structure of the plant is better developed and there are more favorable environmental conditions for plant growth. At the same time it is known that the genotype has a great effect on the yield and yield components obtained from the plants.

3. Conclusion

Soil humic substances play an important role (water retention, drainage, solubility of some nutrients, encouraging plant root growth etc.) in the development of plants. It must be applied to the same soil for several years in order to reveal these effects of humic acids. Due to the fact that our study was only single year, humic acid had no significant effect on the properties examined. According to the findings of this study, it was observed that winter sowing has more yield than spring sowing. This is due to the fact that winter sowing has a longer vegetation period, better development of the plant root structure and more favorable environmental conditions for plant growth. It is also known that genotype has a great effect on yield and yield components obtained from plants. Arslan and Gurbuz cultivars were sown in spring and winter in Yozgat ecological conditions, and the highest seed yield, essential oil ratio and essential oil yield were obtained from the winter sowing of the cv. Arslan. For Yozgat and similar ecologies, we can recommended the winter sowing of cv. Arslan and doses of 100-200 L ha⁻¹ of humic acid containing 36% of total organic matter, 1.5% of total nitrogen (N), 1% of organic nitrogen, 22% of total humic and fulvic acid, water soluble Potassium Oxide (K₂O) value with 4% and pH 4-6.

Acknowledgment

This study was prepared from Master Thesis conducted by Yozgat Bozok University, The Graduate School of Natural and Applied Sciences, Department of Field Crops, Yozgat, Turkey.

References

1. Başer, K.H.C., *Tıbbi aromatik bitkilerin endüstriyel kullanımı*. Anadolu Üniversitesi Tıbbi ve Aromatik Bitki ve İlaç Araştırma Merkezi, TAB Bülteni, 1998. **13-14**: p. 19-43.
2. Baytop, T., *Türkçe bitki adları sözlüğü*. Türk Dil Kurumu Yayınları, Ankara, Türkiye, 1994, 578: p. 508.
3. Zeybek, N. and Zeybek, U., *Farmasötik Botanik*. Ege Üniversitesi Eczacılık Fakültesi, İzmir, Türkiye, 1994, 2-436.
4. Diederichsen, A., *Promoting the conservation and use of underutilized and neglected crops 3 coriander*, 1996. Institute of Plant Genetics and Crop Plant Research. Gatersleben/ International Plant Genetic Resources Institute, ISBN. 92-9043-284-5.
5. Yamanol, A., *Kışniş (Coriandrum sativum L.)'nin farklı ekim zamanı ve tohumluk miktarının agronomik ve teknolojik özellikleri üzerine etkisi*. Yüksek Lisans Tezi, Ege Üniversitesi, Fen Bilimleri Enstitüsü, 1996.
6. Bhatnagar, S.S., *Coriandrum Linn. (Umbelliferae)*. A Dictionary of Indian Raw Materials and Industrial Research, New Delhi, 1950. p. 455-461.
7. Andriessse, J.P., *Nature and Management of Tropical Peats*. FAO Soils Bulletin 59. 1998. FAO, Rome. ISBN:92-5-102657-2: p.165.
8. Lobartini, J.C., Orioli, G.A. and Tan, K.H., *Characteristics of soil humic acid fractions separated by ultrafiltration*. Communication in Soil Science and Plant Analyses, 1997. **28**:p.787-796.
9. Siviero, P., Sandei, L., and Colombi, A., *Results of applying leonardite and humic acids to processing tomatoes*. Informarore Agrario, 1996. **52**: p. 57-60.
10. Kononova, M.M., *Soil organic matter, its nature, its role in soil formation and soil fertility*. 1961. Pergamon Press Ltd. Lib. Oxford.
11. Sözüdoğru, S., Kütük, A.C., Yalçın, R. and Usta, S., *Humik asidin fasulye bitkisinin gelişimi ve besin maddeleri alımı üzerine etkisi*. Ankara Üniversitesi, Ziraat Fakültesi, Ankara, Türkiye, 1996, 1452.
12. Karaca, A., *Kışniş ve rezene bitkilerinde fenolojik, morfolojik ve bazı teknik özellikler üzerinde çalışmalar*. Yüksek Lisans Tezi, Odokuz Mayıs Üniversitesi, Fen Bilimleri Enstitüsü, 1998.
13. Kaya, N., Yılmaz, G. and Telci, İ. *Farklı Zamanlarda Ekilen Kışniş (Coriandrum sativum L.) Populasyonlarının Agronomik ve Teknolojik Özellikleri*. Turkish Journal of Agriculture, 2000. **24**: p. 355-364.
14. Özcan, R., *Seçilmiş kışniş (Coriandrum sativum L.) hatlarının verim ve verim öğeleri üzerine bir araştırma*. Yüksek Lisans Tezi, Ankara Üniversitesi, Fen Bilimleri Enstitüsü, 2001.
15. Kandemir, K., *Farklı azot dozu ve sıra aralığının kışnişin verim ve verim unsurları üzerine etkisi*. Yüksek Lisans Tezi, Ordu Üniversitesi, Fen Bilimleri Enstitüsü, 2010.
16. Kızıl, S. and İpek, A., *Bazı Kışniş (Coriandrum sativum*

- L.) hatlarında farklı sıra arası mesafelerinin verim, verim özellikleri ve uçucu yağ oranı üzerine etkileri. Tarım Bilimleri Dergisi, 2004. **10**: p. 237-244.
17. Okut, N. and Yıldırım, B., *Effect of different row spacing and nitrogen doses on certain agronomik characteristic of coriander (Coriandrum sativum L.)*. Pakistan Journal of Biological Sciences, 2005. **8**(6): p. 901-904.
 18. Özel, A., Güler, İ. and Erden, K. *Harran Ovası koşullarında farklı ekim zamanlarının kişniş (Coriandrum sativum L.)'in verim ve bitkisel özelliklerine etkisi*. HR.Ü. Ziraat Fakültesi Dergisi, 2009. **13**(4): p. 41-48.
 19. Gök, N., *Farklı zamanlarda ekilen kişniş (Coriandrum sativum L.) çeşitlerinin verim ve kalite özelliklerinin belirlenmesi*. Yüksek Lisans Tezi, Yüzüncü Yıl Üniversitesi, Fen Bilimleri Enstitüsü, 2011.
 20. Uzun, A., Özçelik, H. and Özden, Y.G., *Orta Karadeniz Bölgesi için geliştirilen kişniş (Coriandrum sativum L.) çeşitlerinin bazı tarımsal özelliklerinin belirlenmesi, verim ve uçucu yağ oranının stabilite analizi*. GOÜ, Ziraat Fakültesi Dergisi, 2010. **27**: p. 1-8.
 21. Gül, Ö., *Kişniş (Coriandrum sativum L.)'de farklı ekim sıklığının verim ve uçucu yağ oranı üzerine etkisi*. Yüksek Lisans Tezi, Çukurova Üniversitesi, Fen Bilimleri Enstitüsü, 1995.
 22. Kan, Y. and İpek A., *Kişniş (Coriandrum sativum L.) verim ve bazı özellikleri*. 2002. 14. Bitkisel İlaç Hammaeddeleri Toplantısı, Eskişehir, ISBN: 975-94077-2-8.
 23. Karaca, A. and Kevseroğlu, K., *Kişniş (Coriandrum sativum L.) ve Rezene (Foeniculum vulgare Mill.) Bitkilerinde Bazı Önemli Fenolojik, Morfolojik Özellikler Üzerine Bir Araştırma*. Türkiye 4. Tarla Bitkileri Kongresi, Tekirdağ, 2001, 243-248.
 24. Gergerli, B., *Harran Ovası koşullarında kişniş (Coriandrum sativum L.)'de uygun ekim zamanının belirlenmesi*. Yüksek Lisans Tezi, Harran Üniversitesi, Fen Bilimleri Enstitüsü, 2002.
 25. Tunçtürk, R., *Kişniş (Coriandrum sativum L.) çeşitlerinde değişik ekim mesafelerinin verim ve kalite üzerine etkisi*. Yüzüncü Yıl Üniversitesi, Tarla Bitkileri Dergisi, 2011. **21**(2): p. 89-97.
 26. Bahadır , N.P., Türkmen, M. and Mert, A., *Hatay koşullarında yetiştirilen aşotu (Coriandrum sativum L.) bitkisinin uçucu yağ oranlarının ve içeriklerinin belirlenmesi*. Biyoloji Bilimleri Araştırma Dergisi, 2016. **9** (2): p.20-22.
 27. Yalçın, Z., *Bazı kişniş genotiplerinin (Coriandrum sativum L.) Erzurum ekolojik koşullarında verim ve başlıca tarımsal özellikleri*. Yüksek Lisans Tezi, Atatürk Üniversitesi, Fen Bilimleri Enstitüsü, 2016.
 28. Beyzi, E. and Gunes, A., *Kişniş (Coriandrum sativum L.) Bitkisinin Uçucu Yağ Bileşenleri Üzerine Bor Uygulamasının Etkileri*. Gaziosmanpaşa Üniversitesi Ziraat Fakültesi Dergisi, 2017. **34**(1):p.146-152.
 29. Demircan, F., *Kişniş (Coriandrum sativum L.) de sıra arası mesafesinin verim ve kaliteye olan etkisi*. Yüksek Lisans Tezi, Ege Üniversitesi, Fen Bilimleri Enstitüsü, 1997.
 30. Ravi, R., Prakash, M. and Keshava Bhat, K., *Aroma karakterizasyon of coriander (Coriandrum sativum L.) oil sampels*. European Food Research and Technology, 2007. **225**: p. 367-374.
 31. Kırıcı, S., Mert, A. and Ayanoglu, F., *Hatay ekolojisinde azot ve fosforun kişniş (Coriandrum sativum L.) verim değerleri ile uçucu yağ oranlarının etkisi*. II. Tarla Bitkileri Sempozyumu. Samsun, 1997, 347-351.
 32. Lobartini, J.c., Orioli, G.A. and Tan, K.H., *Characteristic of soil humic acid fractions sparated by ultrafiltration*. Communications in Soil Science and Plant Analysis, 1997. **28**(9-10): p. 787-796.
 33. Ergönül, U., *Ayçiçeği (Helianthus annuus L.) çeşitlerine uygulanan humik asit ve leonardit'in verim, verim öğeleri üzerine etkileri*. 2011. Yüksek Lisans Tezi, Ankara Üniversitesi, Fen Bilimleri Enstitüsü, 2011.



Research Article

Production of red fluorescent protein (mCherry) in an inducible *E. coli* expression system in a bioreactor, purification and characterization**Hülya Kuduğ^{a,*} , Bahadır Ataman^a , Rizvan İmamoğlu^b , Duygu Düzgün^a and İsa Gökçe^a** ^a Tokat Gaziosmanpaşa University, Department of Genetic and Bioengineering, Tokat, 60250, Turkey^b Bartın University, Department of Biotechnology, Bartın, 74110, Turkey

ARTICLE INFO

Article history:

Received 01 June 2018

Revised 20 September 2018

Accepted 24 September 2018

Keywords:

Bioreactor

E. coli

Fluorescent proteins

mCherry

pBAD

ABSTRACT

New and improved genetic engineered variants of fluorescent proteins (FPs) have become useful tools for bioimaging in biomedical researches. Red fluorescent proteins (RFPs) first derived from the sea anemone *Discosoma* show high performance *in vivo* labeling and imaging. mCherry is a member of RFPs which has very high photostability, resistant to photo bleaching and rapid maturation. These advantages ensure that mCherry can be successfully fused to many proteins and widely used for quantitative imaging techniques. In this study, the constructed recombinant plasmid pBADCherry was expressed in *Escherichia coli* BL21(AI) then culture conditions, inducer concentration and induction time were optimized. Results of sodium dodecyl sulfate polyacrylamide gel electrophoresis (SDS-PAGE) analysis demonstrated that 5 hours induction at 0.04% of arabinose concentration was optimal for the highest mCherry yield. The expression of hexa histidine-tagged (6xHis) recombinant mCherry was induced by arabinose and purification performed using nickel (Ni²⁺) affinity chromatography. High throughput expression of 81 mg fluorescent protein from a liter of *E. coli* culture carried out in bioreactor.

© 2019 Advanced Researches and Engineering Journal (IAREJ) and the Author(s).

1. Introduction

The story of fluorescent proteins began with discover of green fluorescent protein (GFP) from the bioluminescent jellyfish *Aequorea victoria* [1]. After cloning of GFP and demonstration applications in living cells it has become an important tool for fluorescent labeling in molecular and cell biology [2]. GFP and its variants in different colors have developed into a unique tool for visualization of living cells and organisms. Fluorescent proteins (FPs) are used in a variety of applications for structural studies especially in labeling of proteins, nucleic acids, organelles and organisms. On other respects functional studies such as protein-protein interactions, development of biosensors, production of reactive oxygen species (ROS), drug screening can be carried out using FPs. Mutagenesis studies on production of new versions FPs have led to improve properties of

these proteins as brightness, photostability, maturation rate, oligomerization and performance in fusion labeling [3].

Since discovery of original GFP from jellyfish the broad range of FPs characterized from other organisms (e.g. hydrozoans, corals, anemones) that emit in the yellow-orange to far-red regions of the visible light spectrum [4-6]. Fluorescent proteins with red, orange and far-red emitting fluorescence are assessable quality for multicolor imaging experiments. These proteins have been isolated mostly from corals of class Anthozoa and have longer excitation wavelengths that give advantages for lower phototoxicity and deeper penetration in tissue.

Oligomerization, non-specific localization, interactions with undesired proteins and aggregation are main restrictive results for fusion applications of oligomeric FPs. Non-*Aequorea* FPs are not naturally monomeric,

* Corresponding author. Tel.: +0356 252 16 16 (2839)

E-mail address: hulya.kudug@gop.edu.tr (H. Kuduğ), ataman84@gmail.com (B. Ataman), rizvanimamoglu@gmail.com (R. İmamoğlu), dzgn_duygu@hotmail.com (D. Düzgün), isa_gokce@yahoo.co.uk (İ. Gökçe)

ORCID: 0000-0003-0365-2760 (H. Kuduğ), 0000-0002-8782-2706 (B. Ataman), 0000-0002-6306-4760 (R. İmamoğlu), 0000-0002-5998-8397 (D. Düzgün), 0000-0002-5023-9947 (İ. Gökçe)

they have mostly dimeric or tetramer structure in nature and are not suitable intracellular expression and labeling. Artificial monomerization of these proteins has resulted decrease in performance so hydrophobic surfaces engineered monomeric FPs has been interested recently [7-9].

The first monomeric red fluorescent protein mRFP1 derived from the Indo-Pacific sea anemone, *Discosoma sp.* tetrameric red fluorescent protein, DsRed (Figure 1) has limitations including brightness, chromophore maturation and fast photo bleaching [10,11]. Direct mutagenesis targeting chromophore residues has yielded a series of mRFP1 known as 'mFruits'. mCherry is the best red member in mFruit family which has brightness level is ~75% of EGFP, respectively. mCherry is a 28.8 kDa monomer with 256 amino acids and derived from DsRed. The protein exhibits emitting light in the range of wavelength 610 nm that makes it suitable for multiple labeling. It gives results in a short time during imaging experiments due to the rapid maturation period after transcription. High photostability and other advantages make mCherry presently the most widely used monomeric RFP [11,12].

Recent studies reported that the *araBAD* promoter system in *Escherichia coli* (*E. coli*) performs to manipulate the yield of desired protein induced by L-arabinose added in culture medium [13-16]. The *araBAD* promoter enables to manipulate of the transcriptional rates of the soluble recombinant protein expression levels [17,18].

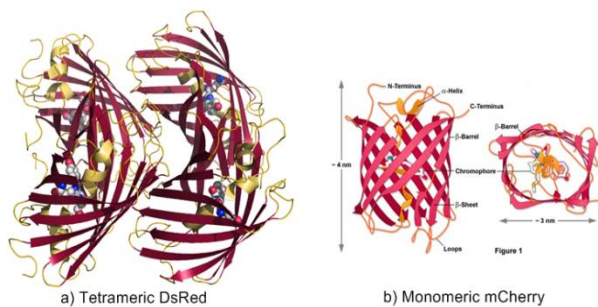


Figure 1. Structure of wild-type tetrameric RFP, DsRed (a) and monomeric RFP, mCherry (b) [9].

Expression systems based on *araBAD* promoter (P_{araBAD}) use for control of expression in *E. coli* which can be induced by external inducer [19]. pBAD system has been designed for high level expression of interested gene(s) that can be induced by arabinose [20,21]. pBAD offers tightly regulated expression resulted in high protein yields, dose-dependent induction for modulating expression levels and optimization of soluble protein expression [14] Besides expression under an effective promoter, cultivation of recombinant *E. coli* cells in bioreactor gives the yield in high level with maximum

cell productivity [22,23].

In this study, we investigated the use of pBAD promoter system to express of red fluorescent protein mCherry. We optimized the inducer concentration and induction time to maximize expression level. The performance for the highest productivity studied in bioreactor. Besides the yield of recombinant mCherry had been purified and characterized. This method provides rapid, practical, cost-effective and high efficient production of soluble mCherry that can be used for further biomedical researches.

2. Material and Method

2.1. Recombinant mCherry vector backbone

The backbone of the mCherry plasmid was pBAD expression system and had ampicillin resistance gene (*bla*). pBADCherry was a gift from Michael Davidson & Roger Tsien (Addgene plasmid #54630). The mCherry coding sequence was cloned into N-terminal backbone with a hexa histidine-tag is shown in Figure 2. The pBADCherry vector contains 708 nucleotides that encoded insert mCherry was transformed into competent *E. coli* DH5 α . The transformed cells were grown overnight at 37°C in LB plates containing 100 μ g/mL ampicillin. Plasmid purification from 5 mL LB culture performed using EZ-10 Spin Column Plasmid DNA Miniprep Kit (Biobasic).

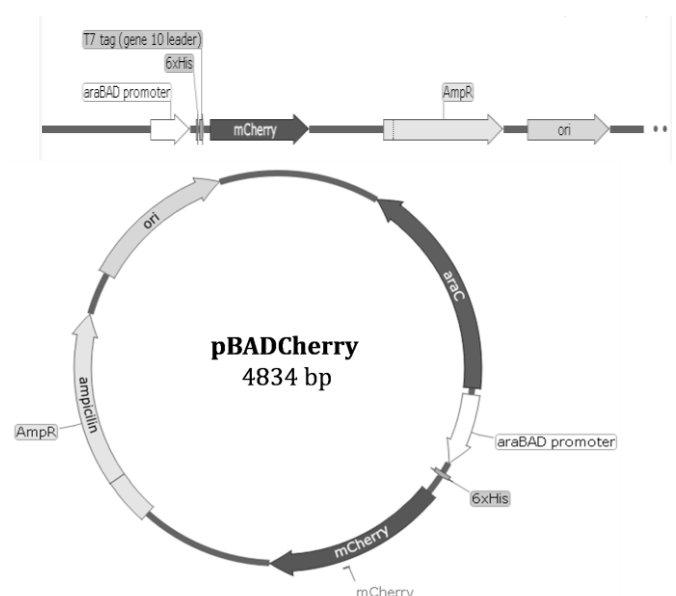


Figure 2. The construction of the pBADCherry plasmid

2.2. Expression of mCherry

High efficiency chemically competent *E. coli* BL21 (AI) cells transformed with recombinant plasmid pBADCherry by heat shock. LB agar containing ampicillin (100 μ g/ml) was utilized as a selective medium for transformants of *E. coli* cells. A single colony from the agar was inoculated into 5 mL LB and cultured at

37°C and 200 rpm overnight in shaking incubator. Glycerol stocks of the transformed cells were made by mixing 1:1 ratio of the overnight culture with 30% (w/v) sterilized glycerol solutions and stored at -80°C. *E. coli* cells carrying any insert were grown as negative control. The preculture was centrifugated at 5000 rpm for 5 min and the pellet was resuspended in fresh medium.

2.3. Optimization of expression of mCherry

Culture parameters (inducer concentration and induction time) were varied to investigate optimal conditions. Initially, small scale in flask contains 50 mL LB used for optimization before large scale protein production. The resuspended culture was inoculated in LB flasks at a ratio of 1:100 and was grown at 37°C until OD₆₀₀ was reached 0.6. Bacterial cultures were then induced with varying concentrations (0.002, 0.004, 0.006, 0.008, 0.01, 0.02, 0.04 and 0.2 %) of arabinose and grown for another 5 hours at 37°C.

The effect of induction time on mCherry expression was investigated. Cultures that induced with the optimum inducer concentration were withdrawn induction at different time (1, 2, 3, 4, 5 and 6 h) intervals. Equal volume from each sample (20 µl) was analyzed by 12% SDS-PAGE.

2.4. Cultivation in bioreactor

The overnight culture of *E. coli* strain BL21(AI) that transformed with a pBADCherry plasmid was inoculated (1%) in 50 mL LB medium in a 250 mL shake flasks and incubated overnight at 37°C with shaking at 200 rpm. Production of mCherry in large scale was performed in 'Sartorius Biostat® A plus' bioreactor that has 5L working volume. 3 L LB medium (containing 100 µg/mL ampicillin and 1% olive oil as a foam breaker) in bioreactor was inoculated with the fresh overnight culture. Cultivation was carried out under controlled conditions at 37°C and pH 7.0. The pH was kept constant at 7.0 by the controlled addition of 5M NaOH. The dissolved oxygen concentration (DO) was maintained at 30% saturation by increasing agitation speed (500–2,000 rpm) and O₂-enrichment if required. The optical density of culture was measured at 600 nm with spectrophotometer. Expression of recombinant mCherry was induced at OD₆₀₀ = 2.0 with optimum arabinose concentration that decided from experimental concentration data for optimization. Batches were finished when no further growth was detected with optical density.

2.5. Purification of target protein

After induction and expression of target protein in high cell density, cells were harvested by centrifugation

at 5000 rpm for 5 min. Cell pellets of 3L *E. coli* culture resuspended in 100 mL of lysis buffer (100 mM sodium phosphate, 100 mM NaCl, pH 7.0). Cell suspension was lysed by sonication (10 cycles of 15s pulse with intervals of 15s each, at 90% amplitude) for 2 hours on ice bath. The lysate was pelleted at 8000 rpm 5 min to separate undisturbed cell contents. Ultra-centrifugation was performed at 30000 rpm for 1 hour to get soluble protein solution.

Preparation of column for purification 10 mL of Ni-NTA resin in column was pre-equilibrated with 5 column volumes (CVs) of washing buffer (100 mM NaH₂PO₄, 100 mM NaCl, pH 7.8). Supernatant that transferred to a fresh tube after ultra-centrifugation was loaded to column. The flow through was collected and all untagged proteins were removed from column using 10 CVs of wash buffer 1 (100 mM sodium phosphate, 100 mM NaCl, 10 mM imidazole pH 7.8) and wash buffer 2 (100 mM sodium phosphate, 100 mM NaCl, 20 mM imidazole, pH 7.8). His tagged mCherry that bound to column was recovered with elution buffer (100 mM sodium phosphate, 100 mM NaCl, 300 mM imidazole, pH 7.8). Purified mCherry fractions were dialyzed overnight in buffer (20 mM Na₂HPO₄, 50 mM NaCl, pH 7.8) at 4°C.

2.6. Protein analysis

Optimal induction time and inducer concentration dependent expression levels, purity and molecular mass of purified mCherry samples were determined by SDS-PAGE. Whole cell lysate samples and collected protein purification samples were mixed 1X sample buffer and denatured at 95°C for 3 min, subjected to a 12% denaturing SDS-PAGE and stained with Coomassie brilliant blue. SDS-PAGE was performed essentially by the methods of Laemmli [24].

The concentration of the purified mCherry by the absorption spectra using a UV-VIS spectrophotometer (Varian Cary® 50). Absorbance was read at 280 nm.

2.7. Fluorescence measurements

The spectral properties of the purified mCherry were measured in a fluorometer (PTI Quanta Master™). The excitation and emission wavelength of mCherry were reported.

3. Results and Discussion

3.1. Construction of pBADCherry

The gene encoding red fluorescent protein mCherry is commercially available cloned in *E. coli* vector (pBAD). The pBADCherry was gift from Dr. Tsien (University of California, San Diego, CA) that used in this study. The gene is 708 nucleotides in size and encodes a start codon, with N-terminal 6XHistidine and was placed under

control of the arabinose-inducible *araBAD* promoter (P_{BAD}) (Figure 1).

3.2. Cytoplasmic expression of mCherry

E. coli BL21(AI) cells was transformed using the constructed pBADCherry expression vector. The mCherry was expressed as a His-tagged protein. A single clone of transformed *E. coli* cells was cultivated for detection of protein expression. The effects of inducer concentration and induction time on soluble mCherry expression were carried out in lab scale shake flasks contain LB medium. The degree of purity of recombinant mCherry was analyzed by 12% SDS-PAGE under denaturing conditions, stained by Coomassie brilliant blue. The molecular size of mCherry with Histidine tag was approximately 28 kDa as expected (as estimated in 12% SDS-PAGE gel) (Figure 3). The purity of the final protein product analyzed by Coomassie-stained gels was greater than 95% .

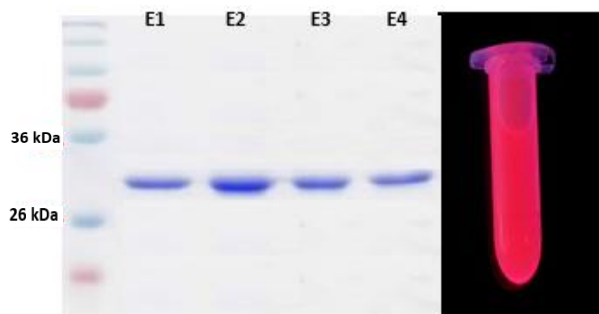


Figure 3. SDS-PAGE analysis of mCherry purified fractions.

Optimum arabinose concentration was decided by working at eight different concentrations at 37°C. As shown in Figure 4 expression levels were increased with arabinose concentrations and the expression was highest at 0.04% arabinose concentration. In addition the optimal induction was performed at 5 hours after addition of 0.04% arabinose shown in Figure 5. Taken together, the optimal culture conditions for highest expression of mCherry was established as 0.04% of arabinose at 37°C for 5 hours. Whole cell lysates of the optimization studies were analyzed by 12% SDS-PAGE.

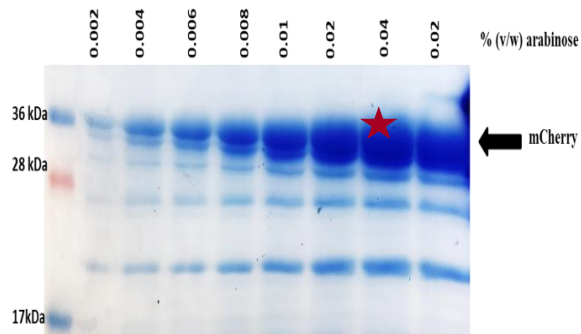


Figure 4. Arabinose induction of the expression of mCherry at different arabinose concentrations. Proteins in the whole cell lysates were analysed by 12% SDS-PAGE.

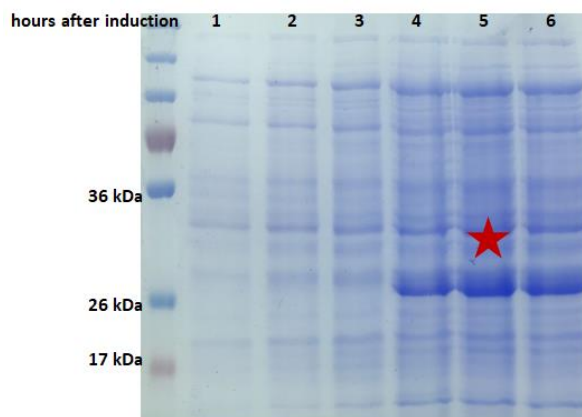


Figure 5. Effect of the induction time on mCherry expression with 0.04% arabinose concentration. Proteins in the whole cell lysates were analyzed by 12% SDS-PAGE.

3.3. Overexpression of mCherry

After determining the mCherry overexpression in *E. coli* in shaking medium the performance was observed under bioreactor conditions. The effects of induction parameters on protein expression were optimized with small culture of *E. coli* in flasks before performing large culture in a bioreactor. All processes in bioreactor were have been carried out in batch culture conditions. Optimized parameters (inducer concentrations and induction time) were applied to bioreactor. In order to determine optimal arabinose concentration for maximum yield of mCherry, induction was performed between 0.002-0.2% arabinose concentrations and analyzed by 12% SDS-PAGE (Figure 4).

Maximum yield of protein was observed at %0.04 arabinose concentration. The optical density of bacterial culture at 600 nm reached to a maximum of 12 after 5 hours of induction. Absorbance measured at 280 nm is used to calculate the concentration of purified mCherry. The yield measured for the fluorescent protein concentration was 81 mg/L from 3 L bacterial culture medium in a bioreactor while the concentration was 15 mg/L in shake flasks.

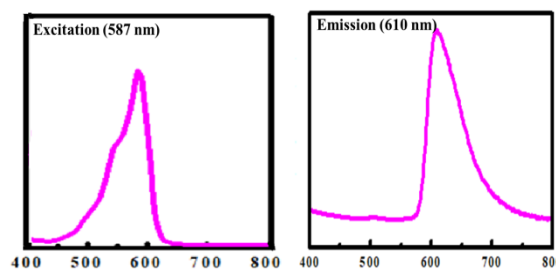


Figure 6. Excitation and emission spectra of mCherry

Figure 6 indicates the fluorescence excitation (587 nm) and emission (610 nm) spectra of purified mCherry. Spectral results were same as the ones reported before in the literature [25,27].

4. Conclusion

The advancement in FPs experimental studies makes FPs very practical tools for broad applications in biosciences, especially *in vivo* imaging. GFP and its variants used as a multicolor labeling of different compartments of cells, tissues or organisms. It is believed that because of increasing in diversity of FPs, they will become favorable tools for clinical, preclinical or therapeutic studies, such as drug screening, tumor monitoring and photodynamic therapies of cancer [7, 8].

Expression and purification of new generation FPs that improved by genetic engineering techniques represent variety of undiscovered opportunities for basic investigations. Production of engineered pure monomeric mCherry protein for structural studies is very important. mCherry has a monomeric structure unlike ancestor of RFPs and the palette of monomeric FPs enables multicolor labelling experiments [3].

Isolation and purification of proteins from organisms such as plant, animal or microorganisms is quiet challenging and very expensive process besides contamination risk of human and animal diseases derived from isolated hosts. Recombinant DNA technology helps to overcome these restrictions and gives product of protein with improved features that close to their natural structures [26].

For overproduction of recombinant proteins both eukaryotic and prokaryotic expression systems are used. Bacterial host systems have many advantages for achieving a very high yield of recombinant proteins. *E. coli* is the most preferred system because of its typical features such as capability to produce large amounts of recombinant protein in a short time at low cost with its well-known genome. Also *E. coli* expression systems are very convenient for the production of proteins such as FPs that don't require specific posttranslational modifications.

The *E. coli* pBAD system based on *araBAD* operon is a tightly regulatable expression system that allows turning expression on/off. Strain BL21(AI) is also the most widely used host for target gene expression. In this study pBADCherry in *E. coli* BL21(AI) cells were grown in bioreactor gives a very high yield of recombinant mCherry protein about 6 times higher than flask culture at 0.04% optimum arabinose concentration. The results of study indicated that by varying the concentration of arabinose, expression of proteins can be regulated at different levels. The expression level of mCherry at different time was shown in Figure 5. It is observed that the expression level of mCherry remained unchanged after 5th hours of induction and there was no significant difference between 5th and 6th hours of induction. Consequently induction with 0.04% arabinose concentration for 5 hours was decided as optimum condition of induction.

In this study expression of recombinant mCherry fluorescent protein in *E. coli* was optimized by an inducible system, overexpressed in bioreactor and also purified in a very high purity. It is hope that expressed pure recombinant FPs will be a control model for further studies to improve their biophysical properties such as brightness, photostability, maturation and tolerance for physical conditions. Taken together, our given method demonstrates that a high-throughput to produce FPs that usable for biophysical, structural and functional studies for instance, mechanisms of maturation, behavior of their chromophore and investigating of FPs for potential use in dye-sensitized solar cells.

In conclusion, we demonstrated an effective method for producing recombinant mCherry. We suggest that soluble mCherry protein yield can be further increased by optimization of vector, strain and bioreactor conditions.

Acknowledgment

This work was supported by the Scientific and Technological Research Council of Turkey (TÜBİTAK), (Project No: 114Z956) and Committee of Scientific Investigation of Gaziosmanpaşa University, Research Funds (Project No: 2017/62).

References

1. Shimomura, O., *The discovery of aequorin and green fluorescent protein*. Journal of Microscopy, 2005. **217**: p. 3–15.
2. Chalfie, M., Tu, Y., Euskirchen, G., Ward, W.W., Prasher, D.C., *Green fluorescent protein as a marker for gene expression*. Science, 1994. **263**(5148): p. 802–805.
3. Chudakov, D.M., Matz, M.V., Lunyakov, S., Lunyakov, K.A., *Fluorescent proteins and their applications in imaging living cells and tissues*. Physiological Reviews, 2010. **90**(3): p.1103–1163.
4. Shaner, N.C., Patterson, G.H., Davidson, M.W., *Advances in fluorescent protein technology*. Journal of Cell Science, 2007. **120**: p. 4247–4260.
5. Haddock, S.H., Mastoianni, N., Christianson, L.M., *A photoactivatable green-fluorescent protein from the phylum Ctenophora*. Proceedings Biological Sciences, 2010. **277**: p. 1155–1160.
6. Chudakov, D.M., Belousov, V.V., Zaraisky, A.G., Novoselov, V.V., Staroverov, D.B., Zorov, D.B., Lukyanov, S., Lukyanov, K.A., *Kindling fluorescent proteins for precise in vivo photolabeling*. Nature Biotechnology, 2003. **21**(2): p. 191–194.
7. Shemiakina, I.I., Ermakova, G.V., Cranfill, P.J., Baird, M.A., Evans, R.A., Souslova, E.A., Staroverov, D.B., Gorokhovatsky, A.Y., Putintseva, E.V., Gorodnicheva, T.V., Chepurnykh, T.V., Strukova, L., Lukyanov, S., Zaraisky, A.G., Davidson, M.W., Chudakov, D.M., Shcherbo, D., *A monomeric red fluorescent protein with low cytotoxicity*. Nature Communications, 2012. **3**(1): p. 1204.
8. Campbell, R.E., Tour, O., Palmer, A.E., Steinbach, P.A., Baird, G.S., Zacharias, D.A., Tsien, R.Y., *A monomeric red fluorescent protein*. Proceedings of the National Academy of Sciences, 2002. **99**(12): p. 7877–7882.

9. Shen, Y., Lai, T., Campbell, R.E., *Red fluorescent proteins (RFPs) and RFP-based biosensors for neuronal imaging applications*. Neurophotonics, 2015. **2**(3): p. 031203.
10. Bin, W., Yan, C., Joachim, D.M., *Fluorescence fluctuation spectroscopy of mCherry in living cells*. Biophysical Journal, 2009. **96**(6): p. 2391–2404.
11. Shaner, N.C., Campbell R.E., Steinbach P.A., Giepmans B.N., Palmer A.E., Tsien R.Y., *Improved monomeric red, orange and yellow fluorescent proteins derived from *Discosoma* sp. red fluorescent protein*. Nature Biotechnology, 2004. **22**(12): p. 1567–1572.
12. Ransom, E.M., Ellermeier, C.D., Weiss, D.S., *Use of mCherry red fluorescent protein for studies of protein localization and gene expression in *Clostridium difficile**. Applied and Environmental Microbiology, 2015. **81**(5): p. 1652–1660.
13. Lee, You-Jin, Jung K.-H., *Modulation of the tendency towards inclusion body formation of recombinant protein by the addition of glucose in the araBAD promoter system of *Escherichia coli**. Journal of Microbiology and Biotechnology, 2007. **17**(11): p. 1898–1903.
14. Guzman, L.-M., Belin, D., Carson, M.J., Beckwith, J., *Tight regulation, modulation, and high-level expression by vectors containing the arabinose P_{BAD} promoter*. Journal of Bacteriology, 1995. **177**(14), p. 4121–4130.
15. Newman, J.R., Fuqua C., *Broad-host-range expression vectors that carry the L-arabinose-inducible *Escherichia coli* araBAD promoter and the araC regulator*. Gene, 1999. **227**: p. 197–203.
16. Patkar, A., Vijayasankaran, N., Urry, D.W., Srienc F., *Flow cytometer as a useful tool for process development: Rapid evaluation of expression systems*. Journal of Bacteriology, 2002. **93**(3): p. 217–229.
17. Boström, M., Markland, K., Sandén, A.M., Hedhammar, M., Hober, S., Larsson, G., *Effect of substrate feed rate on recombinant protein secretion, degradation and inclusion body formation in *Escherichia coli**. Applied Microbiology and Biotechnology, 2005. **68**(1): p. 82–90.
18. Sandén, A.M., Boström, M., Markland, K., Larsson, G., *Solubility and proteolysis of the Zb-MalE and Zb-MalE31 proteins during overproduction in *Escherichia coli**. Biotechnology and Bioengineering, 2005. **90**(2): p. 239–247.
19. Greefield, L., Boone, T., Wilcox, G., *DNA sequence of the araBAD promoter in *Escherichia coli* B/r*. Proceedings of the National Academy of Sciences, 1978. **75**(10): p. 4724–4728.
20. Siegele, D.A., Hu, J.C., *Gene expression from plasmids containing the araBAD promoter at subsaturating inducer concentrations represents mixed populations*. Proceedings of the National Academy of Sciences, 1997. **94**(15): p. 8168–8172.
21. Khlebnikov, A., Risa, Ø, Skaug, T., Carrier, T., Keasling, J.D., *Regulatable arabinose-inducible gene expression system with consistent control in all cells of a culture*. Journal of Bacteriology, 2007. **182**(24): p. 7029–7034.
22. Chae H.J., Delisa M.P., Cha H.J., Weigand W.A., Rao G., Bentley W.E., *Framework for online optimization of recombinant protein expression in high-cell-density *Escherichia coli* cultures using GFP-fusion monitoring*. Biotechnology and Bioengineering, 2000. **69**(3): p. 275–285.
23. Lu, C., Albano, C.R., Bentley W.E., Rao, G., *Differential rates of gene expression monitored by green fluorescent protein*. Biotechnology and Bioengineering, 2002. **79**(4): p. 429–437.
24. Laemmli, U.K., *Cleavage of structural proteins during the assembly of the head of bacteriophage T4*. Nature, 1970. **227**(5259): p. 680–685.
25. Sarabipour, S., King, C., Hristova, K., *Uninduced high-yield bacterial expression of fluorescent proteins*. Analytical Biochemistry, 2017. **449**(1): p. 155–157.
26. Demain, A.L., Vaishnav, P., *Production of recombinant proteins by microbes and higher organisms*. Biotechnology Advances, 2009. **27**(3): p. 297–306.
27. Shaner, N.C., Steinbach, P.A., Tsien, R.Y., *A guide to choosing fluorescent proteins*. Nature Methods, 2005. **2**(12): p. 905–909.



Research Article

Use of various plant extracts to provide hygiene in mattresses and antibacterial film production

Gülsemin Savaş Tuna ^{a,*} , Efe Şafak ^a , Beyza Kara ^a , Gülce Mülayim ^a , Ceren Sert ^a ,
Nazlıcan Ulu ^a , Kemal Göktuğ Eken ^a  and Sercen Cansu Sertel ^b 

^a Aden Science High School, Tekirdağ, 59030, Turkey

^b Bahçeşehir University, Faculty of Medicine, İstanbul, 34734, Turkey

ARTICLE INFO

Article history:

Received 06 April 2018

Revised 30 October 2018

Accepted 27 November 2018

Keywords:

Clove

Antibacterial

Hygiene in mattresses

ABSTRACT

It has been known for many years that microorganisms can grow and proliferate on textile material. Other than clothes, the objects that humans mostly contact with are their mattresses. In this study, it was aimed to produce an antibacterial film in order to prevent growth and proliferation of various bacteria which are dangerous for human health in mattresses and to make mattresses hygienic since they cannot be changed in a short time. In the study, extracts were first obtained from *Saponaria officinalis* L., *Oxalis acetosella* L., *Althaea officinalis* L., *Lavandula officinalis* L., *Aesculus hippocastanum* L., *Thymus vulgaris* L., *Syzygium aromaticum* (L.) Merr at Perry plants. The extracts were used individually and combined to form experimental groups. The antibacterial effects of the extracts were examined by disc-diffusion method applied on Gram-positive rods, Gram-negative rods, Gram-positive cocci and Bacilli colonies obtained from mattresses. In addition, the colony counts were also carried out in total MAB culture. Based on the results of the study, it was determined that *S. aromaticum* and *L. officinalis* + all extracts had the highest inhibitory effect. By using *S. aromaticum* extract, xanthan gum, propylene glycol, tween-20 and distilled water, an antibacterial film, which may provide long-term hygiene in mattresses, was produced. The obtained gel was lyophilized and made available for use. As a result of this study, it was foreseen that with the development of the obtained product, 4-5 million people (e.g., dorm, hospital, hotel) could be protected from the diseases transmitted from mattresses, the money spent on the chemicals used for hygiene and the damages caused by these chemicals on human and environmental health could be reduced, mattresses used for long periods of time could be made healthy, and mattresses can be made hygienic in a cost-effective, practical and natural manner.

© 2019 Advanced Researches and Engineering Journal (IAREJ) and the Author(s).

1. Introduction

Today's modern living and working conditions provide ideal conditions for the microorganisms to reproduce rapidly. The excessive reproduction of some microorganisms causes the deterioration of products (food, textile, healthcare products...), the formation of diseases and infections in the human body, and the increase of allergic reactions [1]. It has been known for many years that microorganisms can grow and proliferate on textile materials. Other than clothes, the objects that

humans mostly contact with are their mattresses. In a study, it was reported that 317 million living organisms were found in one gram of the samples taken from two different hospitals, elderly and child deaths increased in those hospitals, and intestinal infections and diseases like hepatitis A were transmitted through mattresses. In the study conducted by Department of Genetics and Bioengineering of Yeditepe University, Faculty of Engineering and Architecture, it was reported that the examination on mattress samples obtained from 19

* Corresponding author. Tel.: +90 505 253 3430

E-mail addresses: glsvs@yahoo.com (G. Savaş Tuna), efesafak35@hotmail.com (E. Şafak), bezya_karaaa17@hotmail.com (B. Kara),

gulcimim@hotmail.com (G. Mülayim), cerensert99@gmail.com (C.Sert), nazlicanulu2001@hotmail.com (N. Ulu), kemaleken.2000@gmail.com (K.G. Eken), sercen.sertel@gmail.com (S.Sertel)

ORCID: 0000-0003-2089-2790 (G. Savaş Tuna), 0000-0001-8028-7619 (E. Şafak), 0000-0002-5602-8868 (B. Kara), 0000-0003-1772-4171 (G. Mülayim), 0000-0002-5766-7143 (C.Sert), 0000-0002-2176-200X (N. Ulu), 0000-0002-6140-5090 (K.G. Eken), 0000-0002-6631-1835 (S.C. Sertel)

different hospitals, hotels and dormitories had revealed that the mattresses became a biotope comprised of dust mites, scabies, molds and bacteria, and this was a significant threat to human health [2]. In Turkey, the student capacity of the dormitories operating as part of the Higher Education Credit and Hostels Institution (KYK) under the Ministry of Youth and Sports is 601.019 [3]. The student capacity of 2591 dormitories operated by the Ministry of National Education is 483,941 [4]. In addition, according to 2016 data, the bed capacity of 865 state hospitals in Turkey is 217.771 [5]. Hotels are the other areas posing risk for human health. In 2016, the total bed capacity of the hotels in Turkey was 312.912 [6]. However, it is now stated that this figure has reached 1 million as of today. Considering private dormitories and private hospitals, the number of beds and the number of people who benefit from them, that is the people who are under risk, has reached 4-5 million. If we also take into account our beds and mattresses in our homes, it can be said that people face this danger every day.

After the infection incidents occurring in hospitals, more importance has been placed on the hygiene of beds and mattresses, and the application of systems using ultraviolet rays has become a topic of discussion. However, the implementation of such systems is costly and difficult. Nowadays, devices that absorb these wastes with vacuum systems are used more commonly since they are more cost-effective [2]. These devices are for cleaning purposes, but the important thing is to prevent the growth and proliferation of microorganisms. Therefore, antibacterial and antifungal products should be used. Today, arsenic, iron, lead, tin, mercury, silver, vegetable and animal extracts are used as antibacterial agents. In particular, the use of heavy metals (Pb, Hg, As...) causes increase in various health problems, such as cancer, poisoning, skin rash, and itching. For instance, after the widely used tin compounds were examined by the EPA (Environmental Protection Agency), the use of these compounds was banned in Japan and in some European countries [7].

Today, human health constitutes the focus of antibacterial applications. For this reason, high efficiency and non-toxic substances have been introduced to the use of the textile industry with the help of advancing technology. For example, this feature of Bamboo, which is known as an antibacterial tree in the Far East, has been transported to clothes over time. In addition, the products obtained from algae are also known as natural antibacterial agents [8]. Antibacterial and antifungal effects have been primarily investigated in the studies conducted with plants [9-19]. Antibacterial studies have also affected bed and mattress companies and a large number of antibacterial mattresses have been put on the

market. One of those companies produced antibacterial mattresses that provide better sleep quality by combining visco material and soybean oil, whereas another company combined Indian oil and visco material to reach the same result [20]. Only the upholstery of these mattresses has antibacterial properties and their prices are quite high. The aim of this study was to produce a cheap and natural antibacterial film in order to 1- prevent growth and proliferation of various bacteria, which are dangerous for human health, in mattresses, 2- and to make mattresses hygienic since they cannot be changed in a short period.

2. Materials and Methods:

2.1. Material:

In the study, *Saponaria officinalis* L., *Oxalis acetosella* L., *Althaea officinalis* L., *Lavandula officinalis* L., *Aesculus hippocastanum* L., *Thymus vulgaris* L., *Syzygium aromaticum* (L.) Merr at Perry were used as materials.

2.2. Method:

2.2.1. Obtaining extracts from *Syzygium aromaticum* (L.) Merr at Perry, *Thymus vulgaris* L. and *Lavandula officinalis* L. plants:

By using a Clevenger device, extracts were obtained from *S. aromaticum*, *T. vulgaris* and *L. officinalis* plants via steam distillation method [21, 22].

2.2.2. Obtaining extracts from *Althaea officinalis* L. and *Aesculus hippocastanum* L. plants:

50 g *A. officinalis* and 200 ml sterile water were put into a closed container and kept for 2 days (25 °C incubator) under dark environment. After filtration, the extract was sterilized in autoclave (121 °C) for 20 minutes [23]. The same procedure was also performed for the barks of *A. hippocastanum*.

2.2.3. Obtaining extracts from *Oxalis acetosella* L. plant:

The leaves of *O. acetosella* were ground and six 10-gram cartridges were prepared. After the cartridges were placed in the Soxhlet device, hexane, methylene chloride, ethyl acetate and ethyl alcohol were extracted. At the end of extraction, ethyl alcohol was removed by using a rotary evaporator and the extract was obtained [24].

2.2.4. Obtaining Saponin from *Saponaria officinalis* L. plant:

The pieces taken from the root of *S. officinalis* were ground and 3 cartridges (10 g x 3) were prepared. The prepared cartridges were treated with petroleum ether (200 ml) for 6 hours in the Soxhlet device. After the cartridges were dried, the process was continued for 24

hours in Soxhlet device with 80% ethanol. Ethyl alcohol was removed by using a rotary evaporator and the concentrated extract was taken to the beaker. The beaker was taken into an ice container, and acetone was added dropwise to the beaker in order to obtain Saponin precipitate with a white color. After the precipitation was complete, filtration was carried out by using filter paper and the filtrate was dried at room temperature to obtain Saponin [25].

2.2.5. Medium preparation and obtaining samples from mattresses:

At this stage of the study, Müller-Hinton agar (Merck 1.05437) growth medium was used to incubate microorganisms found on beds and mattresses. Petri dishes containing growth medium were placed upside down on the mattresses covered with clean linens for 1 hour, and then incubated at 35 °C for 24 hours. This procedure was repeated every two days in 3 separate beds for two weeks. After incubation, the bacterial colonies were identified [26]. In general, four different colonies were identified in the Petri dishes. These colonies, classified as Gram positive rods (e.g., *Lactobacillus*, *Listeria*, *Eubacterium*), Gram negative rods (e.g., *Enterobacteria*, *Pseudomonas*, *Acinetobacter*), Gram positive cocci (e.g., *Streptococcus*, *Staphylococcus*) and Bacilli (e.g., *Bacillus*), can be produced by various species [27, 28]. Since bacteria could not be identified individually based on their species, the study was carried out based on total bacteria count.

2.2.6. Cultivation of mesophilic aerobic bacteria culture:

In the literature review performed to obtain a clearer result in this study, it was seen that Chinese (CTITC) and Japanese (JTIA) Textile Inspection centers conducted their studies on antimicrobial mattresses in mesophilic aerobic bacteria culture (MAB) or *Staphylococcus* [28]. MAB culture contains bacteria such as *Lactobacillus* and *Staphylococcus* [27]. At this stage of the study, Brain-Heart Infusion Medium (Merck 1.10493) was used for MAB culture inoculation. Inoculation was performed 24 hours after the medium was prepared and left for incubation at 35 °C for 24 hours. After the incubation, 1 loop (~ 10⁹ bacteria) was taken from MAB culture and transferred to 100 ml Bufferd Peptone Water medium.

2.2.7. Investigation of Antibacterial Effects of Plant Extracts:

The antibacterial effects of the extracts were investigated by two different methods.

In the first stage, Disc-Diffusion Method was used to investigate the antibacterial activity of the extracts on the samples taken from the mattresses [29]. The discs to be

used in the method were previously prepared and sterilized by being kept in a dry sterilizer for 1 hour at 180 °C. 28 experimental groups were formed from plant extracts (Table 1). In addition, deionized water was used as a negative control group and Amoxicillin Clavulanate antibiotic was used as a positive control group [30]. By using physiological saline solution, 10⁻² dilutions were prepared from the colonies developed in Petri dishes, and 50 microliters were taken from the dilutions and inoculated onto Petri dishes. 3 discs soaked with 25 micron of extract were placed into these Petri dishes. Petri dishes were incubated at 35 °C for 24 hours and the changes were observed.

The resulting zones were measured by caliper and their averages were taken. The study was carried out in 3 repetitions.

In the second stage, Total Bacterial Count was performed in MAB culture. Bacteria inoculated into BPW medium were used for this process. 0.1 ml of bacterial cultured BPW was taken and inoculated into tubes containing 9 ml Maximum Recovery Diluent (physiological saline solution) and 1 ml plant extract. After inoculation, tubes were kept at room temperature for 30 minutes and total bacterial counting was performed [31]. After counting, data was obtained by using the following formula (Table 2).

$$N = C / [V(n_1 + 0,1 \times n_2) \times d] \quad (1)$$

(N: number of colonies (gram or ml), C: total amount of colonies counted in Petri dishes, n₁: number of Petri dishes in first dilution, n₂: number of Petri dishes in second dilution, d: dilution coefficient of the first counted Petri dish).

2.2.8. Preparation of Antibacterial Film:

In order to prepare antibacterial film, the most effective plant extract (10-15%), Xanthan Gum (1-3%), Propylene Glycol (10%), Tween-20 (5%) and Distilled water (100g) were used. Firstly, ratio of the water was determined according to the percentages and half of the water was added to xanthan gum. The gum was allowed to stand overnight so that it could expand and be homogenous. Propylene glycol was then added. The rest of the water was used to dissolve the Tween-20. The extract was added dropwise on dissolved Tween-20. This mixture was added to Xanthan gum and then taken to a petri dish and dried in a 40 °C incubator. The obtained gel was lyophilized.

3. Results and Discussion

Based on the measurements made by the disc-diffusion method on the experimental groups, it was observed that the plant extracts had different antibacterial properties (Table 1).

When the results obtained by the disk-diffusion method were examined, it was seen that *A. officinalis*, *L. officinalis* + *A. officinalis* extracts had no inhibitory effect on bacteria, and the least inhibitory effect was seen in *A. hippocastanum* extract.

It was determined that *S. aromaticum* extract had an efficient antibacterial effect on all four different colonies identified in the mattresses. Other extracts with high inhibitory effect were *L. officinalis* + all, *S. aromaticum* + all, *T. vulgaris* + *S. officinalis* and *L. officinalis* + *S. officinalis*. At the end of the MAB counting, it was determined that the results in the experimental groups were different (Table 2).

In the studies related to colony count, the counting is performed over 15-300 colonies and these values are taken as criteria [32]. When table 2 is examined with respect to the Positive control group, it was seen that *L. officinalis*, *T. vulgaris*, *A. officinalis*, *A. hippocastanum*, *L. officinalis*+ *A. officinalis*, *L. officinalis*+ *A. hippocastanum*, *T. vulgaris* + *A. officinalis* and *T. vulgaris* + *A. hippocastanum* extracts had no inhibitory effect on mesophilic aerobic bacteria. Similar to the disk diffusion method, it was determined that *S. aromaticum* extract had also the highest antibacterial effect on MAB culture. Other extracts with high antibacterial effect were *L. officinalis* + all and *L. officinalis* + all + salt mixtures. The data obtained from this study is also supported by previous studies [13-16, 18].

Table 1: Results of Disc-Diffusion Procedure Performed on Plant Extracts (mm)

Extract	Gram(+) Rods	Gram (-) Rods	Gram (+) cocci	Bacilli
<i>L. officinalis</i>	1.4	1.6	1.8	1.6
<i>S. aromaticum</i>	9.5	9	9.2	9.4
<i>T. vulgaris</i>	6	5.5	5	6.2
<i>S. officinalis</i>	4	5	3	3
<i>O. acetosella</i>	3	2	2	2
<i>A. officinalis</i>	0	0	0	0
<i>A. hippocastanum</i>	0.5	0	0.5	0
<i>L. officinalis</i> + <i>S. officinalis</i>	6.30	6	6.8	5
<i>L. officinalis</i> + <i>O. acetosella</i>	4	5	4	4
<i>L. officinalis</i> + <i>A. officinalis</i>	0	0	0	0
<i>L. officinalis</i> + <i>A. hippocastanum</i>	1	0.5	0.5	1
<i>L. officinalis</i> + all	8.5	8	7.5	8
<i>L. officinalis</i> + all + salt	4.5	4	3	3.5
<i>L. officinalis</i> + all + carbonate	4.5	5	4	5
<i>S. aromaticum</i> + <i>S. officinalis</i>	6	6.5	5.5	6
<i>S. aromaticum</i> + <i>O. acetosella</i>	6.5	7	6	6.5
<i>S. aromaticum</i> + <i>A. officinalis</i>	3	2	2	2.5
<i>S. aromaticum</i> + <i>A. hippocastanum</i>	4	4.5	4.5	3.5
<i>S. aromaticum</i> + all	7	6	6	6.5
<i>S. aromaticum</i> + all + salt	4	4	5.5	5
<i>S. aromaticum</i> + all + carbonate	3.5	4	4	3.5
<i>T. vulgaris</i> + <i>S. officinalis</i>	6	6	7	6
<i>T. vulgaris</i> + <i>O. acetosella</i>	4.5	3.5	4	4
<i>T. vulgaris</i> + <i>A. officinalis</i>	2	1.5	2	2
<i>T. vulgaris</i> + <i>A. hippocastanum</i>	2	2	2.5	2.5
<i>T. vulgaris</i> + all	5	6	4.5	5.5
<i>T. vulgaris</i> + all + salt	5	6	6	6
<i>T. vulgaris</i> + all + carbonate	3	3.5	2.5	3.5
Negative group	0	0	0	0
Positive group	10.5	11.5	10	12

Table 2: Antibacterial effects of plant extracts in MAB culture (cfu/g).

Extract	MAB
<i>L. officinalis</i>	>300
<i>S. aromaticum</i>	8
<i>T. vulgaris</i>	>300
<i>S. officinalis</i>	14
<i>O. acetosella</i>	20
<i>A. officinalis</i>	>300
<i>A. hippocastanum</i>	>300
<i>L. officinalis</i> + <i>S. officinalis</i>	20
<i>L. officinalis</i> + <i>O. acetosella</i>	15
<i>L. officinalis</i> + <i>A. officinalis</i>	>300
<i>L. officinalis</i> + <i>A. hippocastanum</i>	>300
<i>L. officinalis</i> + all	10
<i>L. officinalis</i> + all + salt	11
<i>L. officinalis</i> + all + carbonate	16
<i>S. aromaticum</i> + <i>S. officinalis</i>	13
<i>S. aromaticum</i> + <i>O. acetosella</i>	16
<i>S. aromaticum</i> + <i>A. officinalis</i>	27
<i>S. aromaticum</i> + <i>A. hippocastanum</i>	18
<i>S. aromaticum</i> + all	16
<i>S. aromaticum</i> + all + salt	19
<i>S. aromaticum</i> + all + carbonate	41
<i>T. vulgaris</i> + <i>S. officinalis</i>	19
<i>T. vulgaris</i> + <i>O. acetosella</i>	47
<i>T. vulgaris</i> + <i>A. officinalis</i>	>300
<i>T. vulgaris</i> + <i>A. hippocastanum</i>	>300
<i>T. vulgaris</i> + all	19
<i>T. vulgaris</i> + all + salt	21
<i>T. vulgaris</i> + all + carbonate	26
Negative group	>300
Positive group	0

In terms of cost, it was decided to produce antibacterial film by using clove extract and the sample film was produced as described in the Materials-Methods section. It was determined that by using this film, Gram positive cocci which cause various infections in hospitals, gram-negative rods which cause various diseases such as pneumonia and antibiotic resistance, and gram-positive rods which cause skin and soft tissue infections [33] can be prevented from settling and proliferating in beds and mattresses.

Based on the results of this study; it was foreseen that by using the produced antibacterial film on mattresses and various surfaces, natural resources of Turkey can be better utilized and 4-5 million people can be protected

from the diseases transmitted from mattresses, the money spent on the chemicals used for hygiene and the damages caused by these chemicals on human and environmental health can be reduced, and mattresses can be made hygienic in a cost-effective, practical and natural manner. It is recommended that the sample antibacterial film produced in this study should be further developed by experts in the field and put into the practice as soon as possible (Figure 1).



Figure 1. Use of antimicrobial film on mattresses

References

1. <http://www.acilservis.org> (Date of access: 2017 27 April)
2. eccelebi@huriyet.com (Date of access: 2017 27 April)
3. <http://www.gsb.gov.tr> (Date of access: 2017 27 April)
4. T.C. Millî Eğitim Bakanlığı Strateji Geliştirme Başkanlığı, Millî Eğitim İstatistikleri, Örgün Eğitim, 2015-2016. [cited 2017 29 June] Available from: <http://sgb.meb.gov.tr>
5. T.C. Sağlık Bakanlığı Kamu Hastaneleri Genel Müdürlüğü, Genel Sağlık İstatistikleri. [cited 2017 29 June] Available from: <http://rapor.saglik.gov.tr/istatistik/rapor/index.php>
6. <https://www.tursab.org.tr> (Date of access: 2017 27 April)
7. <http://www.esasticaret.com/index.php/ueruenler/tektstkmyasallari/antbakteral-kmyasal> (Date of access: 2017 27 April)
8. <http://tektstilmuhendisleri.blogspot.com/2010/01/antibakteriyel-tekstiller.html> (Date of access: 2017 27 April)
9. Nanetti, A., Massi, S., Conti, A. Using Apedin Vapor(R) in

- the control of Varroa mites and in honeybee feeding. Vet Ital. Apr-Jun; 2004. 40(2): p. 46-55.
10. Benli, M. ve Yiğit, N. Ülkemizde Yaygın Kullanımı Olan Kekik (*Thymus vulgaris*) Bitkisinin Antimikrobiyal Aktivitesi. Mikrobiyoloji Dergisi, 2005. p. 1-8.
 11. Hammad, M.M. *Thymus vulgaris* Effect on *Streptococcus mutans* Adhesion to Epithelial Cells. The Preliminary Program for First African and Middle-East IADR Federation Conference, 2007.
 12. Aydın, B.D. Bazı Tıbbi Bitki ve Baharatların Gıda Patojenleri Üzerine Antimikrobiyal Etkisinin Araştırılması. Kafkas Üniv Vet Fak Derg., 2008. 14 (1): 83-87.
 13. Topal, U., Sasaki, M., Goto, M., Otlis, S. Chemical compositions and antioxidant properties of essential oils from nine species of Turkish plants obtained by supercritical carbon dioxide extraction and steam distillation. Int J Food Sci Nutr. Nov-Dec; 2008. 59(7-8): 619-34.
 14. Ayana, B. ve Turhan, K.N. Gıda Ambalajlamasında Antimikrobiyel Madde İçeren Yenilebilir Filmler/ Kaplamalar ve Uygulamaları. GIDA, 2010. 35(2):151-158.
 15. Komes, D., Belščak-Cvitanović, A., Horžić, D., Rusak, G., Likić, S., Berendika, M. Phenolic composition and antioxidant properties of some traditionally used medicinal plants affected by the extraction time and hydrolysis. Phytochem Anal. 2011. 22(2): 172-180.
 16. Soković, M., Glamočlija, J., Marin, P.D., Brkić, D., van Griensven, L.J. Antibacterial effects of the essential oils of commonly consumed medicinal herbs using an in vitro model. Molecules. 2010. 15(11): 7532-7546.
 17. Vale-Silva, L.A., Gonçalves, M.J., Cavaleiro, C., Salgueiro, L., Pinto, E. Antifungal activity of the essential oil of *Thymus x viciosoi* against *Candida*, *Cryptococcus*, *Aspergillus* and dermatophyte species. Planta Med, 2010. 76(9):882-888.
 18. Zu, Y., Yu, H., Liang, L., Fu, Y., Efferth, T., Liu, X., Wu, N. Activities of ten essential oils towards *Propionibacterium acnes* and PC-3, A-549 and MCF-7 cancer cells. Molecules, 2010. 15(5): 3200-3210.
 19. Bagavan, A., Rahuman, A.A., Kaushik, N.K., Sahal, D. In vitro antimalarial activity of medicinal plant extracts against *Plasmodium falciparum*. Parasitol Res. 2011. 108(1): 15-22.
 20. <http://www.viscoyatakmerkezi.com/hint-yagi-ozlu-bitkisel-visco.html> (Date of access: 2017 27 April)
 21. Baytop, T. Türkiye'de Bitkilerle Tedavi, 1999, Türkiye, İstanbul: Nobel Tıp Kitapevleri Yayını, 2. Baskı.
 22. Tanker, M. ve Tanker, N. Farmakognozi, 1990. Türkiye: Ankara Üniversitesi Eczacılık Fakültesi yayınları, No: 65.
 23. Tanker, M. ve Tanker, N. Farmakognozi, 1990. Türkiye: Ankara Üniversitesi Eczacılık Fakültesi yayınları, No: 66.
 24. Sakar, M.K. ve Tanker, M. Fitokimyasal Analizler, 1991. Türkiye: Ankara Üniversitesi Eczacılık Fakültesi yayınları, No: 67.
 25. Özek, T. Türkiye'de Elde Edilen Çöven Kökünden Saponin Ekstraksiyonu Ve Ürünün İncelenmesi. 1987. İstanbul Teknik Üniversitesi Fen Bilimleri Enstitüsü, PhD Thesis.
 26. Dolapçı, İ. Bakterilerde İzolasyon, Tanı ve İdentifikasyon Yöntemleri. Ankara Üniversitesi Tıp Fakültesi Tıbbi Mikrobiyoloji AD, 2016.
 27. Levinson, W. Review of medical microbiology and immunology, 2016. The McGraw-Hill Companies.
 28. <https://www.amerisleep.com> (Date of access: 2017 27 April)
 29. Toroğlu, S. ve Çenet, M. Tedavi Amaçlı Kullanılan Bazı Bitkilerin Kullanım Alanları ve Antimikrobiyal Aktivitelerinin Belirlenmesi İçin Kullanılan Metodlar. KSU. Journal of Science and Engineering, 2006. 9(2): p.12-19.
 30. Erbil, N., Arslan, M. Penisilin Grubu Bir Antibiyotik Olan Amoksisilin-Klavulanik Asit (Amoklavin®)'in Antibakteriyel Aktivitesi ve Mutajenik Etkisinin Belirlenmesi. KSÜ Doğa Bil. Derg., 2016. 20(3): p. 242-246.
 31. Friedman, M., Henika, P.R., Mandrell, R.E. Bactericidal activities of plant essential oils and some of their isolated constituents against *Campylobacter jejuni*, *Escherichia coli*, *Listeria monocytogenes* and *Salmonella enterica*. Journal of Food Protection, 2002. 65 (10): p.1545– 1560.
 32. <https://www.mikrobiyoloji.org> (Date of access: 2017 27 April)
 33. Alvarez-Lerma, F., Grau, S., Gracia-Arnillas, M.P. Gram-positive cocci infections in intensive care: guide to antibacterial selection. Drugs, 2006. 66(6): p.751-68.

**Research Article****Determination of highly effective attributes in fold level classification of proteins****Özlem Polat** * *Department of Mechatronic Engineering, Cumhuriyet University, Sivas 58140, Turkey***ARTICLE INFO***Article history:*

Received 28 February 2018

Received 31 December 2018

Accepted 13 January 2019

Keywords:

Divergence analysis

Fold recognition attributes

Neural networks

Protein fold classification

ABSTRACT

In this paper it is aimed to determine which of the protein features or attributes is the most significant for classification of proteins according to their folds. Proteins in the database used in this study are represented by six feature groups called attributes and by a 125-dimensional feature vector. The representation of proteins with very high dimensional vectors such as 125 causes increasing computational load of the classification process and extending the process time. In this study “dimension reduction” solution is offered for this negative situation. Hence, with two different approaches, the features and attributes having high classification performance are determined. In the first approach, which attribute gives higher performance is determined by testing separately each of the six attributes. In the second approach, the most significant of the 125 features are determined using Divergence Analysis method. In this study, a classic classifier KNN (K-nearest neighbor) and artificial neural network models GAL (Grow and Learn) and SOM (Self-Organizing Map) networks are used as classifier and classification performance is analyzed for reduced dimension datasets.

© 2019 Advanced Researches and Engineering Journal (IAREJ) and the Author(s).

1. Introduction

Proteins are essential and large biological macromolecules that regulate necessary parts of living organisms to control all their living functionalities [1]. Proteins having same or similar shape in a given locus perform the same or similar functions. Structural comparison and classification of proteins is therefore have a great importance in terms of computational biology [2]. Information on all known proteins is stored in the Protein Data Bank [3]. Currently (December 31, 2018) has 147,610 protein structures experimentally identified in this database, and this number is increasing every month by adding an average of 800 new molecules. Thus, many similar structures are formed in this database. The comparison and classification of protein structures is also important in this respect. SCOP (Structural Classifications of Proteins) [4] provides comprehensive evolutionary and structural relationships among all known proteins [5]. Proteins are divided into four main structural classes according to the components of the secondary structure;

all-alpha, all-beta, alpha/beta and alpha+beta; and according to SCOP, these four main classes are divided into folds, folds are divided into superfamilies, and superfamilies are divided into families. Folds represent the 3D shape of proteins and because of that the protein structure defines the protein function. Therefore, classifying proteins according to their folds is an important issue for structural biology.

There are many studies in the literature about proteins. Over the past 30 years, a wide variety of research has been conducted on the classification of protein folds. In these studies, classifiers such as artificial neural networks [5-12], Bayesian classifiers [13], k-nearest neighbors [14-17], support vector machines [18-20] were used as well as ensemble classifiers [1,21-30] using more than one classifier were used. In all these studies, different methods were used to classify the proteins at the fold level, among which only [8,26,30] tested separately the feature groups used in the classification of proteins.

One of the earliest studies on classifying protein at the fold level was performed by Reczko and Bohr [6]. Reczko

* Corresponding author. Tel: +90 346 219 10 10

E-mail address: ozlem.polat@cumhuriyet.edu.tr

ORCID: 0000-0002-9395-4465

Note: Part of this study was presented at International Advanced Researches & Engineering Congress, Osmaniye /Turkey

and Bohr used a special feed-forward artificial neural network model called Cascade-Correlators. In 1999 Dubchak et al. developed a new computational method based artificial neural network to assign the protein sequence to a fold class in SCOP [5]. In 2001 Edler et al. [7] conducted a study showing the role and consequence of statistical methods in predicting protein fold classes. In the same year, Ding and Dubchak [8] applied support vector machines and artificial neural networks as the primary classifier to recognize protein folds. In these studies, Ding and Dubchak used a dataset, which they had generated in previous studies [5], containing 27 protein folds. This dataset contains a total of 694 proteins, 311 in the training set and 383 in the test set. Bologna and Appel used an ensemble of four-layer Discretized Interpretable Multi-Layer Perceptron [9] and used the dataset formed by Ding and Dubchak [8]. In 2003, Huang et al. [31] proposed a hierarchical learning architecture that separates proteins into four structural classes; as a second step, they tried to solve 27-class protein fold classification problem using MLP, GRNN, RBFN and SVM classifiers. In 2004, Okun [14] used a modified nearest neighbor algorithm called the K-Local Hyperplane Distance Nearest Neighbor. In 2005, Chinnasamy et al. [13] presented a system called TAN (Tree-Augmented Network) and based Bayesian Network for classification problem. In the same year, Huang et al. [11] used a hierarchical learning architecture based on artificial neural networks, in which the attributes were selected during learning to classify proteins at the fold level. In 2006 Nanni [22,23] used two different ensemble classifiers. Shen and Chou [15] developed a hybrid classifier called OET-KNN (K-Nearest Neighbor Optimized Evidence Theoretic) and they tested it on the 27-class dataset used in [8]. In 2007, Chen and Kurgan [24] proposed PFRES method for classifying protein folds with an automatized way. Shamim et al. [20] used a SVM-based classifier. Motivated by Shen and Chou, Guo and Gao [25] proposed a new hierarchical composite classifier called GAOEC (Genetic Ensemble Classifier Optimized Algorithm). A different study on classification of proteins at the fold level was also performed by Krishnaraj and Reddy [32]. Krishnaraj and Reddy used the AdaBoost and LogitBoost methods, which are two different variations of Boost algorithms. Later on, Damoulas and Girolami [30] used the variational Bayesian approach and the Kernel combination methodology for classification. In 2009 Shen and Chou [33] used a hybrid classifier; Hashemi et al. [1] used MLP and RBF networks; Chen et al. [26] used a new approach based on genetic algorithm and Jazebi et al. [12] used a fusion method to classify the proteins at the fold level. In 2010 Dehzangi et al. applied Random Forest [34] and Rotation Forest [35] algorithms; Wang and Gao [36] used a two-layer classifier in which OET-KNN is used in

the first layer and SVM is used in the second layer. Motivated by [32,34,35] Dehzangi and Karamizadeh used a heterogeneous classifier including LogitBoost, Random Forest and Rotation Forest algorithms [37] for protein fold classification. In 2012 Suvarnavani et al. [38] applied boosting algorithm called SMOTE and used Triangle Sub division Method (TSM) to extract the feature set; then used a decision tree classifier and obtained 78.25% classification accuracy. In 2013 Bae et al. [39] tried to solve the classification problem by using multi-class linear decomposition analysis method. One of the recent studies on this area has been studied by Lin et al. [28]. They applied K-means clustering algorithm in their study. To the best of our knowledge the most recent study in the literature has been made by Aram et al. [29] in 2015. Aram et al. used a two-layer classification framework (TLCF) and a mixture of MLP, RBFN and Rotation Forest algorithms for classification of protein folds.

The studies mentioned above and available in the literature tried to solve protein fold classification problem. Only three of these studies [8,26,30] have evaluated the feature groups separately to classify the proteins according to their folds.

In this study, three different classifiers, KNN, SOM and GAL, are used to classify proteins at the fold level. In addition, in this study, the feature groups (attributes) are evaluated individually in order to determine the most significant attributes for protein fold classification. Also the Divergence Analysis method is used to array the features according to their effectiveness and determine the most significant features for protein fold classification. Thus, in the literature, the feature size in the dataset which is frequently used in the classification of proteins is reduced to a value lower than 125 and the computation load is reduced, therefore the computation time is reduced.

In Section 2 Materials and methods are introduced. In Section 3 experiments and performances are presented and conclusions are brought in Section 4.

2. Materials and Methods

2.1 Dataset and Features

The dataset used in this paper was taken from [8] and still available at <http://ranger.uta.edu/~chqding/bioinfo.html>. The original training and test sets have 311 and 383 proteins, respectively. This dataset consists of 27 folds. These folds are shown in Table 1.

To cope with the fold classification problem, Ding and Dubchak formed the following six attributes from protein sequences; amino acid composition, predicted secondary structure, hydrophobicity, normalized van der Waals volume, polarity and polarizability [8]. Of the above six attributes, only amino acid composition has 20 components, each

component states the occurrence frequency of one of the 20 native amino acids in a given protein. The other five attributes have 21 components.

The occurrence frequencies of the 20 native amino acids in a particular protein form the components of the composition vector of that protein. The 20 amino acids are denoted with letters in alphabetic order each one is represented as AA_i.

Table 1. The 27 protein folds, structural classes and the number of proteins contained in training and test sets [8]

Fold Number	Fold name	Structural Class	Train set	Test set
1	Globin-like	all-α	13	6
2	Cytochrome c		7	9
3	DNA-binding 3-helical bundle		12	20
4	4-helical up-and-down bundle		7	8
5	4-helical cytokines		9	9
6	Alpha; EF-hand		6	9
7	Immunoglobulin-like sandwich	all-β	30	44
8	Cupredoxins		9	12
9	Viral coat and capsid proteins		16	13
10	ConA-like lectins/glucanases		7	6
11	SH3-like barrel		8	8
12	OB-fold		13	19
13	Trefoil		8	4
14	Trypsin-like serine proteases		9	4
15	Lipocalins		9	7
16	TIM-barrel		29	48
17	FAD (also NAD)-binding motif	α/β	11	12
18	Flavodoxin-like		11	13
19	NAD(P)-binding Rossmann-fold		13	27
20	P-loop containing nucleotide		10	12
21	Thioredoxin-like		9	8
22	Ribonuclease H-like motif		10	12
23	Hydrolases		11	7
24	Periplasmic binding protein-like		11	4
25	B-grasp	α+β	7	8
26	Ferredoxin-like		13	27
27	Small inhibitors, toxins, lectins		13	27

The number of occurrences of AA_i in the given sequence is shown as n_i (i=1,2,...,20). Then, the components of the composition vector are introduced as:

$$\frac{n_1}{L}, \frac{n_2}{L}, \dots, \frac{n_{19}}{L}, \frac{n_{20}}{L} \quad (1)$$

where, L denotes the length of the sequence [24].

Three identifiers are calculated for each of the five attributes; composition (C), transition (T) and distribution (D). Composition introduces the histogram related to the three groups in a protein. Transition shows the percent

frequencies related to the change between the groups. Distribution indicates the distribution of the attributes in the sequence. For each of these five attributes, totally 3(C)+3(T)+5×3(D)=21 scalar components are formed. As a result, the dimension of feature vector is 125 [5].

2.2 K-Nearest Neighbor Algorithm

K nearest neighbor algorithm is a supervised learning method usually used to classify any data and its implementation is simple. In this method, the distances between the samples in the training set and the samples in the test set are calculated one by one. After the distances have been calculated, the closest K neighbors to the one whose class is to be specified is determined. The class of the sample being tested is determined by the majority method [40]. If the number of samples related to the class is in the majority in K neighbors, the class of tested protein is determined as the class of the majority. Different distance metrics can be used in the KNN method and the user usually defines the value of K from small positive integers. In this study, Euclidean metric was used as distance metric. For the K constant, several different values have been tested in order to evaluate the classification performance, for example 1, 3, 5, 7 and 9 values for K constant are tested, but for the K=3 value a high classification performance has been achieved.

2.3 Self-Organizing Maps

SOM, a model of artificial neural networks and using the unsupervised learning method, was developed in 1982 by Tuevo Kohonen [41]. SOM uses competitor learning algorithm indicated in [42]. In this way, the neurons of the network compete each other to become active and ultimately only one neuron win the race. Here, the basic goal is to transform adaptively the n-dimensional input space into two-dimensional map of the output nodes (see Figure 1). After training is completed, a label is assigned to the nodes with a labeling method.

In this method, jth node (w_j) is in the output layer and input vector x is in the input layer. The distance between the jth node and x is calculated as follows:

$$x = [x_1, x_2, \dots, x_n]^T ; w_j = [w_{j1}, w_{j2}, \dots, w_{jn}]^T \quad (2)$$

$$D_j = \sum_{i=1}^n (x_i - w_{ji}(k))^2$$

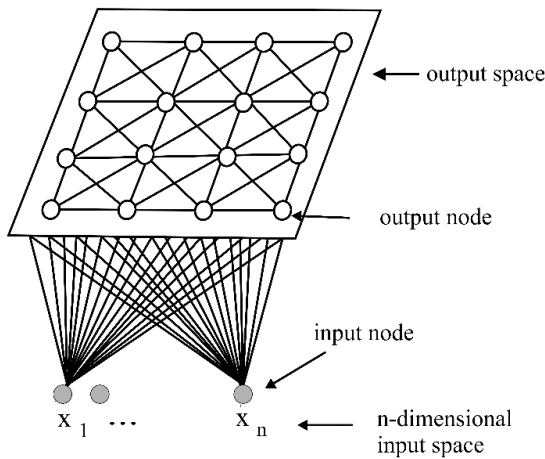


Figure 1. SOM network structure

where n shows the dimension of feature vector.

The weights of the output node and its neighbors are updated as follows.

$$w_{ji}(k+1) = w_{ji}(k) + \eta(k) \cdot (x_i - w_{ji}(k)) \quad (3)$$

Here, η is learning rate and k is the number of iterations. The details of training algorithm of Kohonen's SOM network can be seen in [42].

2.4 Grow and Learn Network

In grow and learn (GAL) network [43], class boundaries are determined by the closest distance measure. The distances between the input vector and all the nodes in the network are calculated. The class of the input vector is determined as the class of the network node closest to this vector. The number of nodes in the network is automatically determined and updated during training if necessary. The network grows when it learns and becomes smaller when it forgets.

The structure of the GAL network is shown in Figure 2. The GAL network consists of two layers. The structure of the nodes in the network is expressed by the following equations.

$$\begin{aligned} D_j &= \sum_{i=1}^n (x_i - w_{ji})^2 \\ E_e &= \begin{cases} 1, & D_e = \min_j (D_j) \\ 0, & \text{otherwise} \end{cases} \\ T_{ec} &= \begin{cases} 1, & \text{if } e \text{ is an exemplar of class } c \\ 0, & \text{otherwise} \end{cases} \\ C_c &= \sum_e E_e \cdot T_{ec} \end{aligned} \quad (4)$$

E_e is the output of the nodes in the first layer, and T_{ec} is the link coefficient that indicates the OR operation that takes only 0 or 1 values.

The first layer is used to find the minimum distance between the node weights and the input vector, while the

second layer is used to define the class to which the nodes in the network belong. The weights in the second layer initially have a value of 0, which is 1 during training. The second layer is used to logically OR the outputs of the same class.

The most important property of the GAL network is that the number of nodes can be automatically specified depending on the structure of the problem (distribution of classes) during training. The structure of the GAL network is highly dependent on the order of the input vectors initially given to the network. There are nodes in the network which are meaningful before, but which have lost meaning with the addition of new nodes to the network. These nodes created during the training algorithm are removed from the network by the forgetting algorithm.

The purpose of the forgetting algorithm is to find nodes that do not affect the success rate of the network when it is

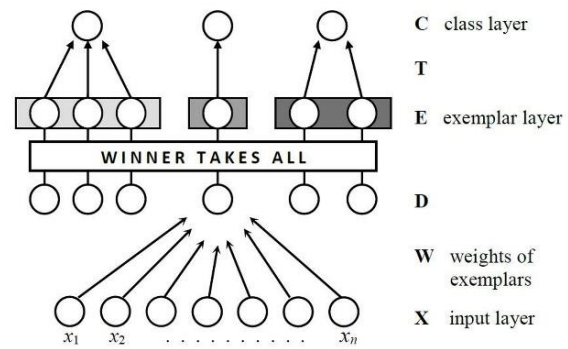


Figure 2. GAL network structure

removed from the network and to remove those nodes from the network. The training and forgetting algorithm of the GAL network [44] is described in detail.

2.5 Divergence Analysis

Divergence analysis is applied to select the best features that do not degrade performance in the desired number of all the features used in problems with two or more classes. In divergence calculations, within-class scatter matrix and between-class scatter matrix are used as criteria for class separation [45].

The selection of the best d feature subset ($d < n$) from n attributes can be done by Divergence Analysis. For example, in this method, firstly one most effective attribute is determined from n features. This feature is a feature that will be placed in the d element final set. After the most effective feature is found, second most effective feature is determined among the remaining $(n-1)$ features so that these two features maximize the separability criterion. This process continues until the d elementary feature set is obtained.

2.6 Performance Analysis

In this paper, to improve the performance, OvO (One-versus-Others) method was used with KNN, GAL and SOM

networks. This method is used in multi-class problems and transforms K-class problem into a two-class problem. One class contains all the proteins belonging to the *i*-th fold that are labeled as positive, and the other class contains all other proteins that are labeled as negative. Thus K binary classifiers are constructed to predict the protein folds.

In the tests for classifying the protein at the fold level, to calculate individual fold success rate (IFSR), the sensitivity, which is mostly used in the literature, was used as seen in Equation (5).

$$IFSR = \frac{\sum True\ Positive}{\sum True\ Positive + \sum False\ Negative} \quad (5)$$

In order to calculate the overall success rate (OSR), the sensitivity formula is generalized for the 27 fold class and the overall success rate is calculated as seen in Equation (6).

$$OSR = \frac{\sum_{n=1}^{27} True\ Positive}{\sum_{n=1}^{27} True\ Positive + \sum_{n=1}^{27} False\ Negative} \quad (6)$$

3. Experimental Results

In the first experiment, KNN classifier was tested for the K=3 value to determine the most significant attribute for protein fold classification. For this purpose, firstly only C (amino acid composition) attribute was used, namely the feature vector only consisted of C attribute and the number of feature vector components was 20. Then S and other four attributes were used individually to determine which attribute is more effective; and the number of feature vector components were 21 for these five attributes. The classification performances obtained for these tests are shown in Table 2. The last column in Table 2 demonstrates the results with the contribution of all six attributes.

According to Table 2 the most significant attribute is C; and the second most significant attribute is S.

In the second experiment, SOM network was used. To train SOM network 15×15 neurons was used; and the neighborhood spread was selected as σ=1, learning rate was determined as η=0.5, lastly iteration number was defined as λ=3000. For each test the average performance over 50 runs is reported. In the last experiment GAL network was used as classifier to determine the most significant attribute for protein fold classification. In the test process, iteration number was determined as 1500. For each test the average performance over 50 runs is given. The results related to performance of SOM and GAL networks are shown in Table 3 and 4, respectively.

According to Table 3 it is observed that attribute C is the most effective and S is the second effective attribute for fold classification. Same conclusions can be made for Table 4.

Table 2. Performance of KNN for each attribute at 27-class protein fold classification

Fold	C	S	H	P	V	Z	All
1	83.3	66.6	66.6	66.6	50	33.3	50
2	33.3	22.2	33.3	22.2	11.1	22.2	33.3
3	35	35	35	20	25	25	40
4	37.5	12.5	25	25	25	25	25
5	77.7	66.6	33.3	55.5	33.3	44.4	66.6
6	33.3	0	22.2	11.1	0	0	0
7	40.9	31.8	31.8	31.8	38.6	36.3	43.1
8	16.6	33.3	8.3	16.6	33.3	16.6	25
9	53.8	15.3	30.7	23	38.4	46.1	46.1
10	33.3	16.6	0	16.6	16.6	16.6	16.6
11	12.5	0	25	37.5	50	37.5	25
12	10.5	21	15.7	26.3	21	26.3	21
13	50	50	25	25	50	50	25
14	50	25	25	25	25	25	25
15	42.8	28.5	28.5	57.1	14.2	28.5	42.8
16	75	70.8	45.8	52	56.2	56.2	81.2
17	50	66.6	33.3	33.3	25	33.3	50
18	23	38.4	15.3	23	15.3	15.3	23
19	29.6	22.2	25.9	22.2	22.2	11.1	18.5
20	41.6	25	50	58.3	33.3	41.6	41.6
21	25	37.5	25	37.5	12.5	25	25
22	41.6	50	50	33.3	50	50	66.6
23	57.1	42.8	42.8	42.8	57.1	28.5	57.1
24	25	50	75	25	75	25	50
25	25	37.5	12.5	12.5	25	37.5	37.5
26	25.9	14.8	14.8	25.9	18.5	14.8	14.8
27	88.8	59.2	25.9	22.2	40.7	18.5	44.4
Suc. Rate	44.4	37.3	30.3	31.9	33.2	30.5	40.5

When considered Table 2, 3 and 4, it can be said that the best classification performance is obtained with GAL; and KNN algorithm is not very well for protein fold classification.

Also, SOM has remarkable results for protein classification at the fold level. Also, it is obvious that the highest success rate can be achieved by the contribution of all six attributes.

Above, to determine the most significant attribute and decrease the dimension of the feature vector the feature blocks including 20 or 21 features were considered. Here, each of the 125 features was individually considered with dynamic programming and the divergence values of each one was calculated. Then, 125 features were put in order according to their significance and; the proteins were classified using the best 10, 30 and 50 features with GAL. The classifier wasn't performed for more than 50 features because as seen from Table 5 very close classification performance (80.9%) to that of Table 4 (81.2%) was obtained. Test results are shown in Table 5.

Table 3. Performance of SOM for each attribute at 27-class protein fold classification

Fold	C	S	H	P	V	Z	All
1	100	83.3	83.3	83.3	83.3	83.3	100
2	77.7	55.5	88.8	88.8	88.8	66.6	88.8
3	55	50	50	45	45	55	80
4	87.5	37.5	75	75	75	62.5	87.5
5	88.8	66.6	77.7	66.6	66.6	66.6	100
6	55.5	55.5	55.5	33.3	33.3	66.6	66.6
7	61.3	54.5	54.5	54.5	54.5	59	72.7
8	50	41.6	41.6	50	50	50	58.3
9	84.6	61.5	53.8	61.5	61.5	53.8	84.6
10	83.3	33.3	50	50	50	50	50
11	62.5	37.5	62.5	62.5	62.5	75	75
12	52.6	36.8	57.8	47.3	47.3	47.3	52.6
13	100	50	50	75	75	75	100
14	100	50	75	50	50	50	75
15	100	57.1	85.7	71.4	71.4	71.4	85.7
16	75	68.7	62.5	62.5	62.5	58.3	72.9
17	66.6	66.6	50	50	50	50	66.6
18	53.8	46.1	46.1	38.4	38.4	38.4	61.5
19	66.6	44.4	37	37	37	37	63
20	75	58.3	58.3	41.6	41.6	58.3	66.6
21	62.5	87.5	62.5	50	62.5	50	87.5
22	66.6	66.6	58.3	58.3	58.3	58.3	75
23	71.4	71.4	71.4	71.4	71.4	57.1	71.4
24	100	50	100	100	100	75	75
25	62.5	62.5	37.5	50	50	50	62.5
26	44.4	55.5	37	44.4	44.4	33.3	55.5
27	100	74	48.1	48.1	48.1	48.1	100
Suc. Rate	69.7	57.2	55.6	54.1	54.3	53.8	73.4

4. Conclusion

In this paper protein fold classification is considered and the most significant attribute and features are determined for protein classification at fold level. Six attributes are tested individually with KNN, SOM and GAL classifiers to determine the effectiveness of them. In KNN, examples are classified based on the class of their nearest neighbors.

SOM uses competitive learning algorithm. In this algorithm the network neurons compete to be activated and eventually only one neuron wins the race. The goal is to train the network and to project the high dimensional data on to low dimensional map in an adaptive way. GAL is an incremental neural network for supervised learning, the number of nodes in the network is automatically determined and updated during training if necessary. The network enlarges when it learns and becomes smaller when it forgets. The results show that the amino acid composition (C) attribute is the most effective attribute and predicted

secondary structure (S) is the second most effective one for all three classifiers at protein fold classification. C attribute gives a reasonable success rate of 71.3% even tested alone with GAL. Also it is obtained that GAL has better classification performance than SOM and KNN.

Table 4. Performance of GAL for each attribute at 27-class protein fold classification

Fold	C	S	H	P	V	Z	All
1	83.3	83.3	66.6	100	83.3	83.3	100
2	77.7	66.6	66.6	66.6	77.7	44.4	100
3	60	75	50	80	90	40	80
4	87.5	75	25	100	75	62.5	87.5
5	100	88.8	55.5	55.5	88.8	77.7	100
6	66.6	44.4	44.4	55.5	66.6	22.2	77.7
7	65.9	93.1	65.9	63.6	68.1	63.6	70.5
8	50	83.3	75	41.6	25	33.3	75
9	92.3	92.3	76.9	46.1	61.5	53.8	84.6
10	66.6	16.6	83.3	33.3	66.6	83.3	66.7
11	62.5	62.5	25	87.5	75	62.5	87.5
12	36.8	47.3	42.1	47.3	78.9	42.1	52.6
13	75	100	75	50	50	100	100
14	75	25	25	25	25	50	75
15	85.7	57.1	85.7	71.4	71.4	57.1	85.7
16	79.1	60.4	83.3	79.1	50	79.1	85.4
17	66.6	75	83.3	75	41.6	50	75
18	61.5	76.9	84.6	69.2	38.4	30.7	84.6
19	66.6	40.7	55.5	59.2	44.4	44.4	81.5
20	83.3	58.3	83.3	66.6	50	100	75
21	62.5	50	62.5	62.5	62.5	62.5	87.5
22	91.6	75	75	58.3	66.6	66.6	91.7
23	85.7	85.7	71.4	85.7	100	71.4	100
24	75	25	50	100	75	75	100
25	50	50	62.5	37.5	37.5	37.5	75
26	51.8	55.5	44.4	48.1	37	25.9	66.7
27	100	70.3	81.4	51.8	37	33.3	100
Suc. Rate	71.3	66.6	65.3	63.4	58.0	54.8	81.2

In addition the effectiveness of the 125 features were studied. In order to reduce the feature vector dimension divergence analysis was applied. The goal of divergence analysis application is that the performance ratio does not change. This method computes divergence values of the features and sorts them by their importance. Here, after divergence analysis, the most significant 10, 30 and 50 features were determined, and they were presented to GAL network. For the most significant 50 features, 80.9% classification performance was achieved, therefore no longer tested. As a result, the feature vector dimension was decreased from 125 to 50 without much decreasing success rate, and so the computational load was reduced.

In the next step of the study, classification performance related to protein folds can be enhanced. The methods can be tested on larger datasets. For better results, new features and new network structures can be analyzed.

Table 5. Performance of the GAL classifier using different dimensional feature vectors formed by divergence analysis

Fold No	Dim=10	Dim=30	Dim=50
1	83.3	100	100
2	88.8	100	100
3	75	85	90
4	87.5	100	87.5
5	100	100	100
6	44.4	77.7	77.7
7	68.1	70.4	70.4
8	33.3	75	75
9	69.2	92.3	92.3
10	66.6	83.3	100
11	75	87.5	87.5
12	47.3	68.4	57.8
13	75	100	100
14	50	75	75
15	57.1	71.4	71.4
16	68.7	87.5	81.2
17	58.3	91.6	91.6
18	61.5	76.9	76.9
19	59.2	74	70.3
20	58.3	83.3	75
21	75	87.5	75
22	83.3	83.3	100
23	57.1	71.4	100
24	50	75	100
25	62.5	75	100
26	37	59.2	55.5
27	81.4	88.8	96.2
Suc. Rate	65.0	80.2	80.9

Acknowledgment

This work is supported by the Scientific Research Project Fund of Cumhuriyet University under the project number TEKNO-011, Turkey.

References

1. Hashemi, H.B., Shakery, A., Naeini, M.P, *Protein fold pattern recognition using Bayesian ensemble of RBF neural networks*, in SOCPAR2009: Malaysia. p. 436-441.
2. Cantoni, V., Ferone, A., Ozbudak, O. and Petrosino, A., *Searching structural blocks by SS exhaustive matching*, Lecture Notes in Bioinformatics. Leif Peterson, Giuseppe Russo, Francesco Masulli (Eds.), 2013. p. 57-69.
3. Protein Data Bank, <http://www.rcsb.org>, last access date: 31.12.2018.

4. Murzin, A.G., Brenner, S.E., Hubbard, T. and Chothia, C., *SCOP: A structural classification of proteins database for the investigation of sequences and structures*, Journal of Molecular Biology, 1995. 247(4), p. 536–540.
5. Dubchak, I., Muchnik, I., Mayor, C., Dralyuk, I. and Kim, S.H., *Recognition of a protein fold in the context of the structural classifications of proteins (SCOP) classification*, Proteins: Structure, Function and Bioinformatics, 1999. 35(4), p. 401–407.
6. Reczko, M. and Bohr, H., *The DEF data base of sequence based protein fold class predictions*, Nucleic acids research, 1994. 22(17), p. 3616-3619.
7. Edler, L., Grassmann, J. and Suhai, S., *Role and results of statistical methods in protein fold class prediction*, Mathematical and Computer Modelling, 2001. 33(12), p. 1401–1417.
8. Ding, C.H.Q. and Dubchak, I., *Multi-class protein fold recognition problem using support vector machines and neural networks*, Bioinformatics, 2001. 17(4), p. 349–358.
9. Bologna, G. and Appel, R.D., *A comparison study on protein fold recognition*, Proceedings of the 9th International Conference on Neural Information Processing, 2002. volume 5, IEEE, p. 2492–2496.
10. Igel, C., Gebert, J. and Wiebringhaus, T., *Protein fold class prediction using neural networks with tailored early-stopping*, , Proceedings of IEEE International Joint Conference on Neural Networks, 2004. volume 3, p. 1693–1697.
11. Huang, C.D., Liang, S.F., Lin, C.T. and Wu, R.C., *Machine learning with automatic feature selection for multi-class protein fold classification*, Journal of information science and engineering, 2005. 21(4), p. 711–720.
12. Jazebi, S., Tohidi, A. and Rahgozar, M., *Application of classifier fusion for protein fold recognition*, Sixth International Conference on Fuzzy Systems and Knowledge Discovery, 2009. volume 7, p.171–175.
13. Chinnasamy, A., Sung, W.K. and Mittal, A., *Protein structure and fold prediction using tree-augmented naive Bayesian classifier*, Journal of Bioinformatics and Computational Biology, 2005. 3(04), p. 803–819.
14. Okun, O., *Protein fold recognition with k-local hyperplane distance nearest neighbor algorithm*, Proceedings of the Second European Workshop on Data Mining and Text Mining in Bioinformatics, 2004. Pisa, Italy, Citeseer, p. 51–57.
15. Shen, H.B. and Chou, K.C., *Ensemble classifier for protein fold pattern recognition*, Bioinformatics, 2006. 22(14), p. 1717–1722.
16. Kavousi, K., Moshiri, B., Sadeghi, M., Araabi, B.N. and Moosavi-Movahedi, A.A., *A protein fold classifier formed by fusing different modes of pseudo amino acid composition via PSSM*, Computational Biology and Chemistry, 2011. 35(1), p. 1–9.
17. Kavousi, K., Sadeghi, M., Moshiri, B. and Araabi, B. N. and Moosavi-Movahedi, A.A., *Evidence theoretic protein fold classification based on the concept of hyperfold*, Mathematical Biosciences, 2012. 240(2), p. 148–160.
18. Markowetz, F., Edler, L. and Vingron, M., *Support vector machines for protein fold class prediction*, Biometrical Journal, 2003. 45(3), p. 377–389.
19. Shi, S.Y.M., Suganthan, P.N. and Deb, K., *Multiclass protein fold recognition using multiobjective evolutionary*

- algorithms*, Proceedings of the IEEE Symposium on Computational Intelligence in Bioinformatics and Computational Biology, 2004. p. 61–66.
20. Shamim, M.T.A., Anwaruddin, M. and Nagarajaram, H.A., *Support Vector Machine-based classification of protein folds using the structural properties of amino acid residues and amino acid residue pairs*, Bioinformatics, 2007. 23(24), p. 3320–3327.
 21. Bindewald, E., Cestaro, A., Hesser, J., Heiler, M. and Tosatto, S.C.E., *MANIFOLD: protein fold recognition based on secondary structure, sequence similarity and enzyme classification*, Protein Engineering, 2003. 16(11), p. 785–789.
 22. Nanni, L., *A novel ensemble of classifiers for protein fold recognition*, Neurocomputing, 2006. 69(16), p. 2434–2437.
 23. Nanni, L., *Ensemble of classifiers for protein fold recognition*, Neurocomputing, 2006. 69(7), p. 850–853.
 24. Chen, K. and Kurgan, L., *PFRES: protein fold classification by using evolutionary information and predicted secondary structure*, Bioinformatics, 2007. 23(21), p. 2843–2850.
 25. Guo, X. and Gao, X., *A novel hierarchical ensemble classifier for protein fold recognition*, Protein Engineering Design and Selection, 2008. 21(11), p. 659–664.
 26. Chen, P., Liu, C., Burge, L., Mahmood, M., Southerland, W. and Gloster, C., *Protein fold classification with genetic algorithms and feature selection*, Journal of bioinformatics and computational biology, 2009. 7(05), p. 773–788.
 27. Yang, T., Kecman, V., Cao, L., Zhang, C. and Huang, J.Z., *Margin-based ensemble classifier for protein fold recognition*, Expert Systems with Applications, 2011. 38(10), p. 12348–12355.
 28. Lin, C., Zou, Y., Qin, J., Liu, X., Jiang, Y., Ke, C. and Zou, Q., *Hierarchical classification of protein folds using a novel ensemble classifier*, PLoS one, 2013. 8(2), e56499.
 29. Aram, R.Z. and Charkari, N.M., *A two-layer classification framework for protein fold recognition*, Journal of Theoretical Biology, 2015. 365, p. 32–39.
 30. Damoulas, T. and Girolami, M.A., *Probabilistic multi-class multi-kernel learning: on protein fold recognition and remote homology detection*, Bioinformatics, 2008. 24(10), p. 1264–1270.
 31. Huang, C.D., Lin, C.T. and Pal, N.R., *Hierarchical learning architecture with automatic feature selection for multiclass protein fold classification*, NanoBioscience, IEEE Transactions on, 2003. 2(4), p. 221–232.
 32. Krishnaraj, Y. and Reddy, C.K., *Boosting methods for protein fold recognition: an empirical comparison*, IEEE International Conference on Bioinformatics and Biomedicine, 2008.
 33. Shen, H.B. and Chou, K.C., *Predicting protein fold pattern with functional domain and sequential evolution information*, Journal of Theoretical Biology, 2009. 256(3), p. 441–446.
 34. Dehzangi, A., Amnuaisuk, S.P. and Dehzangi, O., *Using random forest for protein fold prediction problem: An empirical study*, J. Inf. Sci. Eng., 2010. 26(6), p. 1941–1956.
 35. Dehzangi, A., Amnuaisuk, S.P., Manafi, M. and Safa, S., *Using rotation forest for protein fold prediction problem: An empirical study*, 8th European Conference on Evolutionary Computation, Machine Learning and Data Mining in Bioinformatics, 2010. p. 217–227.
 36. Wang, R. and Gao, X., *A Two-Layer Learning Architecture for Multi-Class Protein Folds Classification*, Interdisciplinary Research and Applications in Bioinformatics, Computational Biology, and Environmental Sciences, 2010.
 37. Dehzangi, A. and Karamizadeh, S., *Solving protein fold prediction problem using fusion of heterogeneous classifiers*, INFORMATION, An International Interdisciplinary Journal, 2011. 14(11), p. 3611–3622.
 38. Suvarnavani, K., Rafiah, S.B. and Kamiseti, N.R., *Multiclass classification for protein fold prediction using Smote*, International Journal of Advanced Research in Computer Science and Software Engineering, 2011. 2(11), p. 290–296.
 39. Bae, S.E., Jung, S., Ahn, I. and Son, H.S., *Protein fold classification with backbone torsional characters using multi-class linear discriminant analysis*, J Proteomics Bioinform, 2013. 6, p. 148–152.
 40. Duda RO, Hart PE. *Pattern Classification and Scene Analysis*. John-Wiley&Sons. Inc. 1973.
 41. Kohonen, T., *Self-Organized Formation of Topologically Correct Feature Maps*, Biological Cybernetics, 1982. 43(1), p. 59–69.
 42. Polat O. and Dokur Z., *Protein fold recognition using self-organizing map neural network*, Current Bioinformatics, 2016. 11, p. 451–458.
 43. Alpaydın E., *Neural models of incremental supervised and unsupervised learning*, Ds. Thesis, Ecole Polytechnique Federale De Lausanne, Switzerland, 1990.
 44. Polat O. and Dokur Z., *Protein fold classification with grow-and-learn network*, Turk J Elec Eng & Comp Sci, 2017. 25, p. 1184–1196.
 45. Ölmez, T., Dokur, Z. *Uzman Sistemlerde Örüntü Tanıma: Yapay Sinir Ağları, Genetik Algoritmalar, Bulanık Mantık, Makine Öğrenmesi* ders notu.

**Research Article**

Resource based view in the Turkish construction sector and resource selection with ANP technique

Ozlem Geylani ^{a,*}  and H. Attila Dikbas ^b 

^aIstanbul Technical University, Maslak Campus, Istanbul 34467, Turkey

^bIstanbul Medipol University, Kavacik Campus, Istanbul 34810, Turkey

ARTICLE INFO*Article history:*

Received 11 September 2018

Revised 20 October 2018

Accepted 25 October 2018

Keywords:

ANP

Building information

Modelling

Construction sector

Resource based theory

Resource selection

ABSTRACT

The competitive environment observed in the international construction sector has reflected in the Turkish construction sector through joint projects. In order to achieve competitive advantage in joint construction projects and to achieve success against national competitors, it is necessary to review resource selection strategies. In this context, the main purpose of this study is to look at the resource selection criteria of the construction companies in terms of International Resource-Based Theory. The 77 resources of the construction firms reviewed during this study were evaluated by taking into consideration their ability to be strategic resource and their competitive advantages. In this study, the Building Information Modelling (BIM) tools and technique, which has been spoken as a resource that will benefit competition in Turkey in recent years, was discussed as an objective and the research problem was whether BIM is a strategic resource or not. In the resource evaluation process, resources should be listed and evaluated by firm employees and managers. In the survey conducted for this purpose, construction firms were asked to select the resources they already had from the resource pool of the research and to score only 9 important resources. To establish vertical hierarchy and horizontal relationships, the obtained results of the evaluation were analyzed by using the Analytical Network Process (ANP) method. In the established hierarchy, the objective was BIM and the selection criteria were VRIO criteria including Valuable, Rare, Inimitable and Organization, which are the resource selection criteria of the Resource-Based Theory. The scores obtained as a result of the survey study applied to the Turkish construction firms were reflected to the ANP technique. While the data processed with the Super Decisions software provides numerical and quantitative comparisons of resources in the construction sector, it also points to a selected set of resources that can work with BIM.

© 2019 Advanced Researches and Engineering Journal (IAREJ) and the Author(s).

1. Introduction

BIM systems and tools used in the Turkish construction sector over the last decade have started to be among the resources used by the construction firms thanks to international projects. Given the development level of the firms, while some firms have a BIM system, the software programs that BIM offers take place as a tool in some other firms. At national or international level, BIM systems and its tools are among the firms' targets as a resource that makes a difference with its absence or presence, and even as a resource that some firms see in their competitors and feel the lack of it. Accordingly, even if they use terms such as administrative strategies, project management, human resources, innovation, vision and mission, Turkish

construction firms have resources that they need support of them to their strategic resources, which they have chosen or created in line with their missing resources or the administrative strategies they have; however, they cannot put these resources into their place.

When firms are defined as organizational structures, resources and capabilities, we start to define them by looking at their internal structures. Moreover, the strategy applied by a construction firm in order to gain competitive advantage depends on everything involved in its internal structure.

In determining competition strategy by taking into account the economic-based literature, there are three different strategies that the firms applied in order to gain a

* Corresponding author. Tel.: +90 212 285 30 30.

E-mail addresses: ozlemgeylani@gmail.com (O. Geylani), hadikbas@medipol.edu.tr (H.A. Dikbas)

ORCID: 0000-0003-4951-7716 (O. Geylani), 0000-0002-1753-5031 (H.A. Dikbas)

competitive advantage; 1. Total cost strategy, 2. Differentiation strategy and 3. Focus strategy. Total cost leadership is defined as the making production of a firm at the lowest cost compared to its all competitors on the market. On the other side, in comparison to their competitors, the effort of firms to produce innovative and high-quality products is called differentiation strategy. Finally, the focus strategy can be defined as the attempt of firms to gain a competitive advantage in a specific product, a specific customer group or a specific market through narrowing down the target market in which they compete.

According to Michael Porter [6], who is pioneer of the concept of competitive strategy, a business must analyze the sector before developing a competitive strategy and determine a strategy that is appropriate for that sector. Thus, the firm will gain a position in which it will be able to protect itself against its competitors in the sector. The firms' acquisition of this opportunity is called position approach, industry-based approach and opportunity approach.

Contrary to Porter's opinion about strategies [6], a resource-based view explaining the situation in which firms aim to gain competitive advantage by focusing on their own internal structures and their own resources and capabilities rather than focusing on the sector has emerged [1].

The resource-based view aims firms to determine their own resources and capabilities. In this respect, when compared to the resources that are not in the hands of their competitors, the current situation will provide competitive advantage to the firms.

Looking at the opportunity-based approach, we face the fact that firms must first analyze the sector they are in and they must pay attention to it when determining their strategies in order to gain competitive advantage.

Among these two different approaches, in order to examine the Turkish construction firms in this study, the Resource-Based Theory (RBT) was preferred. In this context, while the resource-based theory was constituting the basis of the study, the BIM system and tools were selected as a resource for the Turkish construction firms and the firms were asked about their opinions on this resource.

The purposes of this study can be summarized in three items;

1. The fact that RBT is of great importance that can provide benefit for Turkish construction firms when the current strategies and resource selection criteria are examined
2. Listing the most important or strategically defined resources of the firms in line with the answers obtained from the interviews conducted with the construction firms. Matching the resources with the VRIO criteria and production

of the best resource alternatives or combinations with ANP technique.

3. Examination of whether the BIM system and its tools are a strategic source for Turkish construction firms or not.

The results obtained in line with these purposes will be beneficial in the future studies in terms of the key performance indicators and related measurements by listing the result of an original resource selection in construction firms.

2. Background

Edith Penrose (1950) and other researchers [4], [5], [6], [7], [11], have defended for years that in order for firms to grow and develop in an organizational sense, the current situation analysis should be done, industry analysis should be done and strategies should be focused on. Porter initially advised the opportunity-based approach that suggested focusing on market conditions and the environment [6]; later, by combining it with the firm's own structure, he has started to advocate SWOT analysis. While revealing the strengths and weaknesses of the firm, Porter has also foreseen to consider the opportunities and threats that the sectoral conditions, in which the firm is located, present. In addition, Porter evaluated the performance of the firms in terms of competitive insights by taking into account their product and sector structures and the market position they were in [6].

In the late 1980s, Jay Barney stated that the conditions required to gain firm performance and competitive advantage were associated with the firm resources and capabilities. If the resources are the building blocks of the firms, it is necessary to look at the internal structure of the firms in order to identify a resource [1]. By determining objectives for resources and capabilities such as being a valuable resource, being a rare resource, and not being imitated, this strategy, which is described as the resource-based view, has defined the firm as an organizational structure. On the other side, when the resource-based view was considered as a theory, a tool that evaluates the resources emerged. This tool, which is known as the acronym VRIO (V=Valuable, R=Rare, I=Inimitable, O=Organization), divides resources and capabilities into stages step-by-step in order to gain competitive advantage. If a resource meets all the criteria, it means that competitive advantage has been achieved. Sustainability of this depends on structure of the organization and its capability.

All the resources of a firm are more than its strategic resources [2],[3],[12]. Therefore, the protection of resources' strategic resource characteristics depends on the firm's efforts and organizational competence. Barney defines resources as *“everything, such as all assets, abilities, competencies, organizational processes, firm*

characteristics, knowledge, and know-how, that can be controlled by the firm and that provides efficacy and allows them to use strategies providing efficiency.”[3] This opinion is a strategic solution that makes firms to gain a competitive advantage. Here, another issue to be known is that many of the strategic resources are specific to the firm and the firm must be able to establish communication with these resources at the highest level and keep the resources up to date according to the current circumstances and requirements of time. In order to do this, the firm needs to consider the official business processes and production functions together with their strategic resources. Protective measures are essential for the characteristics of the resources. These measures are provided by isolation mechanisms [3].

Considering the same resource selection criteria for construction firms, the resources and capabilities that the firm has in the current situation should be determined, and it should be understood which resources are defined as strategic resources.

3. Methodology

This study begins with a literature review explaining RBT and previous assumptions about competitive strategies. In the context of this research, a face to face interview study was held to determine the resources that might be possessed by Turkish construction firms, whether they had BIM system and tools or they might just aim to establish this system only for using BIM based software. During this research, the evaluation of the resources was done by applying Analytical Network Process (ANP) method in order to construct a logical hierarchy with the definition of the aim, criteria and alternatives. Again, the purpose of the research is connected to that hierarchy and it is questioning the best strategic resource or resource groups in connection with BIM.

It was decided that the best method for this evaluation was the ANP method because this study is a unique study combining ANP method with RBT in the perspective of the construction sector and its actual resources. Moreover, VRIO tool, which is related to RBT, will be a guide in providing competitive advantage by choosing the best resource alternatives specifically to each construction firm in line with the firm’s strategy.

3.1 Decision-Making Process

Data for this research were collected through a survey study that lasted for two years. A total of 41 Turkish construction firms, which were listed in the top 250 contractors list of the ENR 2015 report, constituted the units of analysis of this study.

Comparing to all firms, it was seen that just 10 firms were using BIM system or at least its tools. In order to measure the resources as the number or type, 74 potential

construction resources were chosen to ask the interviewees. This resource list included BIM and its tools. In addition, within the context of RBT, the VRIO tool that examined whether their resources were valuable, rare and inimitable or whether their organizational structure was capable to use them effectively was explained to the firms. After the collection of the appropriate data about the resources of the firms, a logical hierarchy leading to the decision-making process was able to emerge. Furthermore, if there are more than one alternatives in the decision making process, criteria, alternatives and the relations with the aim should be determined first on the way of competitive advantage. There are analytical decision-making methods used for this aim. These are Analytical Hierarchy Process (AHP) and Analytical Network Process (ANP). In AHP method, a relative measurement theory based on the pairwise comparison of the pre-defined criteria and alternatives is preferred. The logic of this method includes pairwise comparison matrices showing the resources as alternatives. In the AHP method, by preparing pairwise comparison matrices, ratios of dominance between the two alternatives are determined via an evaluation based on absolute numbers in the scales between 1 and 9. On the contrary, using the ANP method, not only a comparison between tangible resources is made but also a comparison between intangible resources can be made by depending on the opinions of knowledgeable and expert people [15].

In the decision-making process with ANP, the relationship between factors should also be considered. In other words, because the solution of the problem is not only in hierarchical order, but also in the relationship between the factors, the ANP method provides a more realistic analysis [8], [9], [10]. Also, the AHP structure is similar to a one-way communication system, but the ANP provides more detailed communication including vertical and horizontal connections.

Network structure provides opportunity to rate and grade the alternatives as ineffective, low-impact, high-impact, very high-impact [10]. So, before evaluating the resources, six main steps used for developing decision-making model by applying ANP approach should be defined. Each step of the ANP is described in detail below.

Step 1: Definition of the decision-making problem

Step 2: Identifying relationships

Step 3: Making pairwise comparisons between criteria and alternatives

Step 4: Calculating consistency

Step 5: Creating super-matrix

Step 6: Determining the best alternative

In this study, the use of ANP method was preferred because both the tangible resources and the intangible resources were subjected to pairwise comparisons. However, AHP builds a hierarchy, creates a one-way

model and when making the best decision, it uses priority order for effective factors. Good decision making process includes some steps such as thinking, planning and analysis. If the conditions required for gaining competitive advantage are also added when the evaluation criteria of resource-based theory are added to the resources selected with the firm strategy, determining the VRIO criteria as criteria in the ANP hierarchy is seen reasonable in terms of creating both the criteria and the matchup of the resources.

3.2 Resource Based Theory and ANP

As Barney pointed out, RBT aims to identify and examines resources in a firm as tangible or intangible terms. Since these resources are different from each other with their qualifications, quantities and importance levels, there is a need for an investigation about which resources will benefit from the competitive strategy that is chosen by the firm. [1], [2] [3].

ANP method was used during this research because it helps to investigate the selected resources in line with the survey questions. In order to do that, a total of 30 firms were visited within 2 years in which surveys were completed through face to face interviews. Firms were asked about their strategies and each firm was asked to make a strategic choice from 74 resources to identify their own 9 sources that they believed they are effective.

As it is known, the ANP method creates a network and a vertical hierarchy that are established at the beginning of the decision making process. Then, a horizontal logical link and relationship arrows are defined to show the relationships. Under these circumstances, it is necessary to use the criteria that ANP provides in order to combine it with RBT, while aiming to find the resource or resource groups that will provide competitive advantage.

VRIO, the criteria for the RBT, is a contributing tool at that phase; starting with the selected resources, the adjectives of VRIO (valuable, rare, inimitable) may be used to classify them. Furthermore, each resource may not be a strategic resource, but it may have a potential to transform into a strategic resource. VRIO, as it is mentioned before, evaluates the resources with yes-no question types. If the resource is valuable, its rarity will be questioned as a second step. After that, the potential of its inimitability is important. Finally the organizational effectiveness related to the usage of the resources will matter.

3.3 The ANP Model

First of all, as mentioned previously, determining the problem is the first step of the ANP method. The problem here is that whether BIM is a strategic resource selected during the decision-making process or not.

On the other side, the second step is to identify

relationships. The relationships should be defined between clusters containing alternatives (resources), between criteria and clusters, and finally between clusters, aim and criteria. When the aim of the hierarchy is defined as BIM and if the VRIO criteria and alternatives are determined as resources, a network hierarchy will have been established by showing the relationships. VRIO is defined as criteria of our ANP model and alternatives are defined as resources of a construction firm.

A notable point in the ANP method is the importance of criteria. This importance does not affect the importance of the resources; however, it should not be forgotten that alternatives can affect the criteria [10]. In the context of this study, we can say that the VRIO criteria are a precondition because they are required to establish the hierarchy and network. Reason of this is that the alternative cluster comprised of 9 resources belonging to each criterion actually defines the quality level of resources that will contribute to the aimed competitive advantage. For example, in terms of the likelihood of transforming into a strategic resource and making BIM strategic resource, there are differences between pairing of a resource from a valuable resource list with BIM and pairing an inimitable resource with BIM.

The dependence between nodes (resources) in a cluster (criteria related to the resource list) is defined as an inner dependence and the dependence between two clusters is defined as an outer dependence. The feedback loop is another term for the ANP method and clusters containing nodes. The relationship of a cluster with itself creates a feedback loop. By the way, an ANP model that contains a feedback structure takes the name of the feedback model. Thus, clusters can question themselves in a complex problem [10].

Because the alternative cluster in the subsets (sub-clusters) also contains dependencies, they must depend on the highest level (that is the target level) from the lowest level. Thus, in the decision-making method of ANP, alternatives and resources can establish a pairwise comparison matrix. Pairwise comparisons are equal in terms of number and the scoring status was pre-determined by questionnaires. The purpose of this was to determine the level of dominance among alternatives. While the firms were asked which resources were valuable, rare and inimitable, they were also asked which resources they used organically and productively. The real and productive dominance also show the difference between all resources. Therefore, the resources listed between 1 and 9 by firms were evaluated by firms using scales between 1 and 9. The result of scoring showed the dominance of resources in pairwise comparisons from the sources that meet the dual criteria.

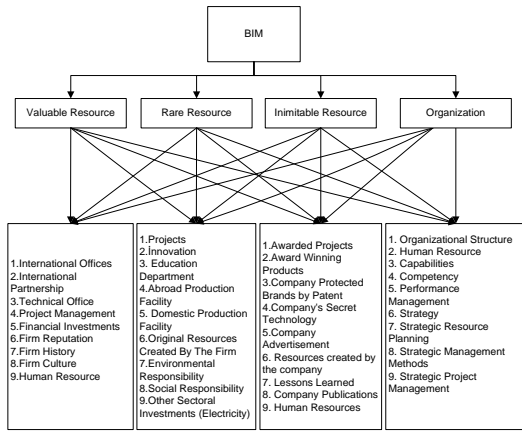


Figure 1. RBT related ANP model with resources.

On the ANP model, the second step is to define relationships. In the previous section, the relationships were defined by establishing links between BIM, criteria and alternatives (resources). On the other side, the third important step is the requirement to make comparisons by establishing links between the criteria and alternatives. The resource lists, which includes BIM system and tools, shown in Figure 1. were essentially chosen by the authors by the time Turkish construction firms tended to use them and these resource lists constitutes the clusters defined in the literature. Accordingly, these resources in each cluster are the nodes in terms of terminology. When defining relationships, it should be noted that the dependence between nodes in a cluster is defined as inner dependence. Moreover, the dependence between two clusters is considered as outer dependence.

Additionally, the feedback loop between the resources in clusters containing alternatives will also be identified by the relationship within them. If resources work together in the same cluster, a feedback is created for each cluster (Figure 1,2,3,4,5).

A simple pairwise comparison matrix is shown in Table 1. If it is assumed that A is a criterion, a comparison can be made between the resources defined as R1, R2, and R3... In the list of references on the left column, R1 is scored between 1 and 9. This scoring can be done for all references. Thereby, this scoring is linked to creating a pairwise comparison matrix [9].

In addition, there is also a software that uses the ANP method. Super Decisions 2.6.0-RC1, which is one of those software, was chosen in order to make resource evaluation for this research. This software allows to create a resource priority list after completion of pairwise comparisons. The resource priority list that is created within this scope and that contains the BIM system and tools is shown in the Table 2.

Table 1. Adaptation of the simple pairwise comparison matrix to the resource selection. [9]

A	R1	R2	Rn
R1	1	4	9
R2	1/4	1	6
R3	1/9	1/6	1

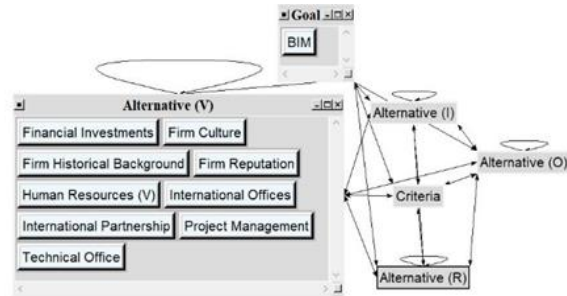


Figure 2. The relation of valuable resources and other resources

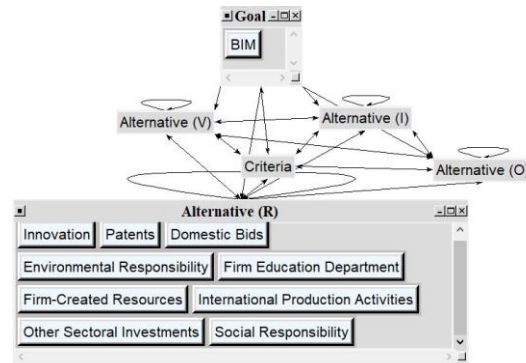


Figure 3. The relation of rare resources and other resources

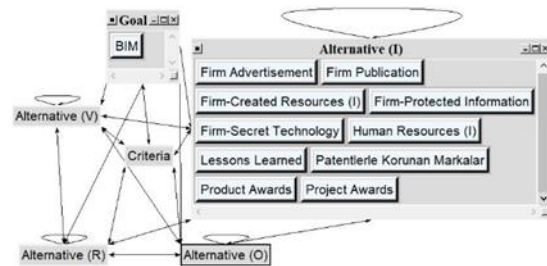


Figure 4. The relation of inimitable resources and other resources



Figure 5. The relation of the organization and other resources

3.6 Calculation of the Consistency

When making comparisons and scoring are performed by using the AHP method, the evaluation of the matrices or written evaluation can be made. No matter what calculation tool is used, the consistency ratio must be included in this calculation [19]. In the context of this study, making the calculation, if “n” is accepted as the number of criteria, random index numbers should be defined. Thus, the eigenvalue is defined by λ . while the largest eigenvalue λ_{max} in the created square matrix, the following equations are used.

Formula used in calculation of the consistency ratio (CR):

$$\text{Consistency Index (CI)} = (\lambda_{max} - n) / n - 1$$

$$\text{Consistency Ratio (CR)} = \text{Consistency Index (CI)} / \text{Random Index (RI)}$$

In this calculation carried out with Super Decisions software, the consistency ratio was accepted as ≤ 0.1 .

3.7 Creating a Super matrix

Creating a super matrix is one of the required steps used to prioritize the resources. Matrix tables divided into three groups (weighted, non-weighted and limit super matrix) are prepared [10]. Moreover, the weighted super matrix is the value that the sum of each column is equal to 1 in the prepared non-weighted super matrix table [8], [9].

The third and final step is to create a limit matrix by increasing the intensity of the weighted Super matrix until its lines change [9], [10]. As a result, for the aim of this study, basic super matrices and limit matrix tables were prepared by using Super Decisions 2.6.0-RC1 software.

4. Results and Discussion

The findings of this study indicates that the value of Turkish construction firm resources with strategically thinking from the view of RBT. Here, the firm resources including BIM were been asked to construction experts and with their comments, an evaluation was tried to be made. However, a resource and its real value will take years to understand in an organization, competitive advantage on the other hand may be gained by the construction firms which are regarded as the organizations here, that they should be capable of using their resources effectively. Moreover, during the time, the technological changes as innovation in construction industry will also affect the strategic value of the resources, so according to the RBT inimitable resources may become a common resource at some time if the firms do not protect their resources against the changes that time brings. Today, BIM system and tools are valuable resources for construction firms and the outputs that are produced by project teams, may help these firms to gain competitive advantage but its sustainability is related to the effort of the firms. So, construction experts' comments are important to protect the strategic position of the resources.

This study discussed and analyzed the potential of BIM system and tools to become a strategic resource for Turkish construction firms. In this study, the applied ANP technique and Super Decisions 2.6.0-RC1 software have been very effective in comparison of 36 firm resources used in Turkish construction sector. More importantly, the RBT, which presents a theoretical background for the research, and VRIO tool have been paired with the ANP technique in order to decide the complex resource selection problem. According to the research findings, examining the table of priorities, it is figured out that if it is strategically seen and associated with BIM, the most effective resource is human resources (in organizational management) with 41.09 % in the ranking. The other important resources are financial investments (31.02%), in-service training (30.91%), organizational structure (27.21%), firm advertisements (25.69%), firm recognition (17.93%), protected information (17.64%), created resources (16.75%), innovation (15.81), Project Management (12.59%), performance management (according to management) (11.17%), and firm's secret technology (10.87%), respectively, these results also show the relation with BIM, if the construction firm are able to match their strategic resources with it.

As a result, the relationship between BIM, strategic resources and percentage values strengthens the opinion that BIM is a strategic resource for Turkish construction firms. Moreover, further research about BIM and other resources may be considered as performance indicators for a construction firm.

5. Conclusion

This study is expected to be beneficial both for the construction industry and for the academia. The results of this research will facilitate to have the big picture of the resources evaluation phenomenon in the construction industry. This is vital since many construction firms had bankruptcy in 2015 during the research interviews were held and at that time strategical way of thinking and the guidance of researchers. Organizations such as construction firm on the other hand should better tailor their solutions for themselves with their strategies for resource choosing criteria. Also, this research will unearth any possibility of firm resources that may related with BIM system and tools are able to support the way to gain competitive advantage from the beginning phase of the resource selection in construction firms.

Until now, no study has attempted to investigate the RBT in construction industry with such comprehensiveness that connected with BIM. With this research, many researchers will be able to get information about construction expert ideas about the construction firm resources. In addition, the effect of RBT on resource selection might provide a good knowledge on the decision strategic resource selections.

Table 2. Priorities of Resources Calculated with Super Decisions 2.6.0-RC1

Priorities Table		
Resource Name	Normalized By Cluster	Limiting
Inimitable (criteria)	0.44570	0.111424
BIM	0.33333	0.083333
Human Resources (O)	0.41097	0.075482
Firm Advertisement	0.25693	0.057135
Firm Education Department	0.30910	0.053600
Financial Investments	0.31022	0.052908
Organizational Structure	0.27219	0.049992
Firm-Protected Information	0.17643	0.039234
Organizational (criteria)	0.13600	0.033999
Firm-Created Resources (I)	0.14702	0.032694
Firm Reputation	0.17931	0.030581
Firm-Created Resources	0.16758	0.029059
Innovation	0.15843	0.027473
Other Sectoral Investments	0.14667	0.025433
Firm-Secret Technology	0.10875	0.024183
Project Management	0.12595	0.021480
Performance Management (O)	0.11173	0.020522
Firm Historical Background	0.11687	0.019932
Firm Publication	0.08140	0.018102
Project Awards	0.06917	0.015381
Patents	0.08298	0.014389
Rare (criteria)	0.05392	0.013481
Lessons Learned	0.05966	0.013268
Technical Office	0.07511	0.012810
Strategy	0.06707	0.012318
Human Resources (I)	0.04821	0.010722
Product Awards	0.04552	0.010123
Firm Culture	0.05504	0.009387
Human Resource (V)	0.05271	0.008990
International Partnership	0.05110	0.008715
Valuable (criteria)	0.03105	0.007762
Strategic Resource Management	0.04207	0.007726
International Production Activities	0.04421	0.007667
Social Responsibility	0.04165	0.007223
International Offices	0.03369	0.005745
Expertise	0.03018	0.005543
Domestic Bids	0.02957	0.005127
Strategic Management Methods	0.02594	0.004765

References

1. Barney, J.B., *Firm Resources and Sustained Competitive Advantage*. Journal of Management, 1991. 17: 99–120
2. Barney, J.B., *Resource-Based Theories of Competitive Advantage*. Journal of Management, 2001. 27: 643–650.
3. Barney, J.B., "Resource-Based Theories of Competitive Advantage: A Ten-Year Retrospective on the Resource-Based View. Journal of Management, 2001. 27: 643–650.
4. Chandler, A., *Strategy and Structure: Chapters in the History of the American Industrial Enterprise*. 1962, Cambridge, MA: MIT Press.
5. Penrose, E., *The Theory of the Growth of the Firm*. 1959, London: Basil Blackwell.
6. Porter, M.E., *Competitive Strategy: Techniques for Analyzing Industries and Competitors*. 1980, New York: The Free Press.
7. Rumelt, R.P., *Towards a Strategic Theory of the Firm.* In "Competitive Strategic Management. 1984, ed. R.B. Lamb, pp 566–70. Englewood Cliffs, NJ: Prentice-Hall.
8. Saaty, T.L., *Decision Making with Dependence and Feedback: The Analytic Network Process*. 1996, RWS Publications, Pittsburgh, 24–29.

9. Saaty, T.L., *Fundamentals of the Analytic Network Process*. International Symposium AHP 1999, Japan, 13–16.
10. Saaty, T.L., *Decision Making For Leaders*. 2000, RWS Publications, Pittsburgh, 47– 52.
11. Selznick, P., *Leadership and Administration*. 1957, Harper & Row: New York.
12. Wernerfelt, B., *Small forces and large firms: Foundations of the RBT*. Strategic Management Journal, 2013. 34(6): 635–643.



Research Article

The evaluation on the effect of effective and repetitive vibration to compressive strength with the fuzzy method

Mahmut Kahraman^a  and **Ferhat Pakdamar^{b, *}** 

^aGebze Technical University, Department of Architecture, Gebze, Kocaeli/TURKEY

^bGebze Technical University, Department of Architecture, N Blok 1-17, Gebze, Kocaeli/TURKEY

ARTICLE INFO

Article history:

Received 25 March 2018

Revised 20 October 2018

Accepted 27 November 2018

Keywords:

Vibration

Repetitive vibration

Compressive strength

Pressure endurance

Fuzzy logic

ABSTRACT

In this study, it was aimed to develop alternative prediction models for estimating the compressive strengths of concrete with different concrete classes and different slump values. An experimental study based on repetitive vibration application was performed in the laboratory environment and prediction models were developed on the basis of fuzzy logic with reference to this experimental study. In the experimental study, the concretes which are in C20 and C35 and have K3, K5 settlement values were produced and determined compressive strengths of the concretes which hides in suitable conditions after 30 minutes, 60 minutes and 90 minutes, 7 and 28 days, respectively. Other results are evaluated with considering the 28 day concrete strength of concretes which once-vibrated. The concrete pressure endurance of the vibration time and its repeated applications are predicted by the graphical representation of fuzzy logic methods. The compressive strength values obtained from the prediction models and the compressive strength values of the experimental data were compared and evaluated. As a result, it is seen that the prediction of the concrete pressure endurance with the fuzzy model is possible and the fuzzy model is predicted more accurately to the concrete pressure endurance.

© 2019 Advanced Researches and Engineering Journal (IAREJ) and the Author(s).

1. Introduction

Throughout the world, as building material concrete is being used most commonly [1]. After its formula prepared according to its project, since the preparation of the ordered concrete consists of the stages such as preparation of the concrete in concrete plants, its transportation to concreting area, placing them into the molds according to the standards, it is certain that each of these stages affects the concrete resistance excessively. The preparation of correctly formulated concrete in the plant is very practical because it is made over computer programs today [2]. The ordered concrete can be produced in large quantities and with different specifications via fabrication system and can be reached to the construction site [3].

Today, depending on the developments in ready mixed concrete technologies, their pressure endurance generally provides good results. Generally, there is no problem faced

with the loss of concrete strength when it is prepared via special computer programs in the plants and also during its transportation by horizontal mixers [4]. In addition, due to the use of high quality pumps in the ready-mixed concrete sector and employment of skilled technical personnel human-caused faults are minimized and very good results are obtained from pressure endurance of the 7 and 28 days old samples taken from the concrete on the construction site [5]. The placement of the concrete into the mold, repeated vibration applications and curing applications seriously affect the strength of the concrete [6]. Since the determination of vibration duration and repeated vibration applications on the concrete are completely dependent on the human factor, by reason of the fact that these intervals and applications are not made according to a certain standard are still seen as a serious problem for the concrete castings in the working sites [7].

* Corresponding author. Tel.: +90 262 605 1614; Fax: +90 262 653 8495.

E-mail address: mahmutkahraman23@gmail.com (M. Kahraman), pakdamar@gtu.edu.tr (F. Pakdamar)

ORCID: 0000-0001-8022-3236 (M. Kahraman), 0000-0002-5594-3095 (F. Pakdamar)

As a result of these casting deficiencies, it causes the loss on the concrete strength and the segregations and deterioration on the concrete surface causes serious quality losses, repair costs and loss of trust of the client companies.

A number of up-to-date methods can be applied for correct placement of the concrete into the molds and accurate determination of the application limits for repeated vibration [8]. Fuzzy solutions of engineering problems, artificial neural networks, genetic algorithms.

By subjecting two different concrete grades that have two different slump features to a revibration, the models calculating their compressive strengths have been tried to be identified and modelled by fuzzy logic methods [10].

Fuzzy logic modeling which has started to be one of the widely used methods is a new mathematical method that has been found by L.A. Zadeh in 1965 and called "Fuzzy Sets". This study of Zadeh L.A. was presented as published in the magazine named Information and Control in 1965. Since then, fuzzy cluster theory was quickly developed by both Zadeh himself and numerous researchers [11].

2. Fuzzy Logic

Fuzzy Logic is a method used to identify and reveal unknowns in an existing system. The fuzzy functions adjust the data at hand to reduce these uncertainties. In addition, fuzzy logic is also being used for making decisions easier to control a system [12].

The most significant difference of fuzzy systems occurs when the inputs are not numerical. The non-digital data is composed of a blurring unit for blurring by processing and a clearing unit for digitizing the blurred output [13].

A common fuzzy inference system has 4 components as shown in Figure 1. These are fuzzification, rule base, inference motor and defuzzification [14].

The membership function for each data entered by fuzzification is transformed into one or more membership functions. It includes the rules covering all possibilities of fuzzy relations between inputs and outputs according to fuzzy rule base. [15].

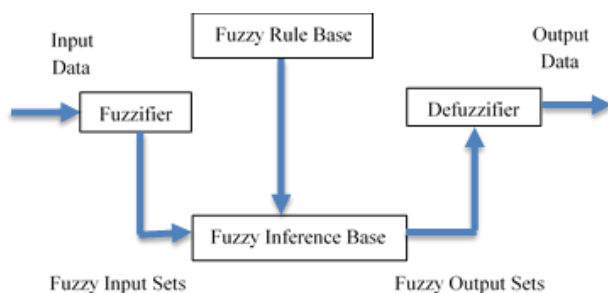


Figure 1. The structure of the fuzzy inference system [15].

These rules are expressed in the form of "if-so" format. The fuzzy inference motor, takes all fuzzy rules in the fuzzy rule base and the findings into consideration to be able to obtain the correct result from the inputs in the transferred set [16].

2.1. Evaluation of Concrete Grades via Fuzzy Logic Method

The following experimental study charts Table 1-4 and Figure 2 are taken from the article [17]. It was taken from the article study. In this section, two different classes of concrete have been tried to be constructed with fuzzy logic method to estimate the repetitive vibration and compression and compressive strength of two different concrete classes [18].

2.2. Experimental Study

Effect of first and second vibrations on the compressive strength in comparison with self-consolidating concrete was examined on the experiment samples which are in the quality classes of C20 and C35 and have slump values of K3 and K5 during the experimental study made in the laboratory environment. In the experimental studies, PC 42.5 type cement, natural Sakarya sand as aggregate and crushed stone aggregate which is also supplied from the same region were used. In the mixture, 0.8% ratio of plasticizer was used [17].

Mixture granulometry is chosen as to be closer to B32. The properties of the cement used are shown in Table 1. The concrete used in the study were C20 and C35 class concrete which were taken from the production facility and they were determined in a way that to obtain two different (K3 and K5) slumps. The compositions of the concrete produced are given in Table 2 and the slump ratios in Table 3 [17]. One side is 150 mm long cube samples from each series were produced [19], [20].

Experiments were carried out by taking samples for three different series for two different concrete grades. For the C20 class concrete, no vibration was applied to the concrete during the first sampling, and the settlement was achieved with its own weight. The concrete in the first series were subjected to vibration for 30 seconds immediately after the production. A single vibration was applied for the second series and for the other samples, a second vibration was applied for 20 seconds after 30, 60 and 90 minutes [17]. This application was repeated for C35 concrete too in the same way and the figures in Table 4 were obtained.

Table 1. Properties of the cement used in the experiment (PC 42.5)

Chemical Properties	Obtained Values	TS-19	
		LEAST	MOST
Chloride(Cl) %	0.0046		
Sulfur Trioxide(SO ₃) %	2.26		
Magnesium Oxide(MgO) %	1.47		
Loss of Ignition %	1.28		
Insoluble Solids %	0.30		
C ₃ A %	-	-	-
2 C ₃ A + C ₄ AF %	-	-	-
PHYSICAL PROPERTIES			
Volume Expansion (mm)	6.0	-	10.0
Specific Surface (m ² /gr)	3598	2800	-
Initial Setting (hour:min)	03:00	01:00	10:00
End of the Setting (hour:min)	04:00	-	-
Pressure Endurance for 2 days (MPa)	21.6	20.0	-
Pressure Endurance for 7 days (MPa)	37.0	31.5	-
Pressure Endurance for 28 days (MPa)	51.9	42.5	-

Table 2. Concrete composition

Concrete Code	Cement kg/m ³	Water kg/m ³	Sand kg/m ³	B.Stone. I kg/m ³	B.Stone. II kg/m ³	S. Plasticizer kg/m ³	Water/ Cement Rate
C20-K3	310	170	912	580	400	2500	0.55
C20-K5	298	190	900	570	390	2500	0.64
C35-K3	390	180	770	515	530	3150	0.46
C35-K5	378	205	755	500	518	3150	0.54

Table 3. Fresh concrete features

Concrete Code	Slump (cm)	Concrete Temperature (°C)	Unit Weight (kg/cm ³)
C20K3	9-11	18	2370
C20K5	20-22	16	2350
C35K3	10	14	2389
C35K5	22	11	2360

Table 4. Pressure test results (MPa)

Concrete Consistency		K3		K5	
		Slump(h)=100 mm		Slump(h)=200 mm	
Concrete Age		7 Days	28 Days	7 Days	28 Days
Concrete Code		Compressive Strength (MPa)			
A	C20-0	22.79 (60)	25.71 (67)	18.64 (59)	26.00 (83)
B	C20-V0	29.04 (76)	38.22 (100)	25.94 (83)	31.39 (100)
C	C20-V30	29.82 (78)	40.44 (105)	28.84 (92)	38.09 (121)
	C20-V60	31.92 (84)	40.33 (106)	29.67 (95)	38.84 (124)
	C20-V90	29.80 (78)	38.21 (100)	29.34 (93)	36.78 (117)
A	C35-0	25.40 (56)	38.42 (85)	22.48 (66)	32.70 (95)
B	C35-V0	39.18 (87)	45.00 (100)	26.00 (76)	34.25 (100)
C	C35-V30	35.37 (79)	46.97 (104)	27.30 (80)	39.74 (116)
	C35-V60	37.87 (84)	48.02 (107)	23.47 (68)	34.84 (102)
	C35-V90	37.54 (83)	43.31 (96)	27.58 (80)	36.84 (108)

*Percentage of single vibration to the 28-day value of the series and given in parentheses.

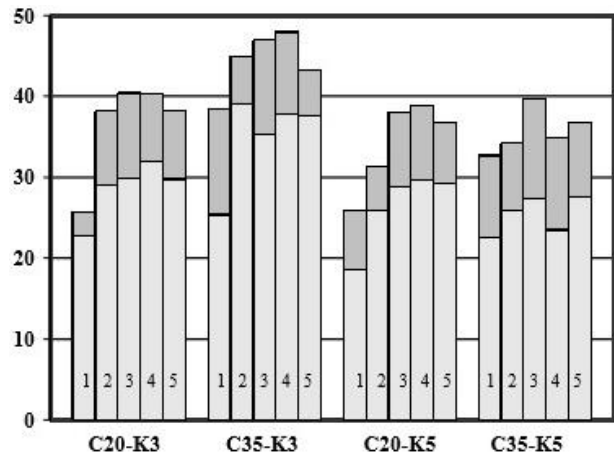


Figure 2. Uniaxial pressure test result changes on compressive strengths in 7 and 28 days as a result of vibration.

2.3. Effect Model of Effective and Repeated Vibration on the Concrete Pressure Endurance Values with Fuzzy Method (EMECSEM).

In this study, use of fuzzy logic in evaluating the effect of effective and repetitive vibration on the concrete pressure endurance has been examined by developing a model that allows the observation of more and qualitative results with diversification of related factors and classes of concrete grade, revibration and slump grades apart from the literature [21]. Thus, with the fuzzy logic model, a decision support system will be provided to be able to develop the limit value that can be obtained according to strength results based on the project sizes and risk-related strategies for determining the variations according to strength values and possible project changes.

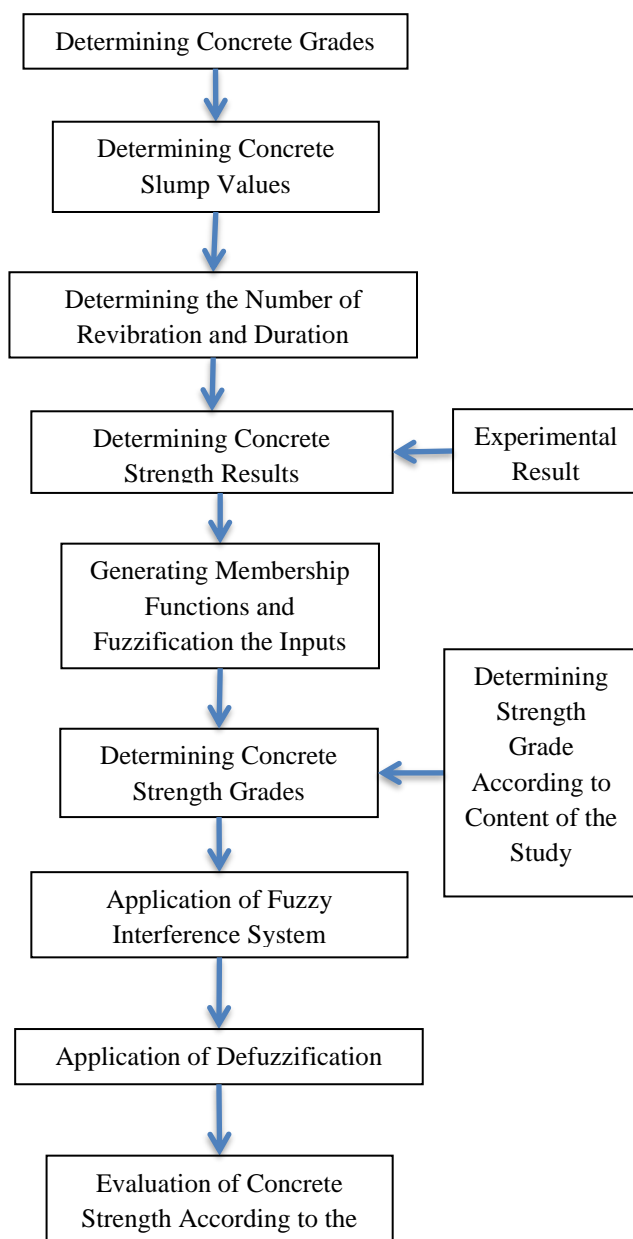


Figure 3. (EMECSEM) process steps of effect model to the concrete pressure endurance values with fuzzy method.

In Figure 3, the steps of the processes applied in the development of the fuzzy strength effect model (EMECSEM) are shown. The structure of the mamdani fuzzy inference system in the generated fuzzy system, determination of the concrete strength values is realizing at four steps according to the sequence of the flow chart given. The first stage is determination of membership functions based on the values such as concrete, slump, the number of revibration and fuzzification the inputs and determination of the concrete strengths obtained by the experiment. The second stage is determining concrete strength grades with reference to the strength values obtained by the experiment and application of the fuzzy inference system. The third phase is defuzzify process. The fourth stage is the evaluation of the concrete strength against the results.

Strength value results related to the variables defined in the studies in which the experimental results were obtained previously were taken and recorded. According to these results, the strength values according to different slump values and revibration applications of different concrete classes are given in Figure 2.

The values to be used in the model are defined in the experiment and their classifications are made. Strength values defined according to the experiment results were determined by simplifying them in a graphical system.

In the first stage of the EMECSEM, concrete grade defined in the model, slump grade, revibration and number of revibration, membership functions for experimental strength values and their fuzzy sets determined and fuzzy rules were generated and fuzzification and defuzzification methods were defined for digitizing the value of strength value obtained.

2.4. Determination of Fuzzy Membership Functions and Fuzzification of the Inputs

The grades of the strength factors that are forming the model inputs are mostly numerical values. For this reason, numerically expressed values must be represented by fuzzy subsets and membership functions in order to be defined in the fuzzy system. Fuzzy subset ranges and membership functions were determined by examining the experimental results.

In this modeling, fuzzy subset ranges and membership functions representing the input and output of the model were determined with reference to the study named "Importance of Active Vibration on Concrete Quality" which is conducted in 2002 by Kemalettin Yılmaz and Fetullah Canpolat and published in Osmangazi University Journal of Engineering and Architecture Magazine Issue XVI.

Fuzzy subset ranges and membership grades used in the model Concrete grades are seen in Figure 4, slump values

are seen in Figure 5, vibration durations are seen in Figure 6 and strength values are seen in Figure 7.

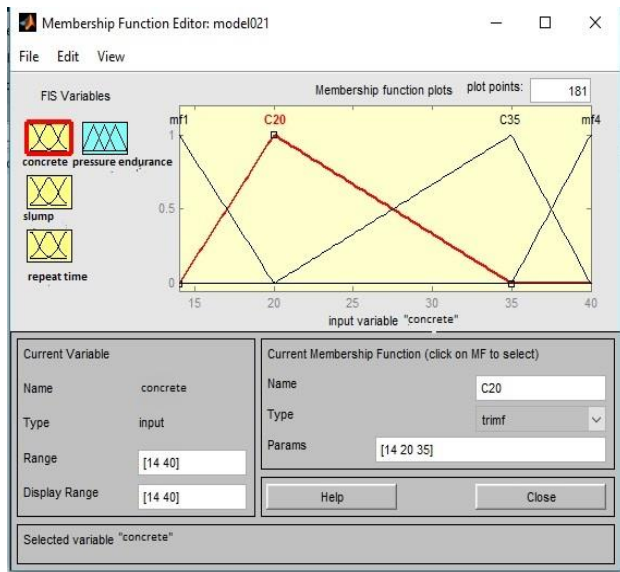


Figure 4. Determination of membership function according to concrete grades

In Figure 4, while determining the membership functions of concrete grades, C20 and C35 concrete were determined, and the input values determined as C14, C20, C35, C40 Concrete class range.

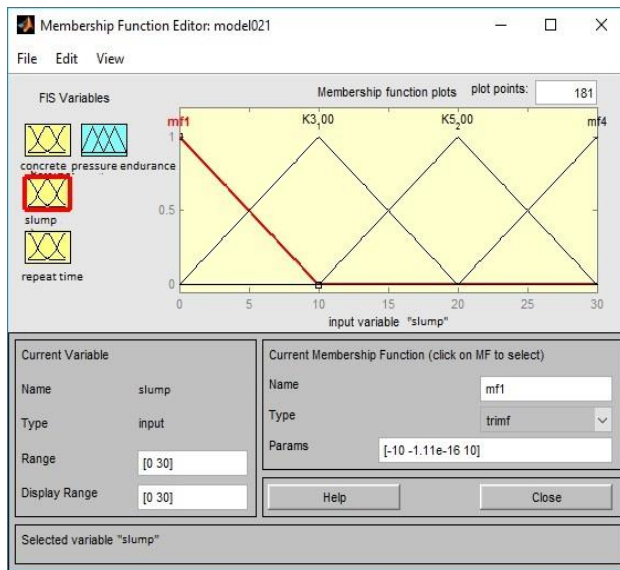


Figure 5. Determination of membership function according to concrete slump values

While determining membership functions according to slump values in Figure 5, K3:10 cm and K5:20cm slump values were determined and Input values determined as mf1:0, K3: 10 cm, K5: 20 cm , mf4: 30 cm concrete slump grade range.

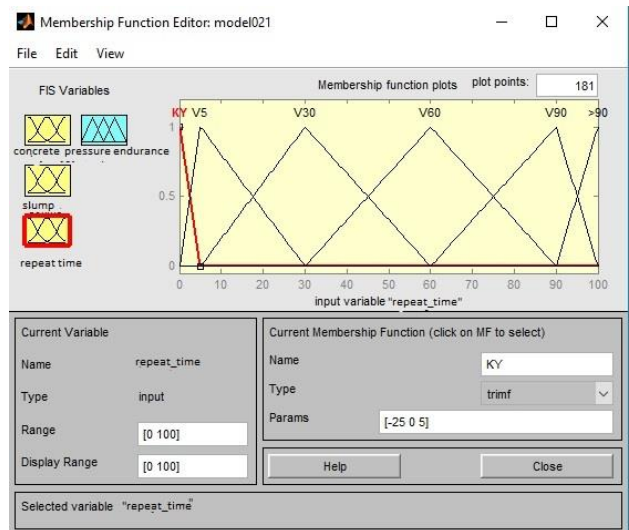


Figure 6. Determination of membership function of revibration number and duration

While the membership functions of membership values of revibration number and duration were being determined in Figure 6, the values determined as KY (Self-Grooving), V5, V30, V60, V90 and above 90 and Input values determined as KY 0 minute, V5: 5 minutes, V30: 30 minutes, V60: 60 minutes, V90: 90 minutes, above 100-minute concrete vibration ranges.

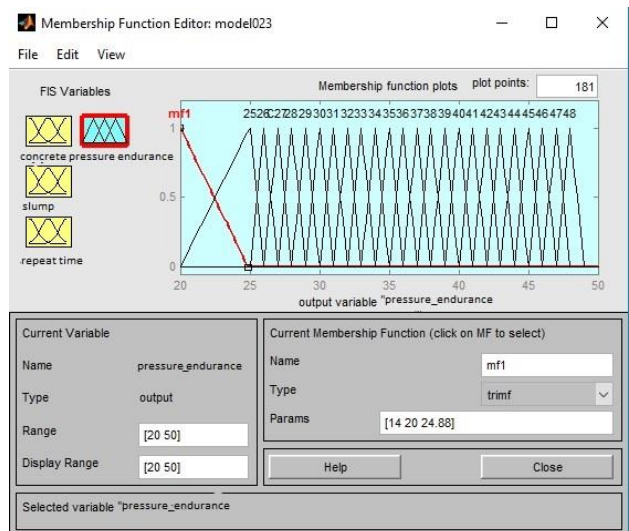


Figure 7. Membership function of concrete endurance values

In Figure 7, when the membership functions of the concrete strength values are determined, values between 20 MPa, 25 MPa, 30 MPa, 35 MPa, 40 MPa, 45 MPa, 50 MPa have been determined starting from 20 MPa, 25 MPa - The strength values of 30 MPa are allocated to the range of 25, 26, 27, 28, 29, 30. The strength values of 30 MPa to 35 MPa are allocated to the range of 30, 31, 32, 33, 34, 35. 35 MPa - 40 MPa strength values are assigned to the range of 35, 36, 37, 38, 39, 40. 40 MPa – Strength values of 45 MPa are allocated to the definition range of 40, 41, 42, 43,

44, 45. 45 MPa - Strength values of 50 MPa are allocated to the identification range of 45, 46, 47, 48, 49, 50.

2.5. Composing Fuzzy Rule Base (Preparing Fuzzy Systems)

For the creation of EMECSEM fuzzy systems; the rules which are stated as IF-THEN type were determined by using the figures close to the strength values which were determined via concrete grade, concrete slump values, revibration values experiment results which constitute the inputs. This is collated with the rules and operator. These rules are defined as "rule base". In Figure 8 and Figure 9, fuzzy outputs were obtained via combining the rules which were written by using the Fuzzy rule base and according to Mamdani fuzzy inference system.

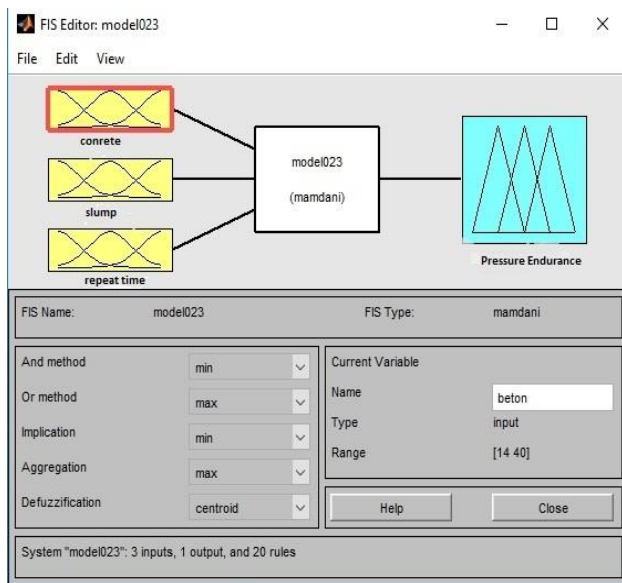


Figure 8. (EMECSEM) Structure of the effect system on concrete strength values with fuzzy method

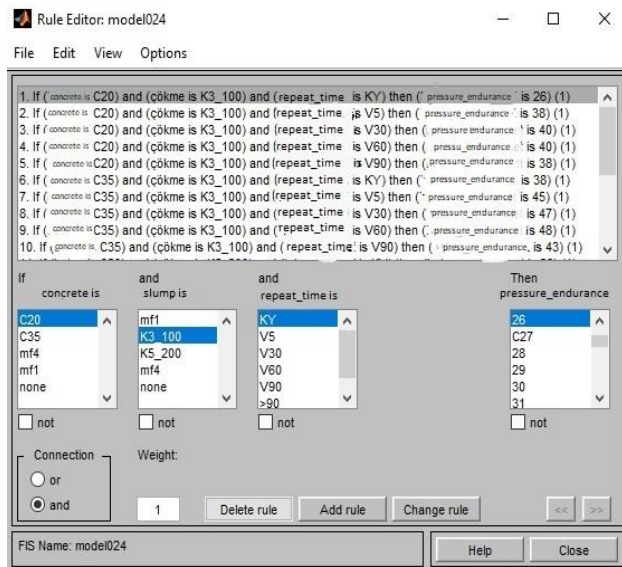


Figure 9. Combining written rules using fuzzy rule base according to fuzzy inference system

Fuzzy Outputs were obtained through combining the rules mixed by using fuzzy rule base according to Mamdani fuzzy inference system. For defuzzification on the outputs which were obtained as fuzzy, "center of gravity" method was used and strength values were determined.

2.6. Application of Defuzzification Process

According to the rules written by using the fuzzy rule base, the strength tables which can be read according to the functions and different variations emerged depending on the fuzzification are shown in Figure 10.

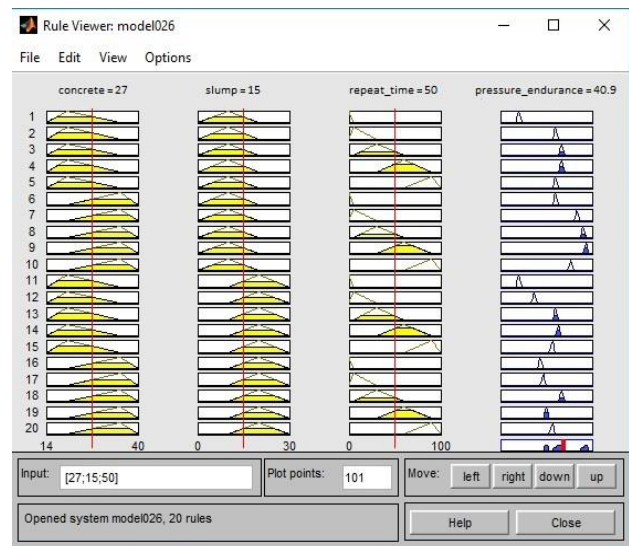


Figure 10. Evaluation of concrete strength according to results

As a result of the defuzzification process, a three-dimensional graph where maximum and minimum values are placed is shown in Figure 10 and Figure 11.

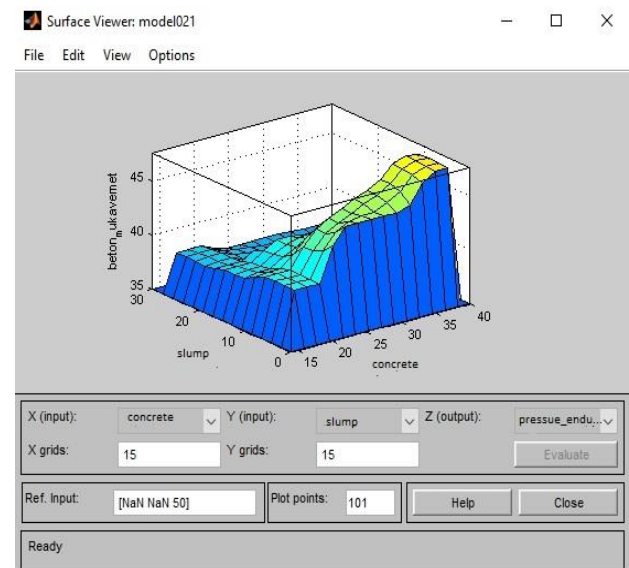


Figure 11. Three dimensional model showing concrete class, slump values and concrete strength values

3. Conclusions

In the study, C20 and C35 fresh concrete samples were subjected to revibrations at K3 and K5 slump values and with 0, 5, 30, 60, 90 min intervals. As a result of revibration applications, their fuzzy logic models are created. Obtained conclusions are listed below:

- A fuzzy logic model is created for revibrations using graphical representation.
- The data in which modeling was obtained with Fuzzy Logic and Pressure Endurance results obtained through experiments were evaluated comparatively. It is believed that this decrease in Pressure Endurance after 60 min of excessive vibration is due to segregation. According to the fuzzy logic model, the error rate was seen as 5-6%.
- With this study, results for no-data values can be found. Computers can make a faster calculation for this method.
- Especially when it comes to the large-budget projects (depending on static calculations, by considering various desired Pressure Endurance and different grades of concrete formulas, different water ratios, different slump values, repetitive vibration applications with different durations, different concrete grades etc.), considering the preparation of appropriate concrete formulas through using fuzzy logic method will provide a great ease.
- Fuzzy logic will expand technical personnel's horizon in terms of preparing different formulas in the construction as well as provide serious economic gains thanks to different formulas obtained for different sections of the construction.
- With this study, clarification of the limits of effective vibration application for accurate concrete casting by the help of fuzzy method will provide serious contributions to architects and engineers in terms of proceeding in line with the work schedule and eliminating repair and correcting costs.

6. Uyan M., Pekmezci B.Y. Effect of Revibration on Concrete Properties, Prefabrikasyon Magazine, 2001. 60 (October): p. 5-8.
7. Vollick C. A., Effect of Revibrating Concrete, ACI Journal, Proceedings, 1958. 54(9): pp.731-732.
8. Khalaf M. N., Yousif M. H. A., Effect of Revibration on the Stability and Compactibility of Concrete, Cement and Concrete Research, 1985. 15: pp. 842-848.
9. Çakıroğlu M.A., Terzi S., Kasap S., Çakıroğlu M.G., Estimating the Concrete Pressure Strength with Fuzzy Logic Method, Yapı Teknolojileri Elektronik Magazine, 2010. 6 (2): 1-8.
10. Terzi, S., Modeling the Effect of Bitumen Amount on Asphalt Concrete Strength with Fuzzy Logic Method, 4th International Advanced Technologies Symposium, 2005: Konya. 28-30 September.
11. Kuşan H., Aytakin O., Özdemir İ. Risks Assessment in Construction Projects with Fuzzy Logic Model, Engineering Sciences, 1A0359, 2016. 11(1): 1-14.
12. Şen Z. Modeling Principles in Engineering with Fuzzy Logic, Su Foundation Publications, Istanbul, 2004. pp:191.
13. Şen Z. Fuzzy algorithm for estimation of solar irradiation from sunshine duration. Solar Energy, 1998. 63(1): pp:39-49.
14. Pakdamar F., Güler K., (2011) "Flexible performance of reinforced concrete beams" ITU Journal Series D: Engineering, 2011. 10(5): pp. 59-70.
15. Özdemir İ., Aytakin O., Kuşan H. Calculating Betterment Fee with Fuzzy Logic Approach, 4th Construction Management Congress, Istanbul, 2007. pp.181-190.
16. Yılmaz K., Canpolat F. Importance of Active Vibration on Concrete Quality, Eng. & Arch. Fac. Osmangazi University Magazine, 2002. 15(2): pp. 1-10.
17. Akan R., Keskin S.,N. Investigation of the Contribution of Jet Grouting to Soil Improvement and the Effects of the Parameters Used in This Method, Suleyman Demirel University Journal of Natural and Applied Science, 2014. 18(2): pp. 22-26.
18. ACI 309R-96, Guide for Consolidation of Concrete, ACI Manual of Concrete Practice, Detroit, 1996.
19. ACI 309.1 R-98, Behavior of Fresh Concrete During Vibration", ACI Manual of Concrete Practice, Detroit, 1998.
20. Subaşı S.,Beycioğlu A., Çullu M., Prediction Of Compressive Strength On Revibrated Concrete Using Fuzzy Logic And Statistical Based Methods" SDU International Journal of Technologic Sciences, 2010. 2(3): pp. 46-52





References

1. Erdoğan T. Y., Concrete, 2003, Ankara: METU Press, 1st Edition, pp. 66-67, 191-198, 652-677.
2. TS 802, "Design Concrete Mixes". Turkish Standards Institute, Ankara, March 2016.
3. TS 1247, Mixing, Placing and Curing of Concrete (Normal Weather Conditions), Turkish Standards Institute, Ankara, 1984.
4. TS EN 206:2013+A1, Concrete - Specification, Performance, Production and Conformity Standard", January 2017.
5. TS EN 12390-2, Concrete – Testing Hardened Concrete", Part 5: Compressive strength of test specimens, Turkish Standards Institute, Ankara, 2003.



Research Article

Investigation of mechanical and microstructural performance of alkali activated electrical arc furnace slag mortars

Murat Ozturk ^a , Umur Korkut Sevim ^a , Muzeyyen Balcikanli Bankir ^{a,*}  and Omer Saltuk Bolukbasi ^b 

^a Civil Engineering Department, Iskenderun Technical University, Hatay, 31200, Turkey

^b Department of Metallurgy and Materials Engineering, Iskenderun Technical University, Hatay, 31200, Turkey

ARTICLE INFO

Article history:

Received 20 April 2018

Revised 25 October 2018

Accepted 27 November 2018

Keywords:

Alkali activation

Electric arc furnace slag

Sodium concentration

ABSTRACT

The production of Portland cement, resulting in the release of CO₂ gas, excessive energy and natural resource consumption, has led to search for alternative materials with similar physical and mechanical properties to the Portland cement of the scientific community. Geopolymers as alternative to conventional cement have a great potential for use in terms of their mechanical and durability properties. For this reason, it is necessary to investigate the usability of a new material alternative to cement, to reduce the environmental impact and for the disposal of Electric Arc Furnace Slag (EAFS), which is produced in large quantities in the primary target world and in Turkey and which causes storage space bottleneck. For this purpose, the mechanical and microstructure of the activated EAFS exposed to different curing conditions at three different sodium concentrations with a silicate module was investigated. When the results are examined, it is obvious that the strength increases with the increase of the sodium concentration. In addition, the literature on which alkali activation of EAFS has been added for the first time.

© 2019 Advanced Researches and Engineering Journal (IAREJ) and the Author(s).

1. Introduction

Cement based materials are the most used materials in the construction sector. The need for cement increased as the need for construction increased. Hence, harmony with nature has been among the priorities of scientists. The release of CO₂ gas, excess energy and natural resource consumption resulting in the production of Portland cement led to the search for alternative materials with similar physical and mechanical properties to the Portland cement of the scientific community [1]. One of the ways of producing eco-friendly concrete or mortar has been proposed by researchers to reduce the use of Portland cement and the active use of by-products pozzolan [2].

Geopolymers or alkali activated Cementitious alkenes are the products of the reactions between solutions with high alkalinities and aluminum silicates [3]. Activated geopolymers have a great potential for use as an alternative to conventional cement in terms of their

mechanical and durability properties. In particular, they exhibited against harsh environmental conditions and have increased their usefulness and environmental benefits as well as their resistance against fire and acid attack. For this reason, aluminum silicates such as metakaolin, slag, fly ash and clay, and pozzolans such as zeolite have been extensively studied as different forms of geopolymers.

Development of compressive strength in the alkali activated blast-furnace slags is possible and the same process can be applied in different additives lime, fly ash and sodium sulphate. Douglas expressed that compressive strength test values of slag mortars showed the slag is potential as a replacement material for ordinary cement concrete [4].

Hydration mechanism and strength gain mechanism of alkali activation of ground granulated blast furnace slag with sodium silicate forms clinker-free binders, with high and early strength development. Due to alkali compound

* Corresponding author. Tel.: +0326 613 56 00-4229; Fax: +0326 613 56 13.

E-mail address: murat.ozturk@iste.edu.tr (M. Ozturk), ukorkut.sevim@iste.edu.tr (U. Korkut Sevim), muzeyyen.balcikanli@iste.edu.tr (M. Balcikanli Bankir), osaltuk.bolukbasi@iste.edu.tr (O. Saltuk Bolukbasi).

ORCID: 0000-0003-3389-4883 (M. Ozturk), 0000-0002-6268-4909 (U. Korkut Sevim), 0000-0001-5091-8766 (M. Balcikanli Bankir), 0000-0002-8862-009X (O. Saltuk Bolukbasi).

of solution setting times were shorter than ordinary cement binder. Three important stages are exist and determined by using isothermal calorimetry. These stages are wetting, gelation of activator and bulk reaction between slag and alkali activator. When looking at the results of X-ray diffraction analysis it is seen that no crystalline products occurred. Also hydration mechanism was investigated by scanning electron microscopy and it is specified that a gel structure filled the initially water-filled space, and gradually make the structure denser as reaction proceeded [5,6].

The primary objective of this study is to develop an alternative method for disposal of slag to use of an alternative material for a new environmental impact reduction and cement material which is produced in large quantities in the world and Turkey, EAFS, causing a huge storage problem. For this purpose, mortar specimens are produced to investigate the mechanical and microstructure of the activated EAFS cement subjected to different curing conditions in three different sodium concentrations in a silicate module.

2. Experimental Study

2.1. Materials

EAFS, Sodium hydroxide (NaOH), Sodium silicate (Na_2SiO_3) solution and fine natural crushed stone aggregate were used for alkali activated EAFS mortars. The Na_2SiO_3 solution contained 8.52% Na_2O , 27.09% SiO_2 and 64.39% H_2O . The properties of the sodium silicate and sodium hydroxide are given in Tables 1 and 2. The maximum particle size distribution of the agglomerate used is 4 mm, fineness modulus and specific gravity are 2.65 and 2.6 g/cm^3 , respectively.

Table 1. Chemical and physical properties of sodium silicate

Chemical and physical properties	Analysis (%)
($\text{SiO}_2/\text{Na}_2\text{O}$)	3.19
Be (at 20 °C)	39.4
Specific gravity (20 °C g/cm^3)	1.373
Na_2O (%)	8.52
SiO_2 (%)	27.09

Table 2. Chemical and physical properties of sodium silicate

Chemical and physical properties	Unit	Analysis (%)
(NaOH)	g/kg	≥ 990
(Na_2CO_3)	g/kg	≤ 4
(Na_2SO_4)	mg/kg	≤ 80
(NaCl)	mg/kg	≤ 200
(Fe)	mg/kg	≤ 10
(Hg)	mg/kg	≤ 0.1
(Pb)	mg/kg	≤ 0.5
(Sb)	mg/kg	≤ 5
(Se)	mg/kg	≤ 5
(Ni)	mg/kg	≤ 2

The used EAFS is taken from Iskenderun Tosçelik Corporation. 500 kg EAFS is grinded through steel mills until reaching grain size of $-45 \mu\text{m}$. After grinding, the metals were separated from the product using magnetic separators (around 150 kg of metal was drawn from 500 kg of product). The final product has a specific gravity of 3.98 g/cm^3 , a blaine value of 2600 g/cm^2 , and also chemical analysis result is shown in Table 3.

Table 3. Chemical composition of EAFS

Component	FeO	Fe_2O_3	SiO_2	CaO	Al_2O_3
%	14.22	17.02	17.04	33.42	11.573
Component	MgO	MnO	K_2O	TiO_2	Na_2O
%	7.62	2.45	0.03	0.04	0.18

2.2. Mix Design

Twelve different test specimens were prepared to determine if EAFS cement was to be activated;

- The silicate module (SM) is selected as 1.
- The curing temperature (CT) is 40 ° C.
- Cure time (CTm) is 6 and 12 hours.
- Cured atmospheric moisture (AM) is 48% and 98%.
- Sodium concentrations (SC) are 4%, 6% and 8%.
- Samples were tested 28 days after curing.

In all test samples, the EAFS : Alkali solution: Aggregate ratio was kept constant at 1: 2.75: 0.485 by mass. Table 4 gives the mix design details. A gradually accelerating concrete mixer was used for the mixture. Mixing fine aggregate and EAFS was poured and dry mixing started, followed by dissolving sodium hydroxide in sodium silicate solution. Since the solution is exothermic, after waiting for cooling, the solution is poured in water and mixing process is continued. After a certain flowability is observed, the mixture is poured into prism molds ($40 \times 40 \times 160 \text{ mm}^3$).

Table 4. Design parameters of alkali activated EAFS mortar

SM.	CT (°C)	SC	AM (%)	CTm (h)	Comp. str. (MPa)	Mix No	
1	40	4	45	6	1,38	M1	
				12	1,56	M2	
			98	6	1,24	M3	
				12	3,06	M4	
			6	45	6	10,75	M5
					12	10,38	M6
		98		6	9,55	M7	
				12	9,84	M8	
		8		45	6	8,86	M9
					12	7,50	M10
			98	6	6,75	M11	
				12	10,19	M12	

After 24 hours the molds were demolded, the samples were removed and stayed at room temperature for 28 days after curing for 6 and 12 hours at 48 and 98% humidity with the help of climatic test cabinet, at 40 ° C. Mechanical tests were applied and then the microstructure analysis were examined.

2.3. Test Method

Compressive strength tests were carried out on 40x40x40 mm³ cubic samples with a press machine with a pressure capacity of 2500 kN. The test procedure was carried out in accordance with ASTM C349.

JEOL JSM-5610LV model equipment was used for Scanning Electron Microscopy (SEM) analysis. Acceleration voltage of the device: 0.1 ~ 30 kV; resolution at high vacuum mode of 5.0 nm; acceleration voltage 30 kV, WD 6 mm; magnification X25 - X300,000; the probe current is from 1 pA to 1 μA.

Mineralogical phase analysis was carried out parallel to the operation of the optical microscope. EAFS material and alkali activated EAFS samples were analyzed using Rigaku SmartLab model equipment. X-ray diffraction (XRD) analyzes were performed using computer controlled Rigaku-SmartLab ranging from 5 ° to 90 ° with Cu Kα radiation (40 kV, 30mA) and 2θ angles.

3. Results and Discussion

In Figure 1, the compressive strength values of different samples are given. As can be seen from the trend in figure 1, the increase in sodium concentration caused an increase in compressive strength. In addition, it can be said that the curing time is increased from 6 hours to 12 hours and the humidity of the environment (RH) is 98% humidity from the room conditions, it has a positive effect on the compressive strength.

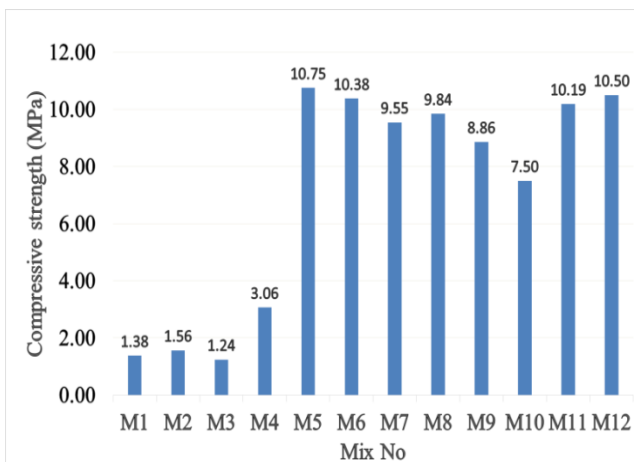
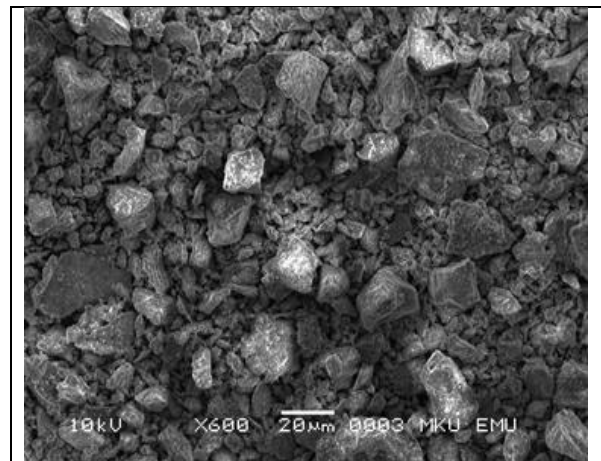
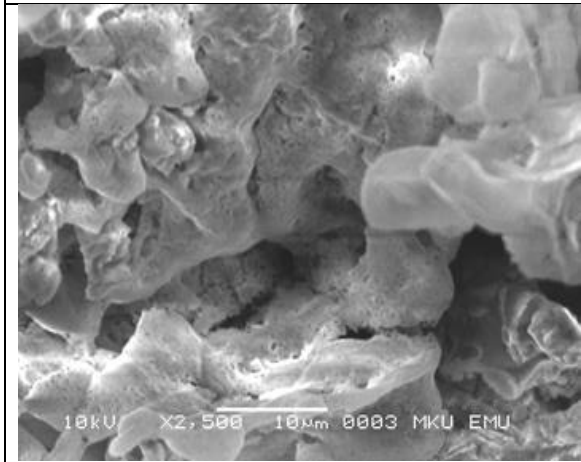


Figure 1. Compressive Strength Values of Alkali Activated EAFS Mortars

Figure 2 shows SEM images of grinded EAFS and activated EAFS (M1). As can be clearly understood, the activation reaction was successfully carried out, and a condensed structure was observed. Figure 3 shows the XRD analysis results of milled EAFS and activated EAFS (M1). When the chemical analysis results are taken into consideration, it is seen that CaCO₃ is formed as a significant hydration product. Therefore it is considered that the subsequent formation of Ca²⁺ ions from the EAFS and OH ions from the alkaline activator to form Ca(OH)₂ as the reaction result in the formation of CaCO₃, which reacts with free CO₂ in the atmosphere.



a) SEM image of EAFS



b) SEM image of Alkali activated EAFS mortar

Figure 2. SEM images of EAFS nad alkali activated EAFS mortar

If the concentration of Na(OH)₂ in the mixture is low, the strength values are not high enough. Increasing the Na(OH)₂ concentration up to a certain level causes an increase in the strength. In Chi's research, the mechanical properties and durability performance of alkali activated slag concrete improved with an increase in the Na₂O dosage and cured at relative humidity of 80% and curing temperature of 60 °C. The specimens has the superior

performance with respect to air and saturated limewater curing. Excessive amount of OH^- ion in the mixture causes excessive production of the $\text{Ca}(\text{OH})_2$ compound, which surrounds the EAFS and reduces the amount of Ca^{2+} soluble in the sludge. This means that the C-A-S-H gel formed after the reaction with Si^{4+} and Al^{3+} ions is less than necessary. At the end of, there is an internal structure that does not provide the necessary conditions in terms of strength [7,8].

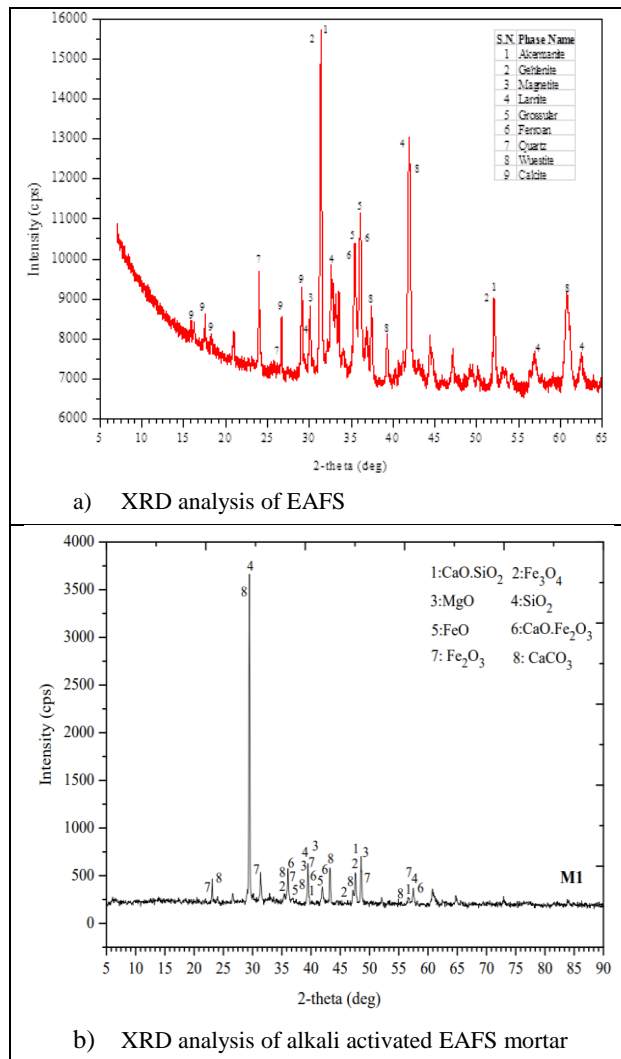


Figure 3. XRD analysis of EAFS and alkali activated EAFS mortar

3. Conclusion

In the present work, EAFS was activated with sodium hydroxide and sodium silicate solutions and mortar samples were produced. Constant silicate modulus as 1, and curing temperature (40°C), three different sodium concentrations (4%, 6% and 8%) for this silicate module and curing temperature were used to determine the effect of different parameters on the behavior of the alkali activated mortar samples in two different relative humidity environments (45% and 98%). The samples

were cured two different curing times (6 and 12 hours) for each relative humidity value. The samples were leaved in an open atmosphere at room temperature for 28 days in laboratory conditions. The results were observed as follows;

1) The mortar sample, labeled M5, achieved the best strength behavior due to the optimum sodium concentration. The highest compressive strength is obtained with silicate modulus, sodium concentration, relative humidity, curing temperature and duration of cure are respectively; 1, 6%, 45%, 40°C and 6 hours.

2) When microstructure analysis (SEM) is examined, a gel is produced as a product of the chemical reactions between EAFS and alkali activators, and it appears that it forms a denser microstructure which is the main factor that influences the development of strength. In addition, (XRD) showed that amorphous phase structure was observed in alkali activated mortar samples.

3) It is important to mention that the alkali activation of EAFS was carried out for the first time in this study. Thus, a new area of use has been introduced in the literature to use EAFS, which is in a waste material condition, as binding material.

Nomenclature

<i>SM</i>	: Silicate modulus
<i>CT</i>	: Curing temperature
<i>CT_m</i>	: Curing time
<i>AM</i>	: Atmospheric moisture
<i>SC</i>	: Sodium concentration
<i>EAFS</i>	: Electrical arc furnace slag

References

1. Scrivener, K.L. and A. Nonat, *Hydration of cementitious materials, present and future*. Cement and concrete research, 2011. **41**(7): p. 651-665.
2. Rostami, M. and K. Behfarnia, *The effect of silica fume on durability of alkali activated slag concrete*. Construction and Building Materials, 2017. **134**: p. 262-268.
3. Duxson, P., et al., *The role of inorganic polymer technology in the development of 'green concrete'*. Cement and Concrete Research, 2007. **37**(12): p. 1590-1597.
4. Douglas, E. and Brandstet, J., *A preliminary study on the alkali activation of ground granulated blast-furnace slag*. Cement and Concrete Research, 1990. **20**(5): p. 746-756.
5. Brough, A. R., and Atkinson, A., *Sodium silicate-based, alkali-activated slag mortars: Part I. Strength, hydration and microstructure*. Cement and Concrete Research, 2002, **32**(6): p. 865-879.
6. Ozturk, M., Bankir, M. B., Bolukbası, O. S., and Sevim, U.K. *Alkali Activation of Electric Arc Furnace Slag: Mechanical Properties and Micro Analyzes*. Journal of Building Engineering, in press, 2018.
7. Chi, M., *Effects of dosage of alkali-activated solution and curing conditions on the properties and durability of alkali-activated slag concrete*. Construction and Building Materials, 2012, **35**, p. 240-245.

8. Oh, J. E., Monteiro, P. J., Jun, S. S., Choi, S. and Clark, S. M. *The evolution of strength and crystalline phases for alkali-activated ground blast furnace slag and fly ash-based geopolymers.* Cement and Concrete Research, 2010, **40**(2):p.189-196.



Research Article

Comparison of contamination on yarns produced from local and us blend cotton types

Gülbin Fidan ^{a,*}  and Yasemin Korkmaz ^b 

^a Kahramanmaraş Sütçü İmam University, Faculty of Engineering and Architecture, Textile Engineering, Kahramanmaraş, Turkey

^b Kahramanmaraş Sütçü İmam University, Faculty of Engineering and Architecture, Textile Engineering, Kahramanmaraş, Turkey

ARTICLE INFO

Research Article
Article history:
Received 15 March 2018
Revised 10 August 2018
Accepted 12 September 2018

Keywords:
Contamination
Cotton fiber
Fabric
Foreign material
Yarn

ABSTRACT

Contamination on cotton fibers is one of the most important problems that shows itself on yarn and fabric. Contamination usually consists of plant leaves, parts, etc. on the cotton and this situation occurs during the harvesting and transporting. Also contamination occurs by bale pieces such as burlap, nylon and polypropylene residues. Developed technologies are using for selection of the foreign material in blowroom and bobbin processes, but it is not possible to completely remove the foreign material from the yarn. In general, the amount of foreign material in the local cotton is more than the US cotton. In this study, yarn production is made in the same specifications with local and US cotton, then yarn foreign material cuttings on bobbin machine and yarn quality values are compared. According to the results, it is seen that yarns produced by US cotton have less contamination than the yarns produced by local cotton. With this situation it is determined that, despite less contamination, yarn technical values of US cotton is worse than local cotton.

© 2019 Advanced Researches and Engineering Journal (IAREJ) and the Author(s).

1. Introduction

Cotton is one of the most favorable and widely used fiber because of its many positive attributes and naturality. One of the most important problems that seen in yarns made from cotton fiber is amount of foreign material that yarns contain.

Foreign material or in other word is contamination, is an important problem that causes many yarn and fabric defects. This situation is one of the major problems of cotton yarn manufacturing. Foreign material causes yarn breaking and causes low level of dye penetration. Nowadays foreign materials on fiber and yarn are cleaned in the blowroom and bobbin machines in spinning mills, but it is not possible to clean completely foreign material from the yarn.

Contamination usually occurs during the harvesting, packaging and storing of cotton fiber. The parts of the cotton plant do not cause contamination. However foreign materials that causes contamination such as fabric pieces that are mixed into during hand picking of the cotton or another materials that involved during ginning. Besides; packing, pieces of baling like burlap, polypropylene and nylon are also causes impurity.

Gençer O. et al. researched that, despite the high volume of cotton production in Turkey, there are problems that affect cotton production negatively and these problems need to be solved. These problems are summarized as, problems related to politics; high production costs of cotton plant raising; problems in cotton varieties, seeds and production techniques; cotton harvesting, ginning and foreign material problems; issues in cotton standardization system; inadequate training on cotton production and processing technique; inadequacy of communication and cooperation between cotton-related sectors [1].

One of the biggest problems observed in cotton produced in Turkey is the amount of contamination. A research by Kaya H. et al. is indicated that spinning mills use local cotton have a number of problems in different percentages. 47% of them have contamination, 28% of them have unstandardization (inhomogeneous balls, unknown fiber properties, and etc), 23% of them have fiber quality properties (low tensile strength, coarse micronaire values, low maturity values, nep and high ratio of short fiber content) and 2% of them have of high cost disadvantage. In the same study, types of contamination were examined and indicated that 48% of them contains foreign material (jute,

* Corresponding author. Tel.: +90 342 337 11 37; Fax: +90 342 337 11 38.

E-mail address: gfidan@gantep.edu.tr (G. Fidan), yorkmaz@ksu.edu.tr (Y. Korkmaz)

ORCID: 0000-0002-7958-2626 (G. Fidan), 0000-0002-0030-6259 (Y. Korkmaz)

Note: This study was presented at International Advanced Researches and Engineering Congress 2017

polypropylene, pieces of coloured clothing), 37% of them contains organic based foreign materials (plant leaves, particles, etc.) and 15% of them have metal pieces (wire, pieces of equipment) as an important contamination material [2].

A research of ITMF (International Textile Manufacturers Federation) indicated that the highest contamination is seen in regions of India, Nigeria, Zimbabwe, China and Turkey. The regions that produced the cleanest raw cotton are the USA (Texas, Arizona, Pima, Memphis and California), Syria, Benin, Brazil, Spain, Argentina, Greece and Australia [3].

Yarn producers prefer US cotton because of the fact that the harvest is made by machine in US and the low level of contamination is guaranteed by the producers. Yarns produced by US cotton contain less synthetic foreign material like nylon and polypropylene and coloured foreign fiber than local cotton produced in Turkey especially in South Eastern Anatolia Region. This study is made for comparison of contamination of yarns produced by local and US cotton.

2. Foreign Material

Foreign materials are visually checked and sorted by the worker, moreover they are sorted out by machines like Truetzschler SP-F, SP-PU and Uster Jossi Vision in the blowroom. Despite this, it can not be cleaned completely and foreign materials can reach to the yarn. Figure 1 shows samples of coloured foreign materials reaching from the blowroom cleaning line to the yarn.

Foreign materials can be classified as vegetable particles, baling materials and trash (Figure 2 and Figure 3).

Vegetable particles:

- Generally in short length range,
- In density spectrum from low to high,
- Can be cleaned after processes like bleaching, so it is not necessary to be cleaned in yarn process.

Foreign fibers and baling materials:

- Spread to the entire spectrum, regardless of length and density,
- Have to be cleaned as soon as when they exceed the limits of disturbing foreign material.

Trash:

- Generally long and rarely contains more faults,
- Must be removed at the relevant cleaning limits [4].

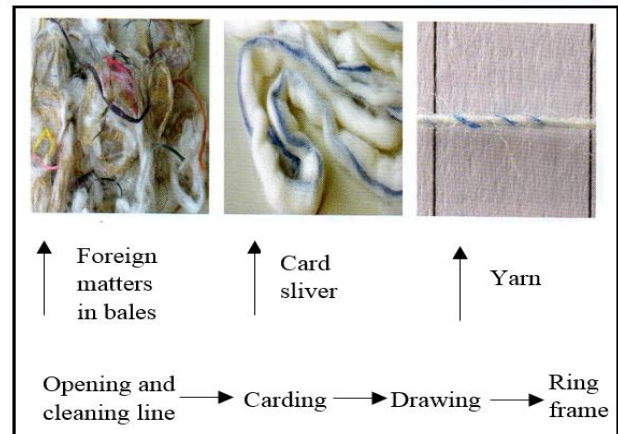


Figure 1. Foreign materials at different stages of the spinning process [5]

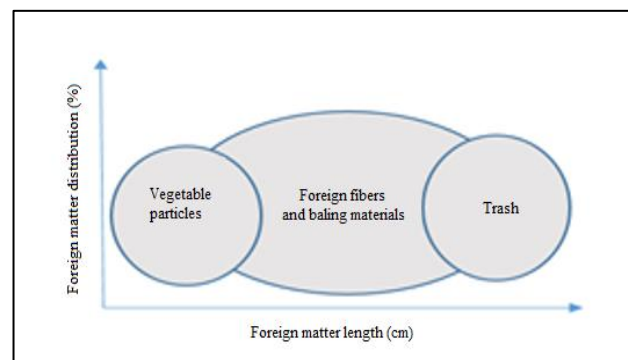


Figure 2. Distribution of foreign fibers on a cotton yarn [4]

Vegetable foreign materials can be removed from the fabric by the bleaching process. In Figure 4, various vegetable foreign material samples are seen on the raw fabric and after pre bleaching process.

Foreign materials can be coloured or synthetic origin (such as nylon, polypropylene). In the case of coloured foreign materials are not to be separated from the yarn, they can appear especially in bleached and light coloured fabrics. Synthetic foreign materials such as polypropylene have a colourless structure. Because of this situation, it is very difficult to remove synthetic foreign material from yarn. They do not absorb dyestuff during dyeing, so there will be uncoloured places on the fabric.

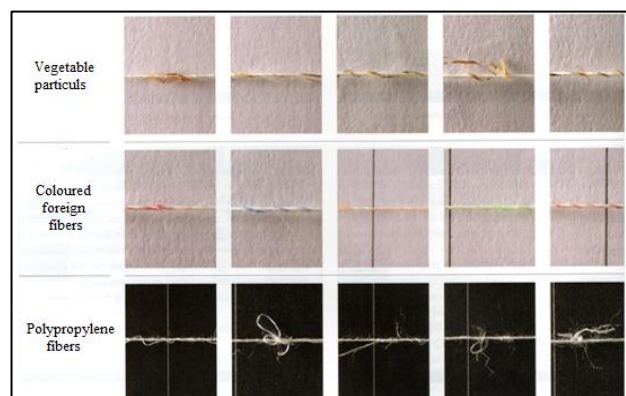


Figure 3. Foreign material types [5]

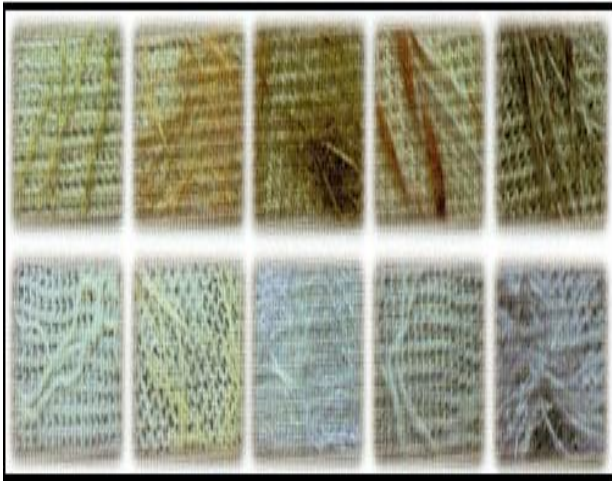


Figure 4. Foreign material images on raw fabric and bleached fabric [5]

On bobbin machine, foreign materials are classified as foreign dark matter, foreign light matter and polypropylene foreign matter. Foreign dark matters are selected from light coloured yarns; foreign light matters are selected from dark coloured yarns. Synthetic foreign materials like polypropylene are cleaned by a separate channel.

In Turkey, during the collection of cotton, many cloth pieces which cause foreign material can be mixed into the collected cotton. These coloured foreign materials are sliced in to very small pieces during the yarn production process, in the case of not being extracted in the blowroom. In bobbin machines, yarns are cleaned by yarn cleaning systems like Uster, Loepfe. When the amount of foreign material is too much and effective cleaning setting cannot be setted, the foreign material fault cannot be removed from the yarn. In Figure 5, non-removable coloured foreign materials are seen on the fabric. The same situation is observed on uncoloured synthetic foreign materials such as polypropylene and nylon. These synthetic foreign materials are sliced in to very small pieces up to the yarn, in the case of not being extracted in the blowroom. When the amount of synthetic foreign material is too much and effective cleaning setting cannot be setted, the synthetic foreign material fault cannot be removed from the yarn. In Figure 6, these non-removable synthetic uncoloured foreign materials are seen on the fabric.

Yarn producers in Turkey prefer US cotton especially for foreign material guaranteed orders, because of the low content of foreign material in US cotton.



Figure 5. A disturbing coloured foreign material sample on knitted fabric [5]

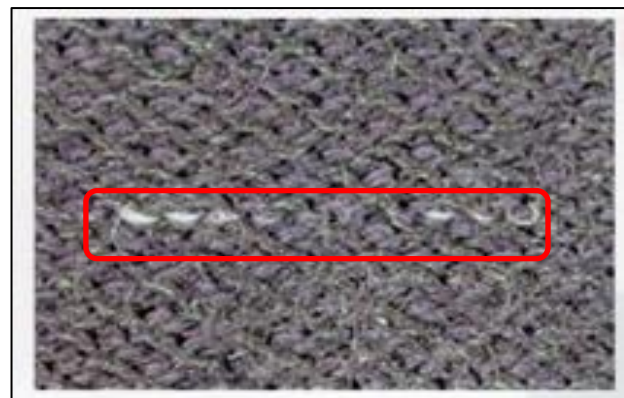


Figure 6. A disturbing polypropylene foreign material sample on knitted fabric [5]

3. Material Method

In this study, combed yarns were produced by using Diyarbakır local cotton and US cotton. The yarn samples were produced by ring spinning frame with the yarn number of Ne 40 and yarn twist multiplier (α_e) was 3,7. Yarns were bobbinned with same cutting settings in the Uster Quantum 3 cleaning system. For determining cotton properties, cotton samples were tested with Uster HVI and Uster Afis devices. For determining the yarn technical values, the yarn samples were tested with Uster Tester 4 device. The Uster Tensojet 4 device was used for determining yarn tensile and yarn elongation.

4. Results and Discussion

According to the results of Uster HVI (Table 1), it was observed that, spinning consistency index, fiber length, short fiber index, uniformity index and strength values of Diyarbakır local cottons are better than those of US cottons. However the values of trash count and trash area are worse than those of US cottons. The same situation can be seen in Table 2, which contains the results of Uster Afis device. Short fiber content of Diyarbakır local cottons is lower than that of US cottons. However the amount of dust and trash count of Diyarbakır local cottons is worse than those of US cottons.

In Figure 7, HVI colour grades for American upland cotton are seen. In this study, green marked area shows US cotton and red marked area shows Diyarbakır local cotton. According to results of Table 1 and Figure 7, colour grades of US cotton is better than Diyarbakır local cotton.

Table 1. Test results of Uster HVI

	Diyarbakır local cotton	ABD cotton
SCI	148	137
Micronaire	4.65	4.14
Length	30.1	29.4
SFI	5.1	7.9
UNF.	83.8	82.3
STR.	33.7	30.7
ELG.	6.2	6.9
C-Grade	31	11-21-31
Rd	76.8	79.0
b+	8.2	8.9
Trash Count	33	17
Trash Area	0.59	0.18

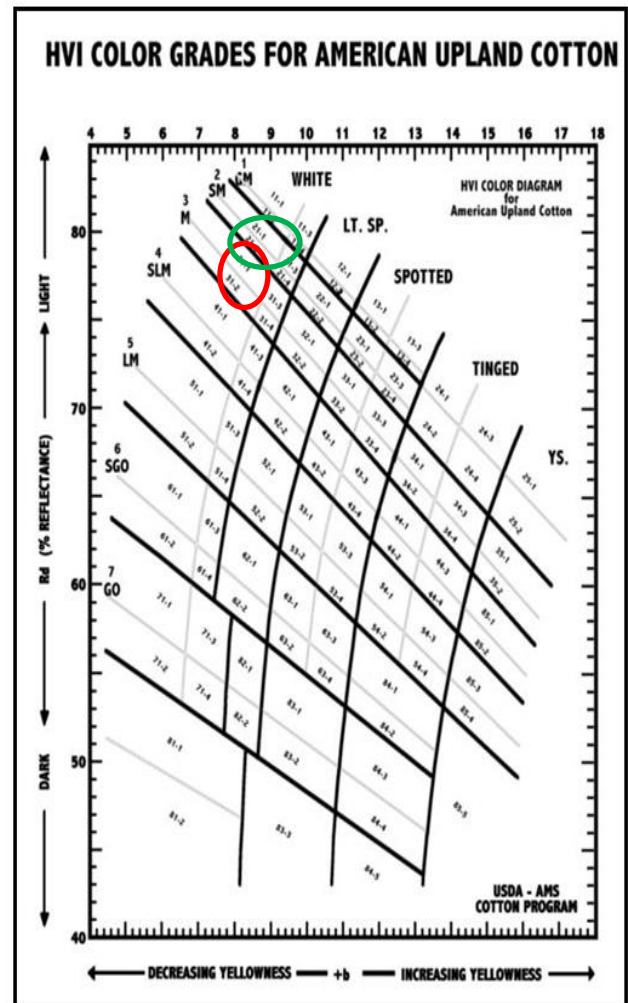


Figure 7. HVI Colour Grades for American Upland Cotton [6]

Table 2. Test results of Uster Afis

	Diyarbakır local cotton	ABD cotton
Nep cnt/gr	114	295
Nep [um]	785	678
UQL(w)[mm]	32.0	31.7
L (w)[um]	25.2	25.5
L (n)[mm]	22.2	23.1
SFC (w)	5.4	8.4
SFC (n)	17.2	26.8
Dust cnt/gr	1193	441
Trash Count	129	55

In this study, Ne 40 combed cotton yarn was produced with Diyarbakır local cotton and US cotton. Yarns were bobbinned with same cutting settings in the Uster Quantum 3 cleaning system and the results are compared.

Diyarbakır local cotton and US cotton compared by visually and it is clearly seen that US cotton is more clean than Diyarbakır local cotton. This situation is parallel to results of Uster HVI and Uster Afis devices. After cleaning of yarns on bobbin machine with Uster Quantum 3, the results of yarn cuttings on 100 km are shown in Table 3. In this study, it was aimed to compare foreign material of yarn samples, so in Table 3 only total yarn faults and foreign dark matter cuttings were given.

Table 3. Total yarn cuttings and foreign material cuttings on 100 km

YARN TYPE	NE 40 COMBED YARN	
BLEND TYPE	DIYARBAKIR LOCAL COTTON	US COTTON
Total Yarn Fault Cuttings	76	48
Foreign Dark Matter Cuttings	22	15

According to these results, it was observed that the yarns produced by US cotton blend have less yarn fault and foreign dark matter cuttings than those of Diyarbakır local cotton blend. When the foreign materials cleaned from the yarns were examined, it can be seen that the foreign materials separated from US cotton yarns are smaller in size than that of local cotton yarns.

After bobbin processes, the yarns are tested in Uster Tester 4 and Uster Tensojet 4 devices. Results of these tests are seen in Table 4.

According to the results of yarn quality tests, it is seen that the yarns produced by Diyarbakır local cotton have less yarn imperfection values (total number of thin places -50%, thick places +50% and neps +200%) than the yarns produced by US cotton. The tensile strength is evidently high with the yarns produced by Diyarbakır local cotton.

Table 4. Yarn quality tests

Ne 40	Diyarbakır local cotton	US cotton
Cv _m %	12.7	13.1
Thin places -40% / km	83	106
Thin places -50% / km	2	1
Thick places 35% / km	263	385
Thick places 50% / km	21	31
Nep 200% / km	36	48
Hairiness	3.4	3.7
Tensile strength cN/tex	20.2	17.8
Breaking elongation %	4.1	4.4

5. Conclusion

In bobbin process, low yarn cuttings are always expected for the performance of weaving and knitting processes. According to the yarn cutting results, the yarns produced by US cotton have less yarn faults and foreign matters than the yarns produced by Diyarbakır local cotton.

In addition, tensile strength is one of the important property of yarn. As clearly visible in the results, US cotton yarns have less tensile strength than local cotton yarns. With this situation, US cotton yarns have higher thick and nep places. If the current prices of US and local cotton are compared, it can be said that US cotton is more expensive than local cotton.

Despite the worse yarn technical values and the high price, the low amount of contamination and yarn cuttings in bobbin process are the reasons for preference of US cotton for foreign product guaranteed production.

References

- Gencer, O., Özüdoğru, T., Kaynak, M. A., Yılmaz, A., & Ören, N. Türkiye'de pamuk üretimi ve sorunları, TMMOB, Ziraat Mühendisleri Odası, Türkiye Ziraat Mühendisliği, VI. Teknik Kongresi 2005.
- Kaya H., Dolunçay A., Toklu P., Türkoglu S., Nasırcı Z., Süllü S., Özbek B., Adana, Kahramanmaraş ve Gaziantep illerinde pamuk ipliği üretimi yapan tekstil işletmelerinin genel durumu, pamuk lifine ilişkin kalite beklentileri, sorunları ve çözüm önerileri. Tekstil ve Mühendis. 2006. 13(62-63): p. 1-15.
- Anonim, *İtmf: Pamukta Kontaminasyon Oranı Arttı*, [cited 2017 05 October]; Available from: <http://www.textotex.com/haber/elyafiplik/itmfpamukta-kontaminasyon-orani-artti.html>.
- Uster®, On-Line Quality Management on Bobbin Machines, Uster Quantum 2 Manuel Application, 2009
- Uster®, Modern Yarn Cleaning on Bobbin Machines, Uster News Bulletin, No:48, September 2011.
- International Trade Centre, Cotton Exporter's Guide, [cited 2018 20 July]; Available from: <http://www.cottonguide.org/>

**Research Article**

Biosynthesis and characterization of iron oxide nanoparticles from *Enteromorpha* spp. extract: determination of adsorbent properties for copper (II) ions

Gizem Ercan ^a , Deniz Uzunoğlu ^a , Memduha Ergüt ^{a,*}  and Ayla Özer ^a 

^a Mersin University, Department of Chemical Engineering, Mersin 33343, Turkey

ARTICLE INFO

Article history:

Received 13 March 2018

Accepted 12 October 2018

Keywords:

Biosynthesis

Cu²⁺ adsorption*Enteromorpha* spp.

Iron oxide nanoparticles

Marine algae

ABSTRACT

Iron oxide nanoparticles (IO-NPs) were synthesized via a biosynthesis method using marine algae *Enteromorpha* spp. extract as a biological reductant agent in this study. Moreover, the total phenolic content of *Enteromorpha* spp. was found as 9.81± 4.8 mg gallic acid equivalents/g dry algae. The biosynthesized IO-NPs were characterized by zeta potential, DLS, SEM/EDX, and FTIR analysis methods and also the formation of IO-NPs was approved with the UV-vis spectrum. The characteristic surface plasmon resonance (λ_{SPR} , nm) value showing the formation of IO-NPs was observed at nearly 410 nm in terms of UV-vis analysis. According to DLS analysis results, the mean hydrodynamic diameter of IO-NPs was determined as 78.83 nm. According to SEM results, spherical nanoparticles are formed, and EDX analysis showed that the signals in the Fe and O elements confirmed the formation IO-NPs. According to FT-IR analysis results, the formation of IO-NPs was approved by the absorption bands at 599.83, and 475 cm⁻¹, which corresponded to the Fe-O stretches of Fe₃O₄ and Fe₂O₃. Subsequently, the synthesized IO-NPs were utilized as an adsorbent for the removal of Cu²⁺ from aqueous solutions. Batch adsorption experiments were conducted to examine the optimum adsorption environmental conditions and the equilibrium, kinetics, and mass transfer modeling was also evaluated. The optimum adsorption conditions were found as initial pH 5.0; temperature 35°C, initial Cu²⁺ concentration 275 mg/L, and adsorbent concentration 0.5 g/L. The experimental equilibrium data were in the best agreement with Langmuir isotherm model, and the maximum monolayer coverage capacity of IO-NPs for Cu²⁺ adsorption found to be 188.68 mg/g at optimum temperature value of 35°C. The adsorption kinetic data were consistent with the pseudo second order kinetic model, and Weber Morris model showed that both the film (boundary layer) and intraparticle diffusion affected the adsorption process.

© 2019 Advanced Researches and Engineering Journal (IAREJ) and the Author(s).

1. Introduction

Copper (II) have been frequently used in several industries like metal cleaning, paints and pigments, paper board, fertilizer, plating baths, and wood pulp. So, it is one of the best known non-biodegradable water pollutants which are causing serious soil and water pollution. Moreover, Copper (II) is extremely toxic and dangerous for ecosystem, agriculture and human health.

The acceptable discharge limit of copper in industrial wastewaters is reported as 1.0 mg/L by the US Environmental Protection Agency [1]. Therefore, to reduce Cu²⁺ to the standard level, effective, eco-friendly

and economic treatment methods are being developed by researchers. There are commonly used treatment methods for discharging copper ions from wastewaters such as ion exchange, adsorption, extraction, reverse osmosis, coagulation, chemical precipitation, and membrane filtration techniques. Among them, adsorption is a frequently-preferred method for heavy metals removal from the wastewaters due to its simple operation, low cost, the capability of trace level pollutant removal and high efficiency [2].

Recently, the usage of metal/metal oxide nanoparticles as an adsorbent has attracted great attention for treatment

* Corresponding author. Tel.: +90-324-361-0001/17371; Fax: +90-324-361-0032

E-mail address: gizemercan16@gmail.com (G. Ercan), denizuzunoğlu@gmail.com (D. Uzunoğlu), memduha.ergut@mersin.edu.tr (M. Ergüt),

ayozer4@gmail.com (A. Özer)

ORCID: 0000-0002-2496-7887 (G. Ercan), 0000-0001-9706-303X (D. Uzunoğlu), 0000-0001-7297-1533 (M. Ergüt), 0000-0002-7824-238X (A. Özer)

of various heavy metals. The advantage of these nanomaterials is high adsorption capacity that is associated with their large specific surface area and high reactivity in the adsorption processes [3]. In this respect, the biosynthesis methods which is environmentally friendly and do not include dangerous substances in the synthesis step have begun to gain importance for the synthesis of metal nanoparticles. Biological methods that are using enzymes, microorganisms, alga, and plants, have been used as practicable environmentally-friendly and safer than other chemical and physical methods which are risky and expensive [4].

Marine algae are divided into macroalgae and microalgae. Marine macroalgae, in other word seaweed, are planted like organisms. They are categorized into three groups considering their pigmentation as brown (phaeophytes), red (rhodophytes), and green (chlorophytes) which are located in the marine or saltwater environment. The latest studies indicated that marine algae could be used for the synthesis of metal nanoparticles owing to their phytochemicals. These phytochemicals include various functional groups such as; amino, hydroxyl, and carboxyl which could act as effective metal-reducing agents [4, 5].

The present study aimed to synthesize iron oxide nanoparticles (IO-NPs) using seaweed *Enteromorpha spp.* algal extract as a reducing/capping agent and to investigate the adsorption of copper (II) ions to IO-NPs.

2. Materials and Methods

2.1 Preparation of Algal Extract from *Enteromorpha spp.*

The green algal genus *Enteromorpha spp.* was picked up from Mediterranean coastline in Mersin, Turkey. Specimens of green seaweed were firstly rinsed with tap water and then washed with pure water. After that, they were dried in an oven at 60°C for 2 h. For the preparation of extract, 5 g of the washed and dried algae samples were boiled in 600 mL of pure water in a beaker under continuously stirring for 180 min. The prepared extract was cooled to room temperature, and then the insoluble fractions and macromolecules were removed by centrifuging the extract. Finally, the obtained green colored extract was kept in the refrigerator at +4°C for the nanoparticle synthesis and the analysis studies.

2.2 Determination of Total Phenolic Content of *Enteromorpha spp.* extract

In order to determine the total phenolic content (TFC) of *Enteromorpha spp.* extract, the Folin-Ciocalteu colorimetric method adapted from Slinkard and Singleton (1977) was applied [6]. According to the method, 100 µL Folin-Ciocalteu reagent and 1.4 mL of distilled water

were put into 200 µL of the extract, and the formed solution was agitated well. After 2 min, 300 µL of 20% (w/v) Na₂CO₃ solution was added to the present solution. Tube content was vortexed again and then left to wait for 2 h at room temperature in the dark. TFC of the extract was stated as gallic acid equivalent (µg of gallic acid/g dry leaf). To determine TFC value, the absorbance of the blue colored solution was recorded at 765 nm with UV-Vis spectrophotometer. For this purpose, a calibration curve ($R^2 = 0.996$) was formed firstly at different concentrations (100 – 700 mg/L) of gallic acid, and then, TFC value of the extract was observed using the absorbance values. The results were reported as the average of three absorbance measurements.

2.3 Synthesis of Iron Oxide Nanoparticles

Iron oxide nanoparticles (IO-NPs) were synthesized via biosynthesis method by using *Enteromorpha spp.* algal extract as a natural reductant/capping agent. The green colored extract was added drop by drop manually into 0.1 M FeCl₃ solution in a 1:2 volume ratio at room temperature and then the color of the yellow solution turned to brown with the creation of nanoparticles in a short time. After that, the resulting nanoparticles were filtered with Whatman # 1 filter paper and dried in an oven at 80°C for 4 h. IO-NPs were crumbled homogeneously by handle-mortar and were kept in closed vessels in a refrigerator at +4°C for further experiments [7]. Biosynthesized IO-NPs were characterized by zetasizer (Malvern, UK) using Dynamic Light Scattering (DLS) technique, zeta potential analyzer (Malvern, UK), UV-vis spectrophotometer (Specord 210 Plus-Analytic Jena, Germany), and Fourier Transform Infrared Spectrometer (FTIR- Perkin Elmer, Shelton).

2.4 Preparation of Cu²⁺ solutions

In order to prepare the stock solution of Cu²⁺ (1.0 g/L), 3.9292 g of CuSO₄.5H₂O was dissolved in 1 L of distilled water. The solutions at different concentrations of Cu²⁺ (50–500 mg/L) were prepared with required dilutions from the stock solution. The initial pHs of the solutions were fixed up to the desired value with 0.1 M solutions of NaOH and HCl.

2.5 Batch adsorption studies

The experiments of Cu²⁺ ions adsorption onto IO-NPs were done in a batch system with artificial wastewater. Two parallel experiments were performed for each adsorption study. The adsorption experiments were conducted in 250 mL Erlenmeyer flasks containing 100 mL of adsorbate solution involving Cu²⁺ ions. 0.1 g of IO-NPs was added to 100 mL of Cu²⁺ solution at the desired initial pH and Cu²⁺ ion concentration. The flasks were shaken in an agitation vessel at the constant

temperature for 210 min to achieve adsorption equilibrium. At foregone time intervals (0.0, 0.5, 2.0, 5.0, 10, 20, 30, 60, 90, 120, 150, 180, and 210 min), the samples from the adsorption solution were taken and centrifuged at 4000 rev/min for 3.0 min. For different environmental conditions such as initial pH, initial Cu²⁺ ion concentration, adsorbent concentration, and temperature, the adsorption experiments were repeated and the experimental data were observed.

2.6 Cu²⁺ analysis

The unadsorbed Cu²⁺ ion concentration in the supernatant was analyzed spectrophotometrically [1]. 1.5 N of 20 mL NH₃ solution and 1% (w/v) of 0.2 mL sodium diethyl di-thio-carbamate solution were put into 1 mL of the supernatant, and it was diluted to 25 mL with pure water. After the yellow-brown solution formed, it was analyzed in terms of UV-vis spectrophotometer at 460 nm. The adsorbed Cu²⁺ ion amounts at equilibrium (q_e (mg/g)) and the adsorption percentages (adsorption, %) were calculated as follows:

$$q_e = (C_o - C_e) / X_o \tag{1}$$

$$\text{Adsorption percentage (\%)} = ((C_o - C_e) / C_o) \times 100 \tag{2}$$

where C_o is the initial concentration (mg/L), and C_e is the equilibrium concentration and X_o is the adsorbent concentration (g/L).

3. Results and Discussions

3.1 Characterization of IO-NPs

The effective hydrodynamic diameter distribution of IO-NPs was analyzed by DLS technique, and the results were represented in Figure 1. According to Figure 1, the smallest IO-NPs (58.77 nm) had the distribution of 10.4 % while the single IO-NPs with the effective hydrodynamic diameter of 78.82 nm were the most frequent ones (32.7 %). Consequently, the mean diameter of IO-NPs was determined as 78.83 nm.

The formation of IO-NPs was firstly noted by visual observation of the color of [IO-NPs-algae extract] solution, and then the UV-vis spectra of the solution were recorded against pure water with 1 mm optical path length quartz cuvette. Accordingly, the color of the solution altered from yellow to brown with the creation of nanoparticles due to the surface plasmon resonance (λ_{SPR}, nm) phenomenon. According to Figure 2, a characteristic and distinct λ_{SPR} value of IO-NPs was obtained at nearly 410 nm.

The SEM images of the synthesized IO-NPs were presented in Figure 3(a) and (b) before and after adsorption, respectively. As seen from Figure 3(a), the nanoparticles have spherical and porous morphology and agglomerated. Moreover, the mean hydrodynamic

particle size of IO-NPs was calculated to be 62 nm by using the Image J program using randomly selected 50 particles from SEM images. The mean hydrodynamic diameters of nanoparticles were found a bit higher than DLS analysis results may be due to the absorption effects and particle scattering because of agglomeration. After Cu²⁺ adsorption, as shown in Figure 3(b), a smooth surface was obtained. The nanoparticles were more agglomerated, and the pores were closed because of the adsorption of Cu²⁺ ions onto the surface of the adsorbent.

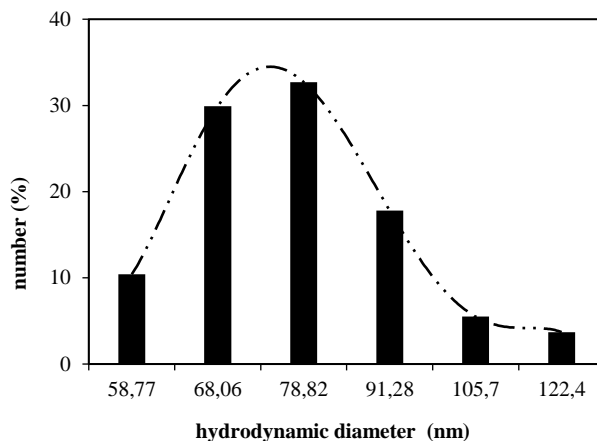


Figure 1. The effective hydrodynamic diameter distribution of IO-NPs

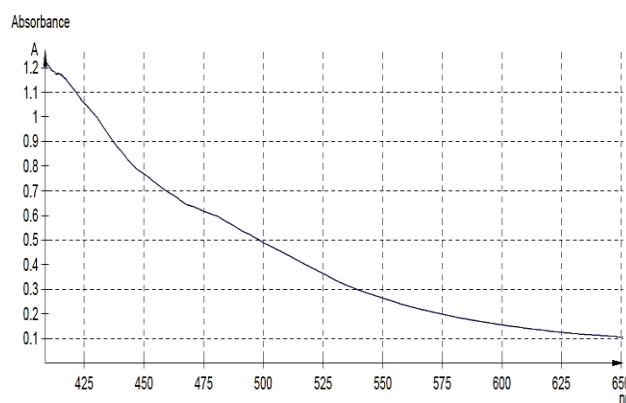


Figure 2. UV-vis spectra of [IO-NPs-algae extract] solution

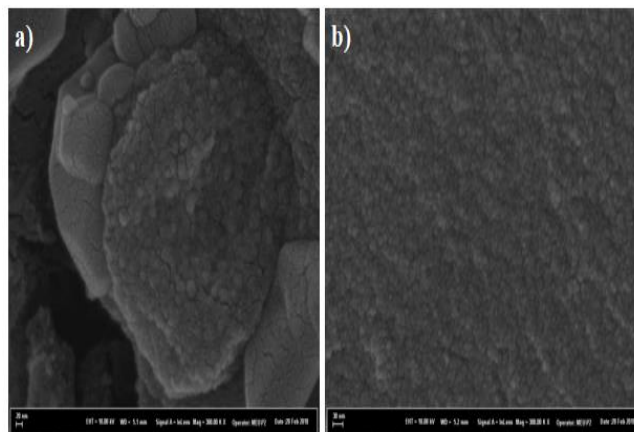


Figure 3. SEM images of IO-NPs (a) before and (b) after adsorption

According to EDX analysis results, the elemental and quantitative weight composition (wt.%) of synthesized IO-NPs was composed of 33.05 % Fe, 32.96 % O, 15.53 % C, 7.02 % Na, 3.68 % S, 3.12 % Cl, 2.59 % N, 1.24% Mg and 0.84% Ca elements. Elemental analysis (EDX) spectrums of IO-NPs before and after adsorption were given in Figure 4(a) and (b) respectively. According to Figure 4(a), the prepared IO-NPs involve the elements of Fe, O, C, Na, S, Cl, N, Ca, and Mg (the peaks of the elements of Pt and Pd stem from the coating of the sample), before adsorption. EDX analysis results revealed that the signals in the Fe and O elements confirmed the formation IO-NPs, whereas the elements of C, a part of O, Na, S, Ca and Mg derived from the aqueous algal extract. The presences of these elements ascribed to the polyphenol groups and other C-containing molecules [8]. Also, Cl element must be arisen from FeCl_3 precursor used in IO-NPs synthesis. After adsorption, in addition to Fe, O, C, N, S, Na, Ca and Mg elements also, Cu element was detected in EDX analysis results after adsorption. The presence of Cu element in the elemental composition confirmed the binding of the Cu^{2+} ions onto IO-NPs surface.

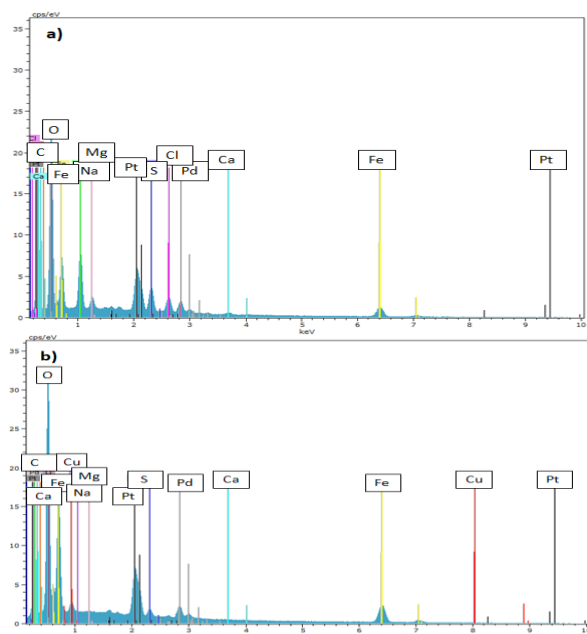


Figure 4. EDX spectrum of IO-NPs a) before and b) after adsorption

The FT-IR spectrum of the synthesized IO-NPs before and after Cu^{2+} adsorption was exhibited in Figure 5. As shown in Figure 5, no important changes in the structures were observed between pre- and post-adsorption. According to the FT-IR spectrum of biosynthesized IO-NPs (Figure 5.a), the broad band at between $3200\text{--}3300\text{ cm}^{-1}$ is attributed to O-H stretching vibration. The slight bands at 2030 and 2187 cm^{-1} related to C-H stretching vibration of $-\text{CH}_2$ and $-\text{CH}_3$ functional groups. The stretching vibration band at 1216 cm^{-1} is due to the

characteristic asymmetric stretching vibration of the sulfate group. Sulfate, carboxyl, hydroxyl, and amino groups are bioactive compounds that exist in a marine alga. These functional groups can be responsible for the formation of nanoparticles. For instance, it was indicated that the sulfated polysaccharides isolated from the marine alga had a powerful capability to synthesize nanoparticles. Therefore, the sulfate group may be responsible for the reduction of iron ions by oxidation of aldehyde groups to carboxylic acids [4]. The band at 1039.55 cm^{-1} is identified as the symmetric C-O vibration related to a C-O-SO₃ group. These peaks demonstrate the presence of sulfated polysaccharides in the *Enteromorpha spp.* algal extract. Therefore, *Enteromorpha spp.* algal extract containing hydroxyl, sulfate, and aldehyde groups may result in the reduction of Fe^{3+} and synthesis of IO-NPs. Moreover, the peak at 1617.53 cm^{-1} corresponds to the conjugated carbonyl (NH) ($-\text{C}=\text{O}$) group stretching vibration that is characteristic of proteins. This peak became slight broader and slightly shifted from 1622.05 cm^{-1} . The result showed a member of (NH) ($-\text{C}=\text{O}$) group within the cage of cyclic peptides acting a role in stabilizing the nanoparticles [5]. Another peak at 1400 cm^{-1} represents the C-C groups result from aromatic rings that are involved in the algal extract. The formation of IO-NPs was characterized by the absorption bands at 599.83 and 475 cm^{-1} which related to the Fe-O stretches of Fe_3O_4 and Fe_2O_3 [9], confirming the formation of IO-NPs.

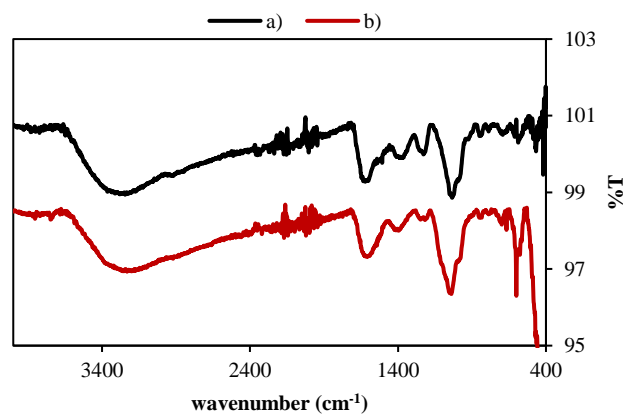


Figure 5. The FT-IR spectrum of the biosynthesized IO-NPs a) before adsorption b) after adsorption

3.2. Total phenolic content of *Enteromorpha spp.* extract

The polyphenols in many plants and alga contain mainly flavonoids (flavonols, flavones, flavanones, isoflavones, flavanols, and anthocyanins) and phenolic acids (hydroxycinnamic and hydroxybenzoic acids). They are synthesized as a defense mechanism against microorganisms, and they have shown hydrogen-donor potentials and metal chelation abilities [10]. Many studies

which are based on the green synthesis of metal/metal oxide nanoparticles, fundamentally cited that plants and alga with high polyphenolic content had a capping/stabilizing ability to reduce metal precursors to their nanoforms [11]. Therefore, TFC of *Enteromorpha spp.* extract was determined to show the potential of reducing capability for IO-NPs synthesis. TFC of *Enteromorpha spp.* extract was determined as 9.81 ± 4.8 mg gallic acid equivalents/g dry algae. Some studies about the phenolic content of *Enteromorpha* species reported in the literature. Ganesan et al., [12], investigated TFC of three species of green seaweed *Enteromorpha* (*E. compressa*, *E. linza*, and *E. tubulosa*). They found the total phenol content (%), calculated with a phloroglucinol standard, in the extract of water as (2.98 ± 0.39), (1.33 ± 0.08) and (1.33 ± 0.08) for *E. compressa*, *E. linza* and *E. tubulosa* respectively. In another study, the phenolic content of *Enteromorpha intestinalis* (L.) Kütz. seaweed, collected from Acıgöl Lake in Turkey, was investigated by Akköz et al., [13]. The researchers found TFC of it was 0.025 ± 0.004 mg gallic acid equivalent/g dry algae. Our study showed that TFC of *Enteromorpha spp.* grown in Mediterranean Sea of Turkey seems significantly high, therefore owing to its high phenolic content, *Enteromorpha spp.* extracts can be used as a bioreductant for preparing metal nanoparticles owing to their reducing capability of metal salts. Consequently, the IO-NPs were synthesized successfully by using *Enteromorpha spp.* extract as a non-toxic, cost-effective, and an environmentally friendly reductive agent.

3.3 Effect of environmental conditions to adsorption

3.3.1 Initial pH

The initial pH value of aqueous solution containing heavy metal ions is a significant factor affecting the adsorption processes. Because, the dissolution of metal, as well as the activity of such as amino, carboxyl, sulfate, and phosphate functional groups that present on adsorbent, are affected from pH [14]. The effect of initial pH on the adsorption of Cu^{2+} ions onto IO-NPs was presented in Figure 6. As shown in Figure 6, the maximum equilibrium uptake value was observed at pH 5.0. The maximum adsorption capacity at the initial pH 5.0 could be defined by the interaction of Cu^{2+} ions and surface charge of adsorbent. The net surface charges of synthesized IO-NPs were determined by measuring ζ (zeta) potential in the pH range of 2.0–6.0 and the change of ζ potential with pH were presented in Figure 7. As shown in Figure 7, it was determined that the IO-NPs surface was negatively charged for all pH values and had a maximum negative charge at pH 5.01 (-33.7 mV). So, the adsorbed Cu^{2+} amount was maximum due to strong electrostatic attractions between Cu^{2+} cations and

negatively charged surface at pH 5.0. The aforementioned electrostatic attraction was illustrated in Figure 8, similar to previously proposed by Brunkesh et al., [15].

3.3.2 Initial Cu^{2+} ion concentration

The effect of initial Cu^{2+} ion concentration on the adsorption was shown in Figure 9. From Figure 9, it was indicated that the uptake amounts at equilibrium increased with increase in the experimental initial Cu^{2+} ion concentration up to 275 mg/L, and then remained constant after that as a result covering of active sites of IO-NPs with the Cu^{2+} ions.

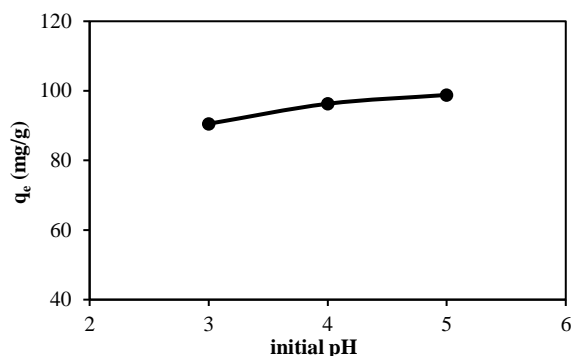


Figure 6. Effect of initial pH ($T=25^\circ\text{C}$, $C_0=100$ mg/L, $X_0=1$ g/L)

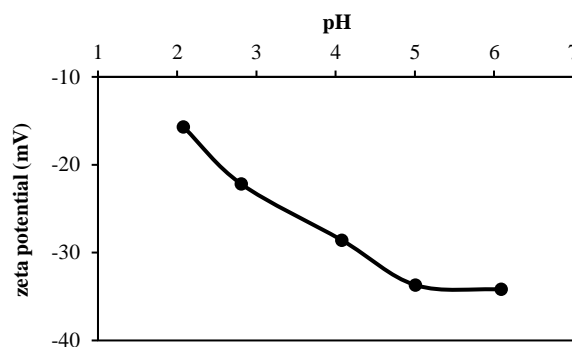


Figure 7. The plot of zeta potential value of the synthesized IO-NPs vs. pH

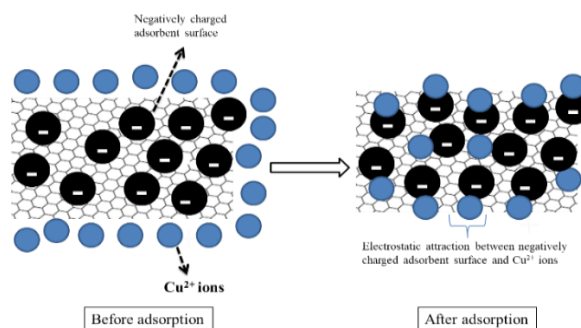


Figure 8. The proposed mechanism of Cu^{2+} adsorption onto IO-NPs

However, the adsorption percentages decreased with increase in the experimental initial Cu^{2+} ion concentration

because of the high ratio of initial Cu^{2+} ion concentration to the available adsorption surface area. Thus, the optimum Cu^{2+} ion concentration was found as 275 mg/L.

3.3.3 Adsorbent concentration

The adsorbent concentration effect on the equilibrium uptake and percentage of adsorption was presented in Figure 10. According to Figure 10, the equilibrium uptakes of Cu^{2+} ion concentrations increased with decreasing the adsorbent concentration from 3.5 g/L to 0.5 g/L. Also; the adsorption percentage slightly increased up to 2.0 g/L of adsorbent concentration, and then indistinctly remained constant with further increase in adsorbent concentration. The increase in uptake values with decreasing adsorbent concentration may arise from the interaction between adsorbent particles such as aggregation, resulting from high adsorbent concentration. The higher adsorption capacities were obtained at lower adsorbent concentrations due to the agglomeration of the adsorbent particles. The agglomeration would cause a decrease in the active surface area of the adsorbent and an increase in diffusional path length. Consequently, the optimum adsorbent concentration was selected to be 0.5 g/L for Cu^{2+} ion adsorption onto IO-NPs.

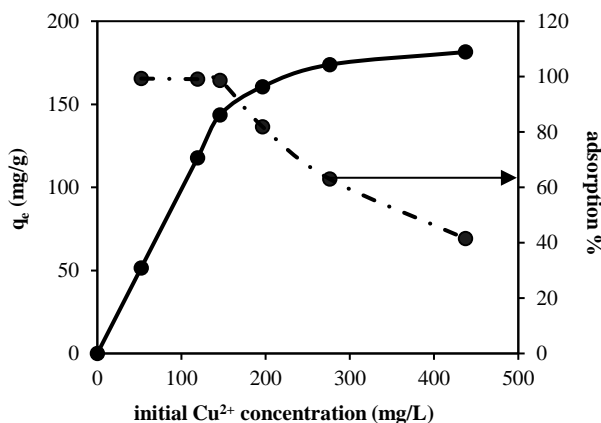


Figure 9. Effect of initial Cu^{2+} concentration (initial pH= 5, $T=35^\circ\text{C}$, $X_0=1$ g/L)

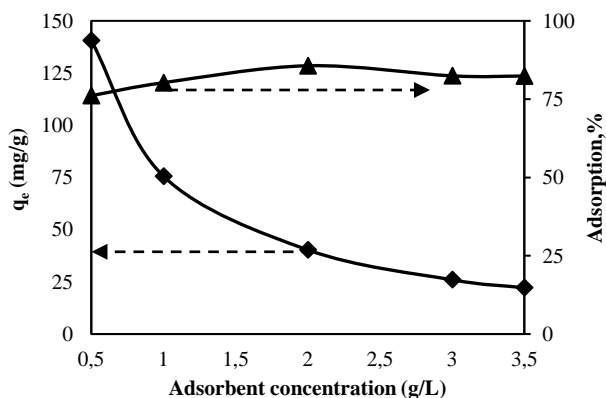


Figure 10. Effect of adsorbent concentration (initial pH= 5, $T=35^\circ\text{C}$, $C_0=100$ mg/L)

3.3.4 Temperature

The variation of the adsorption capacities of IO-NPs with temperature values was depicted in Figure 11. According to Figure 11, the uptake amounts at equilibrium increased up to 35°C , and after that, it slightly decreased by the further increase in temperature. So, the optimum temperature was determined as 35°C for Cu^{2+} ion adsorption onto IO-NPs.

3.4 Equilibrium, kinetic, and mass transfer modeling

3.4.1 Equilibrium modeling

The adsorption isotherm models could be used for modeling the relationships between adsorbate and adsorbent at adsorption equilibrium. The well-established isotherm models of Langmuir and Freundlich were applied to the experimental equilibrium data at different temperatures.

The Langmuir model, that is applicable for monolayer adsorption onto the exactly homogeneous surface with limited availability of identical sites and with too weak interaction between adsorbed molecules is presented by Equation (3):

$$q_e = \frac{Q^0 \cdot b \cdot C_e}{1 + b \cdot C_e} \quad (3)$$

Freundlich isotherm defines the heterogeneous surface energies by multilayer adsorption, and it is stated by Equation (4) [16]:

$$q_e = K_F \cdot C_e^{(1/n)} \quad (4)$$

The isotherm constants calculated from the linearized isotherm equations along with the regression coefficients were presented in Table 2. Also, the isotherm graph at optimum temperature was plotted in Figure 12.

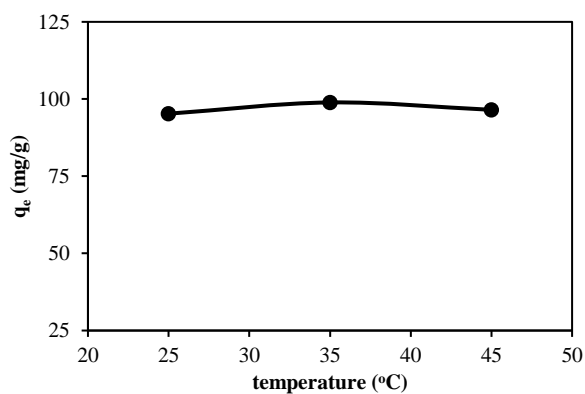


Figure 11. Effect of temperature (initial pH=5, $C_0=100$ mg/L, $X_0=1$ g/L)

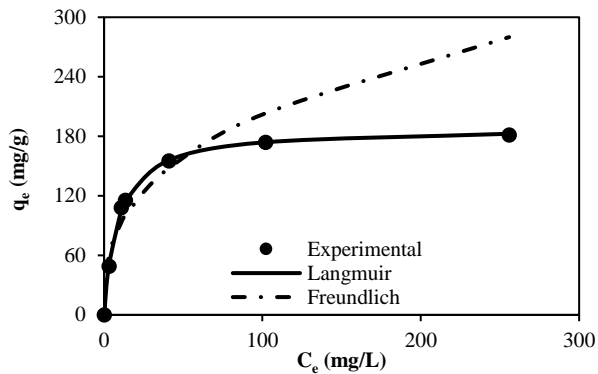


Figure 12. The isotherm graphs (q_e vs C_e) (initial pH=5, $T=35^\circ\text{C}$, $X_0=1$ g/L)

As shown in Table 2, higher regression coefficients ($R^2 > 0.99$) and lower ARE of the Langmuir isotherm model indicated that Cu^{2+} adsorption equilibrium data were well-described by the Langmuir isotherm model. The consistency between experimental q_e values and calculated q_e values from Langmuir isotherm model also approved that the experimental equilibrium data of Cu^{2+} adsorption best fitted to the Langmuir isotherm model. It can be concluded that Cu^{2+} adsorption onto IO-NPs was monolayer in nature. It meant that only one Cu^{2+} ion could adsorb onto the active sites of the adsorbent surface. Therefore, no further adsorption could take place at that site on the surface of the adsorbent. Besides, as it was expected from the results of temperature effect (Figure 11) that Q^0 values were close to each other and the maximum Q^0 value (188.68 mg/g) was obtained at optimum temperature.

The comparison of Q^0 values of various types of iron nanoparticles for Cu^{2+} adsorption was shown in Table 1. Accordingly, it was seen that IO-NPs had relatively higher adsorption capacity compared with the iron-containing adsorbents reported in the literature.

Table 1. The maximum monolayer adsorption capacity values (Q^0) of various types of iron nanoparticles in the literature

Adsorbent	Q^0 (mg/g)	Reference
NiFe ₂ O ₄ magnetic nanoparticles	200.00	[18]
Fe ₃ O ₄ -NPs	188.68	This study
Magnetic nanoparticles coated by chitosan	96.15	[19]
Fe-Fe ₃ O ₄ /GO	90.90	[20]
Nano-scaled zerovalent iron	40.82	[21]
Amino functionalized Fe ₃ O ₄ @SiO ₂ nanoparticles	29.85	[22]
Amino-functionalized magnetic nanosorbent	25.77	[23]

3.4.2 Mass transfer modeling

Several steps, such as intraparticle diffusion, external diffusion, and adsorption, or a combination of more than one step can occur during the transport of adsorbate molecules from the liquid phase to the adsorbent surface. The external resistance greatly reduces the process at highly-stirred systems that the stirring rate effect is unremarkable. Also, the effect of intraparticle resistances can be reduced by decreasing the size of adsorbent, in other words by using nano-sized materials. Weber-Morris intraparticle diffusion model is stated by Equation (5);

$$q_t = K_i \cdot t^{0.5} + I \quad (5)$$

The intraparticle diffusion rate constant (K_i), and I value corresponded to external diffusion are calculated from the slope and intercept value of the plot of q_t vs. $t^{0.5}$ give, respectively. According to the theory of the model, if the plot of q_t vs. $t^{0.5}$ is a straight line and it passes through the origin, the adsorption system is controlled by only intraparticle diffusion. Conversely, if the plot is also linear but it has an intercept value, both intraparticle and film diffusion take place in the adsorption system [17]. Table 3 presented the Weber-Morris model parameters with regression coefficients of Cu^{2+} ion adsorption onto IO-NPs. According to Table 3, the model plots were linear ($R^2 > 0.99$) and also had intercept values (I); thus, the adsorption of Cu^{2+} ion onto IO-NPs followed both intraparticle and film diffusion.

3.4.3 Kinetic Modeling

It is required to assess the adsorption process kinetics for selecting the optimum running conditions for batch processes. The kinetic parameters are useful for the estimation of the adsorption rate and give information for modeling the processes.

The widely used kinetic models for the adsorption processes are the pseudo first order and the pseudo second order kinetic models. The adsorption kinetics was elucidated by correlating the adsorption kinetic data of the Cu^{2+} onto IO-NPs using the linear forms of the pseudo first order and the pseudo second order kinetic models that were given in following Equations 6 and 7, respectively [24].

$$[\log(q_e - q_t) = \log(q_e) - \frac{k_1 t}{2.303}] \quad (6)$$

$$[\frac{t}{q_t} = \frac{1}{q_e^2 k_2} + \frac{t}{q_e}] \quad (7)$$

Table 2. The constants of the adsorption isotherm models (initial pH=5.0, X₀=1.0 g/L)

T (°C)	Langmuir isotherm model (1/q _e)=[(1/(Q ⁰ ·b)·(1/C _e)] + (1/Q ⁰)				Freundlich isotherm model ln(q _e)=ln(K _F)+(1/n)·ln(C _e)			
	Q ⁰ (mg/g)	b (L/mg)	R ²	ARE	K _F (mg/g)/(L/mg) ^{1/n}	n	R ²	ARE
25	181.8182	0.1316	0.991	5.9947	40.2067	0.3351	0.947	10.2815
35	188.6792	0.1165	0.999	0.7109	40.5460	0.3485	0.891	20.7332
45	185.1852	0.07397	0.994	2.2514	47.7673	0.2757	0.927	14.5122

$$[ARE=(100/n) \cdot \sum_i^n (q_{e,cal}-q_{e,exp})/(q_{e,exp})]$$

For Cu²⁺ adsorption onto IO-NPs, the kinetics model parameters and R² values were exhibited in Table 4 (a) and (b). From Table 4 (a) and (b), the adsorption kinetics of Cu²⁺ onto IO-NPs was well-defined by the pseudo second order kinetic model due to the consistency of the experimental and calculated q_e values and high regression coefficients than the pseudo first order model at all initial Cu²⁺ ion concentrations.

Table 3. The parameters of Weber-Morris model (initial pH=5.0, T=35°C, X₀=1.0 g/L)

C ₀ (mg/L)	K _i (mg/g.min ^{0.5})	Intercept (I)	R ²
52.0566	0.0103	47.39	0.990
119.0377	4.2274	74.50	0.994
145.4717	4.7436	80.18	0.993
275.6981	5.8955	93.69	0.995

Table 4.a. The parameters of the pseudo first order kinetic model (initial pH=5.0, T=35°C, X₀=1.0 g/L)

C ₀ (mg/L)	q _{e,exp} (mg/g)	Pseudo first order		
		k ₁ *10 ³ (min ⁻¹)	q _{e,cal1} (mg/g)	R ²
52.0566	56.98	24.41	41.96	0.952
119.0377	118.94	24.41	68.36	0.882
145.4717	143.49	20.73	100.74	0.965
196.0755	160.60	16.58	120.67	0.821
275.6981	173.81	16.58	128.53	0.943
437.2075	181.43	1.45	128.17	0.871

Table 4.b. The parameters of the pseudo second order kinetic model (initial pH=5.0, T=35°C, X₀=1.0 g/L)

C ₀ (mg/L)	q _{e,exp} (mg/g)	Pseudo second order		
		k ₂ *10 ⁴ (g/mg.min)	q _{e,cal2} (mg/g)	R ²
52.0566	56.98	15.39	53.69	0.991
119.0377	118.94	12.50	114.66	0.997
145.4717	143.49	7.74	138.66	0.993
196.0755	160.60	4.85	149.91	0.991
275.6981	173.81	3.04	157.26	0.991
437.2075	181.43	6.29	173.01	0.990

4. Conclusions

The present work revealed that iron oxide nanoparticles (IO-NPs) could be synthesized through the fast and facile biosynthesis method using *Enteromorpha spp.* extract as a biological reductant/capping agent. Algae are abundant resources exist in both fresh and saltwater; also, they cause water pollution. This study showed that they can be converted into economic value by evaluating them in nanoparticle biosynthesis and also the water pollution arising from algae can be reduced by this means.

Acknowledgment

This work supported by the Scientific Research Projects Management of Mersin University is gratefully acknowledged (Project number: 2018-1-TP2-2779), Turkey.

Nomenclature

- b : Freundlich isotherm model constant (L/mg)
- C_e : Residual Cu²⁺ ion concentration at equilibrium (mg/L)
- C₀ : Initial Cu²⁺ ion concentration (mg/L)
- K_F : Freundlich constant indicating adsorption capacity ((mg/g)/(L/mg)^{1/n})
- K_i : Rate constant of intraparticle diffusion (mg/g.min^{1/2})
- k₁ : Rate constant of pseudo first order kinetic model (1/min)
- k₂ : Rate constant of pseudo second order kinetic model (g/mg.min)
- I : Intercept value of Weber-Morris plot
- q_e : Uptake amount per unit mass of adsorbent at equilibrium (mg/g)
- q_{e,cal1} : Calculated uptake amount per unit mass of adsorbent from pseudo first order kinetic model (mg/g)
- q_{e,cal2} : Calculated uptake amount per unit mass of adsorbent from pseudo second order kinetic model (mg/g)
- q_{e,exp} : Experimental uptake amount per unit mass of adsorbent (mg/g)
- q_t : Uptake amount per unit mass of adsorbent at any time (mg/g)
- Q⁰ : Maximum monolayer adsorption capacity (mg/g)

- R^2 : Regression coefficient
 T : Temperature ($^{\circ}\text{C}$, K)
 t : Time (min)
 $1/n$: Freundlich constant indicating adsorption intensity

References

- Uzunoglu, D., and A. Özer, *Adsorption of hazardous heavy metal copper (II) from aqueous effluents onto waste material fish (Dicentrarchus labrax) scales: optimization, equilibrium, kinetics, thermodynamic, and characterization studies*. Desalination and Water Treatment, 2016. **57**(48-49): p. 22794-22798.
- Ajouyed, O., C. Hurel, M. Ammari, L.B. Allal, and N. Marmier, *Sorption of Cr (VI) onto natural iron and aluminum (oxy) hydroxides: effects of pH, ionic strength and initial concentration*. Journal of Hazardous Materials, 2010. **174**(1): pp. 616-622.
- Abhalaxmi, S., and S.K. Sahoo, *Magnetic nanoparticles: a novel platform for cancer theranostics*, Drug Discovery Today, 2014. **19**(4): p. 474-481.
- Mahdavi, M., F. Namvar, M.B. Ahmad, and R. Mohamad, *Green biosynthesis and characterization of magnetic iron oxide (Fe_3O_4) nanoparticles using seaweed (Sargassum muticum) aqueous extract*. Molecules, 2013. **18**(5): p.5954-5964.
- Azizi, S., M. B. Ahmad, F. Namvar, R. Mohamad, *Green biosynthesis and characterization of zinc oxide nanoparticles using brown marine macroalga Sargassum muticum aqueous extract*. Materials Letters, 2014. **116**: p. 275-277.
- Slinkard, K., & Singleton, V. L. *Total phenol analysis: automation and comparison with manual methods*, American journal of enology and viticulture, 1977. **28** (1), 49-55.
- El-Kassas, H. Y., M. A. Aly-Eldeen, and S. M. Gharib, *Green synthesis of iron oxide (Fe_3O_4) nanoparticles using two selected brown seaweeds: characterization and application for lead bioremediation*. Acta Oceanologica Sinica, 2016. **35**(8): p. 89-98.
- Shahwan, T., Sirriah, S. A., Nairat, M., Boyacı, E., Eroğlu, A. E., Scott, T. B., & Hallam, K. R. *Green synthesis of iron nanoparticles and their application as a Fenton-like catalyst for the degradation of aqueous cationic and anionic dyes*. Chemical Engineering Journal, 2011.**172**(1):p. 258-266.
- Iram, M., C. Guo, Y. Guan, A. Ishfaq, and H. Liu, *Adsorption and magnetic removal of neutral red dye from aqueous solution using Fe_3O_4 hollow nanospheres*. Journal of Hazardous Materials, 2010. **181**(1): p. 1039-1050.
- Döker, O., Ergüt M. *Recovery of Bioactive Phenolic Compounds from Lemon (Citrus limon (L.) Burm. f.) and Orange (Citrus Sinensis L. Osbeck) Pomaces*. Chemical and Process Engineering Research, 2017. 51:p.18-33.
- Kumar, K. M., Mandal, B. K., Kumar, K. S., Reddy, P. S., & Sreedhar, B. *Biobased green method to synthesise palladium and iron nanoparticles using Terminalia chebula aqueous extract*. Spectrochimica Acta Part A: Molecular and Biomolecular Spectroscopy, 2013. 102: p. 128-133.
- Ganesan, K., K. Suresh Kumar, and PV Subba Rao. *Comparative assessment of antioxidant activity in three edible species of green seaweed, Enteromorpha from Okha, Northwest coast of India*. Innovative food science & emerging technologies, 2011. **12**(1): p.73-78.
- Akköz, C., Arslan, D., Ünver, A., Özcan, M. M., and Yilmaz, B. *Chemical composition, total phenolic and mineral contents of Enteromorpha intestinalis (L.) Kütz. and Cladophora glomerata (L.) Kütz. seaweeds*. Journal of Food Biochemistry, 2011. **35** (2): p.513-523.
- Uzunoglu, D., N. Gürel, N. Özkaya, A. Özer. *The single batch biosorption of copper (II) ions on Sargassum acinarum*. Desalination and Water Treatment, 2014. **52**(7-9): p. 1514-1523.
- Brungesh, K. V., B. M. Nagabhushana, M.N.K. Harish, and R. Hari Krishna, *An Efficient Removal of Toxic Cr (VI) from Aqueous Solution by MnO₂ Coated Polyaniline Nanofibers: Kinetic and Thermodynamic Study*. Journal of Environmental Analysis Toxicology, 2017. **7**(442): p. 2161-0525.
- Fan, L., C. Luo, M. Sun, X. Li, F. Lu, and H. Qiu, *Preparation of novel magnetic chitosan/graphene oxide composite as effective adsorbents toward methylene blue*. Bioresource Technology, 2012. **114**: p. 703-706
- Benhouria, A., M. A. Islam, H. Zaghoulane-Boudiaf, M. Boutahala, B.H. Hameed, *Calcium alginate–bentonite–activated carbon composite beads as highly effective adsorbent for methylene blue*. Chemical Engineering Journal, 2015. **270**: p.621-630.
- Moeinpour, F., and S. Kamyab. *Adsorption characteristics of Cu^{2+} on NiFe_2O_4 magnetic nanoparticles*. Journal of Water Reuse and Desalination, 2015. **5**(2): p. 223-230.
- Zhou, Y. T., H. L. Nie, C. Branford-White, Z. Y. He, and L. M. Zhu. *Removal of Cu^{2+} from aqueous solution by chitosan-coated magnetic nanoparticles modified with α -ketoglutaric acid*. Journal of Colloid and Interface Science, 2009. **330**(1): p. 29-37.
- Le, G. H., A. Q. Ha, Q. K. Nguyen, K. T. Nguyen, P. T. Dang, H. T. Tran, and T. A. Vu. *Removal of Cd^{2+} and Cu^{2+} ions from aqueous solution by using Fe– Fe_3O_4 /graphene oxide as a novel and efficient adsorbent*. Materials Research Express, 2016. **3**(10): p. 105603.

21. Dada, A. O., F. A. Adekola, and E. O. Odebunmi. *Kinetics, Isotherms and Thermodynamics Studies of Sorption of Cu²⁺ onto Novel Zerovalent Iron Nanoparticles*. Covenant Journal of Physical and Life Sciences, 2014. **2**(1): p. 24-53.
22. Shoueir, K. R., A. Sarhan, A. M. Atta, and M. A. Akl. *Adsorption studies of Cu²⁺ onto poly (vinyl alcohol)/poly (acrylamide-co-N-isopropylacrylamide) core-shell nanogels synthesized through surfactant-free emulsion polymerization*. Separation Science and Technology, 2016. **51**(10): p. 1605-1617.
23. Hao, Y. M., C. Man, and Z. B. Hu. *Effective removal of Cu (II) ions from aqueous solution by amino-functionalized magnetic nanoparticles*. Journal of Hazardous Materials, 2010. **184** (1): p. 392-399.
24. Yan, Y., Q. An, Z. Xiao, W. Zheng, and S. Zhai, *Flexible core-shell/beadlike alginate@PEI with exceptional adsorption capacity, recycling performance toward batch and column sorption of Cr (VI)*, Chemical Engineering Journal, 2017. **313**: p. 475-486.



Research Article

Removal of Acid Orange 74 from wastewater with TiO₂ nanoparticle

Gamze Topal Canbaz^{a,*} , Neşe Keklikcioğlu Çakmak^a , Atakan Eroğlu^a  and Ünsal Açikel^a 

^a Sivas Cumhuriyet University, Engineering Faculty, Department of Chemical Engineering, Sivas, Turkey

ARTICLE INFO

Article history:

Received 13 April 2018

Revised 03 September 2018

Accepted 07 September 2018

Keywords:

Acid Orange 74

Adsorption

TiO₂ nanoparticle

Sol-gel

ABSTRACT

The use of nanomaterials in wastewater treatment has gained importance. Nano-structured adsorbents have good adsorption potential due to their properties such as large surface area. In this study, removal of AO74 (Acid Orange 74) from the waters with TiO₂ nanoparticles were investigated. TiO₂ nanoparticles were synthesized by sol-gel method. The X-ray diffraction (XRD), Scanning electron microscopy (SEM), Fourier-transform infrared spectroscopy (FTIR) and Ultraviolet-visible spectroscopy (UV-VIS) spectrometer techniques were used to characterize the synthesized products. Stability analysis was performed by zeta potential analysis. The anatase phase of the TiO₂ nanoparticles was confirmed by XRD analysis. The SEM micrographs revealed the spherical-like morphology with average diameter of about 32 nm which agrees with XRD results. FTIR spectra show the vibrational mode of TiO₂ around 600 cm⁻¹. Absorption peak in the UV region at 320 nm are observed. This peak is characteristics of nano-sized TiO₂ nanoparticles. If the measured zeta potential absolute value is greater than 35 mV, it can be said that the produced nanofluid is stable. The zeta potential value greater than 35 mV in all measurements in this study, so that the synthesized TiO₂ nanoparticle is stable in the fluid medium. pH (2-5), contact time (10-120 min) and initial dye concentration (20-100 mg / L) were investigated to determine the adsorption potential of TiO₂ nanoparticles. The optimum parameters for adsorption of AO74 were determined as pH and contact time, respectively: 5 and 75 minutes. The adsorption system is compatible with Langmuir and Freundlich isotherms. As a result, TiO₂ nanoparticles were identified as suitable adsorbent for removal of AO74.

©2019 Advanced Researches and Engineering Journal (IAREJ) and the Author(s).

1. Introduction

Dyes are generally used in textile, leather, plastic, paper industry, paints, cosmetics, color additives and biomedical area [1]. The dyes are very stable against light and oxidation due to their complex chemical structure. Due to these properties, their biodegradation is very difficult [2,3]. Textile wastes are one of the most important and dangerous environmental contaminants. Because many dyes are toxic and carcinogenic, they cause damage to the aquatic life and people.[4]. For this reason, it is very important to remove waste from the environment and dye elimination from wastewaters before their release into the environment is very substantial [2,5]. Basic dyes, acid dyes, azo dyes and disperse dyes are commonly used in the textile industry. [6,7]. Most of these dyes such as Acid orange 74 is an

azo dye and used for dyeing wool, fibers, silk and carpet (Figure 1).

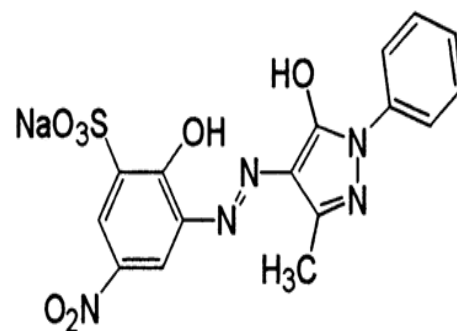


Figure 1. Acid orange 74 molecular structure

* Corresponding author. Tel.: +90 346 2191010(2487)

E-mail addresses: gtopal@cumhuriyet.edu.tr (G. Topal Canbaz), nkeklikcioglu@cumhuriyet.edu.tr (N. Keklikcioğlu Çakmak), ataknovv.eroğlu@gmail.com (A. Eroğlu), uacikel@cumhuriyet.edu.tr (Ü. Açikel)

ORCID: 0000-0001-7615-7627 (G. Topal Canbaz), 0000-0002-8634-9232 (N. Keklikcioğlu Çakmak), 0000-0003-4544-5225 (A. Eroğlu), 0000-0003-4969-8502 (Ü. Açikel)

In recent years, many methods such as adsorption, biological treatment, chemical oxidation, photocatalysis, coagulation/flocculation, etc. have been improved for separating organic pollution from water and wastewaters. Among these methods, adsorption process has been demonstrated as a highly effective removal method due to its simplicity, applicability and this technique also generally preferred in terms of cost. Several natural and synthetic adsorbents such as zeolites, polymers, resins, activated carbon, chitin and some nanoparticles like TiO₂, Al₂O₃, etc. have been used to remove contaminants from waste waters. Particles between 1-100 nm are defined as nanoparticles. Their at least one dimension less than 100 nm. Nanoparticle research is presently an area of deep scientific research because a wide variety of potential applications in medicine, energy and electronics, manufacturing and materials, environmental applications. The use of nanoparticles in environmental applications with the developing technology has become widespread. [8]. Nano materials used in water treatment are produced with small size, large surface area and renewable properties. [9]. The reason for the wide use of nanoparticles is the small size and high surface area. Among the nanoparticles, TiO₂ nanoparticles have commercial interests for their nontoxicity, low cost, hydrophilic, photocatalytic activity, large specific surface area, long service life, high efficiency.

In this study, the synthesis of TiO₂ nanoparticles and the AO74 removal potential from aqueous solutions were investigated. TiO₂ nanoparticles were synthesized by sol-gel method. The X-ray diffraction (XRD), Scanning electron microscopy (SEM), Fourier-transform infrared spectroscopy (FTIR) and Ultraviolet-visible spectroscopy (UV-VIS) spectrometer techniques were used to characterize the synthesized products. Adsorption potential of TiO₂ nanoparticles; pH, contact time and initial dye concentration were determined.

2. Materials and Method

2.1 Synthesis and characterization of TiO₂ nanoparticle

Ethanol, iso-propanol and Titanium (IV) butoxide were mixed in a ratio of 160 ml:20ml:20ml and the mixture was sonicated. To prepare a white precipitate, a solution containing 2 g of cetyltrimethyl ammonium bromide (CTAB) in 100 ml of water was added. The mixture was kept at 80 °C for 4 hours. Excess water in the mixture was removed by evaporation under constant stirring in a water bath. The synthesized material was first dried at 110 ° C for 12 hours and then calcined at 500 ° C in a muffle furnace for the get high degree of crystallization [10].

In this study, TiO₂ were used as the nanoparticles and deionize water (DIW) were chosen as the base fluid. The morphologies of TiO₂ were characterised by the XRD pattern. X-ray diffraction (XRD) analysis was conducted on a Rigaku DMAX IIIC using CuKα radiation at Department of Geological Engineering of Cumhuriyet University in Sivas, Turkey. Scanning electron microscope (SEM) analysis was carried out on TiO₂ nanoparticles by TESCAN MIRA3 XMU electron microscope. To determine the functional groups of TiO₂, FTIR(Bruker: Tensor II) analysis was done in the range 4000-400 cm⁻¹. UV-Vis spectrophotometer (UV-1280, Shimadzu, Japan) was utilized to record the spectra of prepared TiO₂-DIW nanofluids range from 200 to 800 nm. Zeta potential of the TiO₂ nanoparticles in aqueous phase was measured using a malvern Zetasizer Nano Z. The electrophoretic mobility of the particles is determined by this instrument automatically and converts it to the zeta potential [11].

2.2. Adsorption experiments

AO74 (Sigma-Aldrich) stock solution was prepared at 1000 mg / L concentration. AO74 in the desired concentrations was obtained by dilution from stock solution. Adsorption experiments were performed in batch system. The parameters affecting the adsorption were investigated (pH, contact time, starting dye concentration). The experiments were carried out in glass flasks with a working volume of 250 ml. The adsorptive quality of the TiO₂ nanoparticles were tested as a function of pH (2–5), contact time (10–120 min) and initial dye concentrations (20–100 mg/L). The pH of the dye solutions was adjusted with NaOH(0.1-0.01 M) and HCl(0.1-0.01M). After the adsorption system reached equilibrium, the adsorbent was separated by centrifugation. AO74 (λ_{max}455 nm) concentration in the solution was determined by spectrophotometer. The amount of dyes adsorbed (q_e; mg/g) was determined by Eq (1) and the percent dye adsorption (%) was determined by Equations (2).

$$q_e = \frac{(C_o - C_e) * V}{m} \quad (1)$$

$$(\%)adsorption = \frac{C_o - C_e}{C_o} * 100 \quad (2)$$

C_o is the initial dye concentration, C_e is the final dye concentration (mg/L). m is the mass of adsorbent (g) and V is the volume of the dye solution (L).

3. Results and Discussion

3.1 XRD results

XRD characterized the crystal structures of TiO_2 sample, and Figure 1 shows the results. Well-defined (1 0 1) peak at 25.42° and 37.89° , 48.12° , 55.16° , 62.79° were displayed by the XRD pattern of TiO_2 . These peaks belong to the typical anatase phase TiO_2 [12].

The average crystallite size of TiO_2 nanoparticles using the Scherrer equation [13] was calculated from the XRD patterns (Figure 2). The average crystallite size of the TiO_2 nanoparticles was found to be about 12 nm.

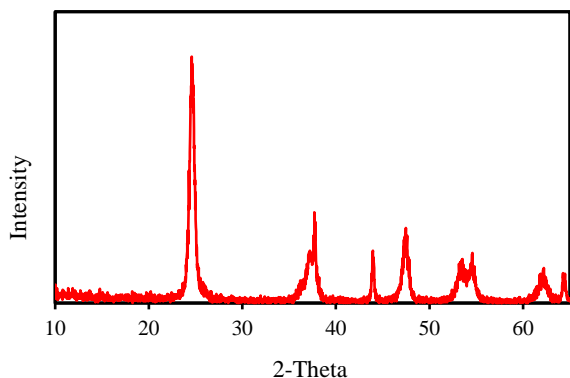


Figure 2. XRD pattern of the sol-gel TiO_2 nanoparticles.

3.2 SEM results

According to the scanning electron microscopy data (Figure 3), TiO_2 nanoparticles are well dispersed systems. As can be observed from the below mentioned micrograph, the particles are spherical. From SEM images, the average particle size was evaluated to be around 32 nm for TiO_2 nanoparticles which is consistent with the XRD results.

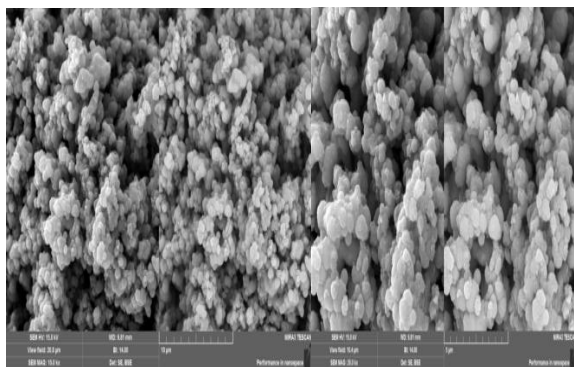


Figure 3. SEM micrographs of sol-gel TiO_2 nanoparticles.

3.3 FTIR results

The FTIR spectrum of TiO_2 nanoparticles was displayed in Figure 4. 700cm^{-1} band is available and it is conformed to the Ti-O stretching vibration and is present in TiO_2 .

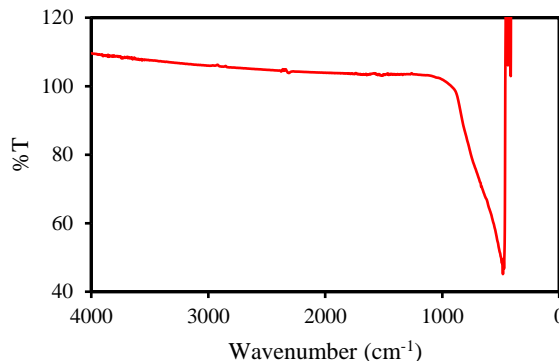


Figure 4. FTIR spectrum of sol-gel TiO_2 nanoparticles.

3.4 UV-Vis results

UV-Vis absorbance spectrum of TiO_2 nanoparticles is shown in Figure 5. Absorption band in the UV region at 320 nm are observed in Figure 4. This is characteristics of nano-sized TiO_2 nanoparticles [14].

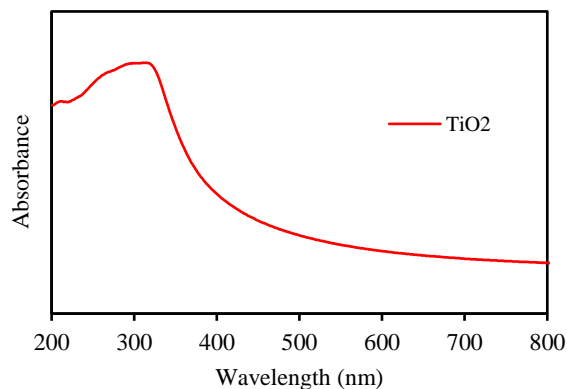


Figure 5. UV-Vis absorbance spectrum of sol-gel TiO_2 nanoparticles.

A Zeta Potential Analyzer was utilized for the purpose of examining the Zeta potential measurement of nanoparticles in the nanofluid. Zeta potential is defined as the electrical potential existing between the nanoparticle surface and the base fluid, and the zeta potential absolute value is related to the nanoparticle stability. If the measured zeta potential absolute value is greater than 25 mV, it can be said that the produced nanofluid is stable. The zeta potential value greater than 35 mV in all measurements in this study. The zeta potential is related to the stability of nanofluids; higher the absolute value of

the zeta potential, the higher its stability. It was concluded that the zeta potential of TiO₂-water nanofluid prepared in this study is very stable.

3.5 pH results

pH is an important parameter in adsorption processes. For this reason, AO74 adsorption at different pH values was investigated. The studies were carried out at room temperature and at constant TiO₂ concentration (10 g / L) and pH values were measured at 2-5. The results obtained from pH experiments are given in Figure 6. The concentration of AO74 adsorbed with increasing pH increased and the maximum adsorption was determined as 52% at pH 5. The optimum pH value for AO74 adsorption was determined as 5.

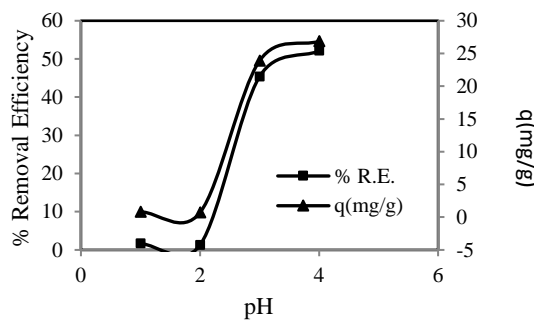


Figure 6. Effect of pH (Co: 50 mg/L, amount of TiO₂ nanoparticles: 10 g/L, T: 23°C)

3.6 Contact time results

Experiments were conducted at different contact times to determine the optimum adsorption time in the adsorption of AO74 with TiO₂ nanoparticles (10-120 minutes). After 75 minutes from the start of the adsorption experiment, the amount of adsorbed dye was determined to reach equilibrium and the optimum contact time for AO74 dye adsorption was determined as 75 minutes (Figure 7).

In another study for AO74 dye removal, activated sludge was used and the removal time was determined to be 240 minutes. In this study, removal time with TiO₂ nanoparticles was determined to be 75 minutes [15]. With TiO₂ nanoparticles, removal was achieved in a shorter time.

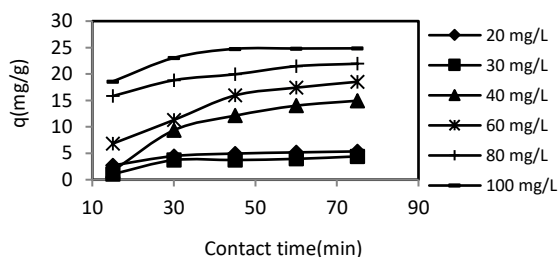


Figure 7. Effect of contact time (pH:5, amount of TiO₂ nanoparticles: 10 g/L, T: 23°C)

3.7 Initial dye concentrations results

Initial dye concentrations results from 20 to 100 mg/L are given in Figure 8. To investigate the effect of initial dye concentration on adsorption, dye concentration was investigated in the range of 20-100 mg / L. An increased concentration of dye was observed with increasing initial dye concentration. Adsorption at 20 mg / L and 100 mg / L dye concentrations was determined as 9.47 mg / g and 30 mg / g respectively.

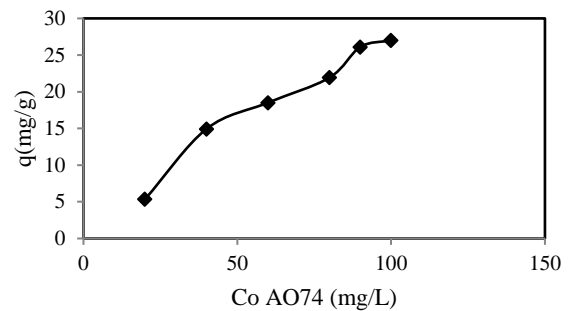


Figure 8. Effect of initial dye concentration (pH: 5, contact time: 75 min, TiO₂ nanoparticles: 10 g/L, T: 23°C)

3.8 Adsorption isotherms

Langmuir and Freundlich isotherm models were calculated by nonlinear regression method using Excel software. The Langmuir model determines the maximum adsorption capacity by assuming that every adsorption site is equivalent in monolayer and energetically. Non-linear Langmuir isotherm equation is given in Equation 3 [16]:

$$q_e = \frac{Q_o b C_e}{1 + b C_e} \quad (3)$$

Here q_e is the amount of equilibrium adsorption capacity and Q_o is the maximum adsorption capacity (mg/g). C_e is the equilibrium solution concentration (mg/L); b is the Langmuir constant (L/mg).

The Freundlich model is applied to adsorption on heterogeneous surfaces [17]. Non-linear Freundlich equation is given in Equation 4.;

$$q_e = k_F C_e^{1/n} \quad (4)$$

k_F is the adsorption capacity (L/g), n is the adsorption intensity.

Langmuir adsorption capacity was determined as 37.03 mg / g for AO74 dye. The results show that the TiO₂ nanoparticles are an effective adsorbent for AO74 removal (Table1).

When using activated sludge in AO74 dye removal, the maximum adsorption capacity was determined to be 142.85 mg / g [15]. Lower results were obtained with TiO₂ nanoparticles in this study.

Table 1. Adsorption isotherm parameters (T=23°C)

Langmuir		Freundlich			
Q ⁰ (mg/g)	b (L/mg)	R ²	K _F (L/g)	n	R ²
37,03	0.023	0.93	0.65	1.66	0.94

3.9 Adsorption kinetic

The data obtained from the adsorption experiment were analyzed using the pseudo-first order kinetic model, pseudo second-order kinetic model and intraparticle diffusion model [18].

$$\log(q_e - q_t) = \log q_e - \frac{k_1}{2.303} t \tag{5}$$

Where q_t (mg/g) is the at a given moment, the adsorbent adsorbed pollutant concentration and k₁ (min⁻¹) is the rate constant of pseudo first order kinetic model.

The second order kinetic model is explained by the following equation by Equation 6 below:

$$\frac{t}{q_t} = \frac{1}{k_2(q_e)^2} + \frac{1}{q_e} t \tag{6}$$

where k₂ (g/mg/min) is the rate constant of pseudo second order kinetic model.

The particle diffusion model is given by Equation 7 below:

$$q_t = k_d t^{0.5} + C \tag{7}$$

where k_d (mg/g/min^{0.5}) is diffusion rate constant and C is intercept.

Kinetic data from TiO₂ nanoparticle and AO74 adsorption data are presented in Table 2.

Table 2. Adsorption isotherm parameters (T=23°C, Co: 40 mg/L, q_e : 37.03mg/g)

Pseudo first order	k ₁	q ₁ (mg/g)	R ²
	0.011	3.97	0.90
Pseudo second order	k ₂	q ₂ (mg/g)	R ²
	0.0008	24.39	0.97
Intraparticle diffusion	k _i	C (mg/g)	R ²
	2.09	3.68	0.89

According to the results of adsorption kinetics given in Table 2, the adsorption process conforms to the pseudo second order kinetic model. The experimental q_e (37.03mg/g) values were also compatible with adsorption capacities (q₂) obtained from the pseudo second order model.

4. Conclusion

Here in, we report for synthesis TiO₂ nanoparticles via sol-gel technique. Nano-size TiO₂ powders were synthesized using sol-gel method. The synthesized material was characterized by XRD, SEM, FTIR and UV-Vis spectroscopy techniques. The XRD pattern of synthesized sample confirms the formation anatase phase with very good crystallinity. Also, SEM image displayed the uniform morphology in the form of nano clusters and spherical shape. FTIR spectra show the vibrational mode of TiO₂ around 600 cm⁻¹. Strong and sharp peak was observed between 200-700 nm in the UV-Vis region optical absorption study. Absorption peak in the UV region at 320 nm are observed. This peak is characteristics of nano-sized TiO₂ nanoparticles. The zeta potential value greater than 35 mV in all measurements. A route of sol gel method was performed for synthesis pure anatase TiO₂ nanoparticles with high quality production. As a result, TiO₂ nanoparticles were successfully obtained by sol gel method by indicating different characterization analysis results.

In this study, TiO₂ nanoparticles were used for AO74 dye removal from aqueous solutions. pH, contact time and initial dye concentration were determined in order to determine the optimum parameters in the adsorption process. The optimum pH and contact time were determined as pH 5 and 75 min at AO74 dye adsorption. With increasing AO74 dye concentration, it was observed that the amount of adsorbent adsorbed to AO74 per unit weight increased. The Langmuir adsorption capacities for AO74dye was 37.03 mg/g. The results show that the TiO₂ nanoparticles are an effective adsorbent for AO74 removal.

Thus, these results verify the encouragement that titanium nanoparticles propose new dimensions toward reliable and economically applicable water treatment of colored effluents. TiO₂ nanoparticles synthesized by sol-gel method were determined to be useful in removing dyes from aqueous solutions.

Acknowledgment

This work is supported by the Scientific Research Project Fund of Cumhuriyet University under the project number M-648.

References

1. Ellass, K., Laachach, A., Alaoui, A., and Azzi, M., *Removal of methyl violet from aqueous solution using a stevensite-rich clay from Morocco*. Applied Clay Science, 2011. 54(1): p. 90-96.
2. Mane, V. S., and Babu, P. V., *Kinetic and equilibrium studies on the removal of Congo red from aqueous solution using Eucalyptus wood (Eucalyptus globulus) saw dust*. Journal of the Taiwan Institute of Chemical Engineers, 2013. 44(1): p. 81-88.
3. Haque, E., Jun, J. W., and Jhung, S. H., *Adsorptive removal of methyl orange and methylene blue from aqueous solution with a metal-organic framework material, iron terephthalate (MOF-235)*. Journal of Hazardous materials, 2011. 185(1): p. 507-511.
4. Karagozoglu, B., Tasdemir, M., Demirbas, E., and Kobya, M., *The adsorption of basic dye (Astrazon Blue FGRL) from aqueous solutions onto sepiolite, fly ash and apricot shell activated carbon: kinetic and equilibrium studies*. Journal of hazardous materials, 2007. 147(1-2): p. 297-306.
5. Hameed, B. H., and Daud, F. B. M., *Adsorption studies of basic dye on activated carbon derived from agricultural waste: Heveabrsiliensis seed coat*. Chemical Engineering Journal, 2008. 139(1): p. 48-55.
6. Turabik, M., *Adsorption of basic dyes from single and binary component systems onto bentonite: simultaneous analysis of Basic Red 46 and Basic Yellow 28 by first order derivative spectrophotometric analysis method*. Journal of hazardous materials, 2008. 158(1): p. 52-64.
7. Mahmoud, D. K., Salleh, M. A. M., Karim, W. A. W. A., Idris, A., and Abidin, Z. Z., *Batch adsorption of basic dye using acid treated kenaf fibre char: equilibrium, kinetic and thermodynamic studies*. Chemical Engineering Journal, 2012. 181: p. 449-457.
8. Brame, J., Li, Q., and Alvarez, P. J., *Nanotechnology-enabled water treatment and reuse: emerging opportunities and challenges for developing countries*. Trends in Food Science & Technology, 2011. 22(11): p. 618-624.
9. Ali, I., *New generation adsorbents for water treatment*. Chemical reviews, 2012. 112(10): p. 5073-5091.
10. Mahbulbul, I. M., Elcioglu, E. B., Saidur, R., and Amalina, M. A., *Optimization of ultrasonication period for better dispersion and stability of TiO₂-water nanofluid*. Ultrasonics sonochemistry, 2017.37: p. 360-367.
11. Leroy, P., Tournassat, C., and Bizi, M., *Influence of surface conductivity on the apparent zeta potential of TiO₂ nanoparticles*. Journal of Colloid and Interface Science, 2011. 356(2): p. 442-453.
12. Vlazan, P., Ursu, D. H., Irina-Moiescu, C., Miron, I., Sfirloaga, P., and Rusu, E., *Structural and electrical properties of TiO₂/ZnO core-shell nanoparticles synthesized by hydrothermal method*. Materials Characterization, 2015. 101: p. 153-158.
13. Langford, J. I., and Wilson, A. J. C. (1978). *Scherrer after sixty years: a survey and some new results in the determination of crystallite size*. Journal of Applied Crystallography, 11(2), 102-113.
14. Aware, D. V., and Jadhav, S. S., *Synthesis, characterization and photocatalytic applications of Zn-doped TiO₂ nanoparticles by sol-gel method*. Applied Nanoscience, 2016. 6(7): p. 965-972.
15. Canbaz, G. T., Acikel, U., and Acikel, Y. S. *Investigation of Acid Orange 74 Dye Adsorption with Anaerob Activated Sludge*. International Journal Of Food And Biosystems Engineering, 2017. 4(1):p. 91-96.
16. Khan, T. A., and Khan, E. A., *Removal of basic dyes from aqueous solution by adsorption onto binary iron-manganese oxide coated kaolinite: Non-linear isotherm and kinetics modeling*. Applied Clay Science, 2015. 107: p. 70-77.
17. Özcan, A. S., Gök, Ö., and Özcan, A., *Adsorption of lead (II) ions onto 8-hydroxy quinoline-immobilized bentonite*. Journal of Hazardous materials, 2009. 161(1): p. 499-509.
18. Gulnaz, O., Kaya, A., and Dincer, S., *The reuse of dried activated sludge for adsorption of reactive dye*. Journal of Hazardous Materials, 2006. 134(1-3): p. 190-196.